



HAL
open science

The study of neural oscillations by traversing scales in the brain

Axel Hutt

► **To cite this version:**

Axel Hutt. The study of neural oscillations by traversing scales in the brain. Modeling and Simulation. Université Nice Sophia Antipolis, 2011. tel-00603975

HAL Id: tel-00603975

<https://theses.hal.science/tel-00603975>

Submitted on 28 Jun 2011

HAL is a multi-disciplinary open access archive for the deposit and dissemination of scientific research documents, whether they are published or not. The documents may come from teaching and research institutions in France or abroad, or from public or private research centers.

L'archive ouverte pluridisciplinaire **HAL**, est destinée au dépôt et à la diffusion de documents scientifiques de niveau recherche, publiés ou non, émanant des établissements d'enseignement et de recherche français ou étrangers, des laboratoires publics ou privés.

The study of neural oscillations by traversing scales in the brain

Axel Hutt
Chargé de Recherche (INRIA)

Habilitation à Diriger Des Recherches
Université Nice - Sophia Antipolis

Rapporteurs: Stephen Coombes, Alistair Steyn-Ross et Thomas Wennekers

Examineurs: Frederic Alexandre et Bruno Cessac

Jour de la soutenance: 27 mai 2011

Contents

I	Research contributions and perspectives	5
1	Introduction	7
2	Contributions	11
2.1	Neural Fields and their properties	11
2.1.1	Derivation of the basic evolution equation	12
2.1.2	Axonal transmission delay	14
2.1.3	Relation to partial differential equations	16
2.1.4	Numerical simulation of IDEs	18
2.2	Linear response theory in neural fields	21
2.2.1	The stationary state and its stability in the absence of noise	22
2.2.2	The stability in the presence of external stimuli	25
2.2.3	General response theory	26
2.2.4	Application: Induction of oscillations in certain frequency bands by external stimuli	29
2.2.5	Application: Model for EEG in general anaesthesia	33
2.3	Non-linear response in neural fields	37
2.3.1	Additive noise tunes the stability of stationary states	37
2.3.2	Traveling fronts	41
2.4	Multivariate signal analysis	41
3	Research perspective	47
3.1	Generation of oscillations in weakly-electric fish	48
3.2	Frequency switch in the mammalian olfactory system	49
3.3	Frequency tuning during general anaesthesia	52
	Project 1: Analysis of dendritic activity subject to the anaesthetic action of propofol on GABA _A -receptors	55
	Project 2: Novel population rate-model based on anaesthetic action on single neurons	58

Project 3: Novel population time-coding model based on a single neuron model . . .	60
Project 4: Nonlinear analysis of neural fields subjected to external inputs	62
Project 5: Cortical layer network of neural populations	66
Project 6: Linking neural populations and EEG by an electromagnetic forward solution	67
Project 7: Multivariate analysis of EEG obtained during general anaesthesia	72
Further perspectives	76
Bibliography	77
II Dossier	89
1 Curriculum Vitae	91
2 Supervision of students	95
3 Summary of PhD-project	97
4 List of publications	99

Part I

Research contributions and perspectives

Chapter 1

Introduction

Physiological rhythms are essential in living beings, such as the circadian rhythm (Moore-Ede et al, 1982), which is endogenous and has been found in various biological systems, the heart as single and double circulatory system in various species (Phibbs, 2007), the neural α -rhythm during relaxed wakefulness (Niedermeyer and Lopes da Silva, 2004) in mammals or the sleep cycles (Siegel, 2002) found in many species, from many reptiles and fish to all mammals. Moreover, most neurological disorders are accompanied by rhythmic activity, as observed in epilepsy (Fisher et al, 2005) or observed as motor tremors in Parkinson disease (Deuschl et al, 2001) and multiple sclerosis (Koch et al, 2007). All these rhythms are endogenous, i.e. self-sustained, and not directly induced by external stimuli. Healthy subjects also may exhibit such endogenous neural oscillatory activity, e.g. during mental tasks (Harmony et al, 1996; Michels et al, 2010).

In addition to these input-independent oscillations, stimulus-triggered neural oscillations are always present due to the omnipresence of sensory stimuli in every day's life. For instance, visual flickers may induce visual hallucinations (Billock and Tsou, 2007) of spatial rotations of ~ 1.5 Hz and the smell of an odour induces neural oscillation in the mammalian olfactory bulb (Cenier et al, 2009) in the β - (12 – 20Hz) and γ -band (20 – 60Hz).

A further important effect of external stimuli is the modification of endogenous neural oscillations by external stimuli. In fact, this modification is the most prominent effect since the brain is known to exhibit always-present on-going activity (Sadaghiani et al, 2010; Deco et al, 2011). Since the neural rhythms in neurological disorders are prominent symptoms, one aim in clinical medicine is the removal of such rhythms by stimulation. Recent corresponding experimental techniques have shown successfully the clinical application of electromagnetic brain stimulation, such as the Deep Brain Stimulation (Kringelbach et al, 2007) for the treatment of Parkinson disease and Transcranial Magnetic Stimulation in multiple sclerosis (Cruz-Martinez et al, 2000).

In addition to the external stimulations, drugs also affect neural oscillations and are applied, e.g. in the medical treatment of the multiple sclerosis (Coles et al, 2008) and in general anaesthesia during

surgery (Orser, 2007). In this context, the drugs change the properties of the neurons, their connections to each other and hence their interplay and modify the oscillatory activity in the neuron population. Consequently, the understanding of the drug effects on the neuron elements and how the changed dynamics in single neurons affect the global activity of the neural population is essential for the understanding of the neural rhythms observed and the development of improved drugs.

To give an example, the combination of a drug treatment and the application of external stimuli can be found in everyday hospital practice during operation. General anaesthesia is an indispensable tool during operation and has been optimized during over a century of medical research. Although today's general anaesthesia works well in most cases, it depends strongly on the healthy situation of the patient, the patient's medical history and physical condition such as the body-weight index. In spite of the knowledge of suitable medical procedures for each of such parameter, there are still unknown components such as the body reaction of the patient on certain anaesthetics. Moreover, in about one of thousand cases patients become conscious during operation and even sometimes are able to move, cf. the nice article of Orser (2007). These cases are very dangerous and result from badly adapted anaesthesia procedures for the individual patient. They also originate from the missing understanding of the underlying neural processes during anaesthesia. For instance, during the operation the medical team typically monitors the heart rhythms and/or the EEG of the patient and adapts the anaesthetic drug concentration constantly to control the depth of anaesthesia. Although this procedure is well-established, it is mainly based on the experience of the anaesthetist, while the effect of the drug action on the neural system and so on the EEG or the heart rate is still poorly understood. The improved knowledge on these actions would yield the development of more optimized medical protocols involving novel drugs and novel procedures of their administrations. To achieve this goal, it is necessary to perform model studies linking the microscopic action of drugs on neural receptors to the macroscopic EEG on the scalp. The present work illustrates this link by a set of detailed projects in section 3.3.

Most of the neural oscillations observed experimentally result from the coherent activity of many neurons, i.e. of a neural population. Consequently, to understand the origin of neural oscillations of neural population activity, their response to external stimulations and maybe their sensitivity to drug medication, it is necessary to study in detail

- single neuron activity to understand better the action of drugs to neuron membranes and receptors,
- neural populations to understand how the single neuron activity affects the population activity and how the populations generate the oscillations and
- the measured neural activity to reveal dynamical features and link these to the dynamics of neural populations.

Hence, the understanding of observed neural oscillations stipulates theoretical models that traverse the multiple scales in neural structures. This is the major aim of the present work.

The subsequent chapter illustrates previous basic contributions to the analytical and numerical study of neural populations on a mesoscopic spatial scale. An additional study of experimental data on the macroscopic scale complements the theoretical work. These contributions investigate the neural dynamics on a mesoscopic and a macroscopic scale, while no link is made between the two description levels. Chapter 3 aims to establish this link. At first, it outlines future work on two oscillatory neural systems driven by external stimuli to reveal a general mechanism how external stimuli may modify or generate oscillations and neural populations. Then the subsequent section explains in detail the investigation on the effect of drugs on EEG-oscillations in general anaesthesia. This combination of models for three different neural systems aims to reveal common principles for oscillation generation in the systems and hopefully gives a clear picture on the origin of neural oscillations.

Chapter 2

Contributions

The chapter reports on the previous contributions on the spatio-temporal dynamics in neural fields and the multivariate data analysis of brain signals. The first section introduces the notion of a neural field and its mathematical complexity followed by section 2.2 discussing the linear and nonlinear response to external stimuli. The latter section provides important mathematical tools, which are the basis for the future research described in chapter 3. Finally, the last section presents previously developed data analysis methods and their application to experimental brain signals providing the essential basis for future work on real data.

2.1 Neural Fields and their properties

The studies of neural population activity in theory and experiment have been triggered mainly by the work of Richard Caton (1875) and Hans Berger (1927), who detected as the first electric activity on the animal and human scalp and are supposed to be the founders of EEG (Haas, 2003). This macroscopic activity is measured by electrodes with a size of few centimeters and thus results from the activity of a large number of neurons, i.e. a population of neurons. This population activity can also be measured by other techniques, such as non-invasive magnetoencephalography (Cohen, 1972) or the invasive dye-imaging techniques (Baker et al, 2005). In cognitive experiments, detailed investigations of the measured population activity reveal that the neural activity is rather robust towards repetitions of experimental trials in certain time intervals and hence is supposed to reflect specific stages of neural information processing. In other words, research of the last decades indicate that cognitive tasks are processed by the brain on the level of neural populations and not of single neurons (Nunez, 2000; Nunez and Srinivasan, 2006).

The mammalian brain exhibits different sensory brain areas which are responsible for specific functions. For instance, visual stimuli are processed by the visual cortices, which decompose the

incoming signal into different features, such as shape, color or orientation. The sensory areas represent large neural populations and exhibit physiological sub-structures specific for each area and task. Consequently, the study of neural populations may yield deeper insights into the neural information processing. To investigate the neural information flow theoretically, it is essential to consider a population model taking into account both the physiological properties of single neurons and their interactions. Since the physiological topology of real neuronal networks is rather unknown, difficult to extract and very complex, it is reasonable to focus on an abstract model. The current work studies a neural field model that considers neural populations on a mesoscopic spatial level on a typical spatial scale of hundreds of micrometers. Such a mesoscopic model permits to bridge the various spatial scales in the brain, from the microscopic scale of single neurons at a scale $\sim 10\mu\text{m}$ to the macroscopic scale of centimeters, i.e. the size of scalp electrodes.

A good mesoscopic model has to simplify microscopic properties of neurons, but takes into account their major features (Hutt, 2009). Moreover, it has to consider physiological features to represent a good model for macroscopic activity. The choice of these features depends on the experiments to be modelled. For instance, macroscopic EEG is considered to be independent of the time between spikes of single neurons, but rather depends on the mean population firing rate in a short interval (Nunez, 2000; Nunez and Srinivasan, 2006; Hutt and Atay, 2005; Wright and Kydd, 1992). Hence, it is sufficient to consider mean population firing rates and neglect inter-spike intervals of single neurons. Moreover, neural fields do not consider explicitly the spatially extended dendritic branches, the spatial distribution of single synapses on the branch and their dynamics in space and time, but just assumes an effective temporal response function. This simplification is a strong approximation but which can be relaxed, see e.g. the work of Coombes et al (2003). In addition, some versions of neural fields, e.g. the one considered below, consider the spatial topography of axonal connections and allow the study of quite general spatial interactions.

The subsequent section derives briefly the evolution equation of an integral neural field model, followed by the motivation to include axonal transmission delays. Then section 2.1.3 shows the relation of the integral model to partial differential equation models. Finally the last section discusses the numerical simulation of the integral model in one and two spatial dimensions.

2.1.1 Derivation of the basic evolution equation

The neural field model considers the neural population as a recurrent network of densely packed neurons and assumes small spatial patches of a diameter of few millimeters, see the original work of (Wilson and Cowan, 1972). These patches are motivated by experimental findings of macroscopic functional units in primary sensory areas, such as visual cortex or auditory cortex, that have a columnar structure. Such patches are called macro-columns or neuronal pools and represent ensembles of interacting neurons, which evolve coherently over time.

More detailed, the model may be seen as a recurrent network with weighted axonal connections

from all nodes to all other nodes and it neglects the spatial extension of dendrites. The chemical synapses on dendrites generate evoked postsynaptic potentials (PSP) according to $V(t) = h(t)H(t)$ with

$$h_1(t) = \frac{1}{\tau_s} e^{-t/\tau_s} H(t) \quad \text{or} \quad h_2(t) = \frac{1}{\tau_2 - \tau_1} \left(e^{-t/\tau_1} - e^{-t/\tau_2} \right) H(t) \quad (2.1)$$

and the Heaviside function $H(t)$. According to this approach, the response functions of single synapses on an incoming spike represents a good approximation for the synaptic response in the neural populations Freeman (1975). The spatial distribution of synapses, their corresponding propagation delays on the dendritic tree and their different time scales are lumped in this effective formulation.

The effective membrane potential at the soma in single neurons is a sum of PSPs propagated along the dendritic tree and finds its equivalent in neural populations. It is called \bar{V} in the following and represents the average effective membrane potential in the population, while the average is taken over the small spatial patch and a short time window of few milliseconds. Recall that the neuron generates an action potential (AP), i.e. a propagating spike, when its effective membrane potential exceeds the spike threshold of the neuron. In an ensemble of neurons, there is a distribution of firing thresholds and the average firing activity is computed as the weighted integral over this firing threshold distribution Hutt and Atay (2005); Amit (1989). Since the typical distribution of firing thresholds is unimodal, i.e. has a single maximum, the average firing activity has a sigmoidal shape Hutt and Atay (2005); Amit (1989)

$$f(x,t) = S_m S(\bar{V}(x,t))$$

with the sigmoid function S and the maximum population firing rate S_m . Since S transfers membrane potentials to firing rates, S is also called the transfer function and may be modeled by the logistic function $S(\bar{V}) = 1/(1 + \exp(-d(\bar{V} - \bar{V}_{th})))$ with the mean firing threshold \bar{V}_{th} and the constant d which is related to the variance of the underlying threshold distribution.

To close the circle of model elements, let us consider the axonal connections between neurons which link the neuron somata to dendritic structures of terminal neurons at distant spatial locations. By virtue of the short- and long-ranged axonal connections in neural systems, the corresponding spatial interactions are nonlocal in space. The neural field model under study considers the probability density of axonal connections between spatial patches, i.e. between two spatial locations x and y . Hence, the population firing rate activity \bar{P} that arrives at synapses before they are converted to PSPs read

$$\bar{P}(x,t) = \alpha \int_{\Omega} K(x,y) f[\bar{V}(y,t)] dy \quad (2.2)$$

where Ω denotes the spatial domain of the field, α is the global synaptic gain and the kernel $K(x,y)$ denotes the probability density of axonal connections from neurons at spatial location y to synapses

at x . Moreover the model (2.2) assume a single neuron type, e.g. pyramidal cell or interneuron, and considers a constant transfer function f over the space.

Moreover, in some brain areas (Hellwig, 2000) it is reasonable to assume that the probability density of axonal connections is identical at each spatial location and, hence, the connection probability density just depends on the distance between two spatial locations. Considering this homogeneity assumption and all elements described above, the evolution of the average effective membrane potential in the population obeys

$$\hat{L}\bar{V}(x,t) = \alpha \int_{\Omega} K(d(x,y))S[\bar{V}(y,t)] dy + I(x,t) \quad (2.3)$$

with the distance function $d(x,y) = |x - y|$ and the temporal differential operator $\hat{L} = \hat{L}(\partial/\partial t)$. For instance, we find

$$\hat{L} = \tau_s \partial/\partial t + 1 \quad \text{and} \quad \hat{L} = \tau_1 \tau_2 \partial^2/\partial t^2 + (\tau_1 + \tau_2) \partial/\partial t + 1$$

for the synaptic response functions h_1 and h_2 in (2.1), respectively. In addition Eq. (2.4) considers an external input $I(x,t)$ which may represent an external stimulation or may reflect neural activity originating from other neural populations.

2.1.2 Axonal transmission delay

The model (2.3) considers axonal spatial connections, which are instantaneous in time. However, it takes the time d/c for a spike to travel from one location to another at distance d due to the finite transmission speed c along axonal fibres. Consequently, the transmission along axons deserves some more attention.

Axons are fibres and may be observed in bundles, i.e. a pack of parallel axonal fibers, or as tree-like axonal branches showing a rather random structure. Moreover, axons may be wrapped by neuroglia cells which maintain the neurons in a mechanical stable condition, see Fig. 2.1. Some neuroglia cells form the so-called myelin sheath around the fibres. These cells are called oligodendrocytes in the central nervous system and Schwann cells in the peripheral nervous system. The myelin sheath is built by the neuroglia cells and covers the axons while leaving gaps, the so-called nodes of Ranvier. It represents several layers of lipids and proteins and affects the signal propagation along axons: the thicker the myelin sheath the faster the spike propagation in the axon. Interestingly, axonal connections in a single brain area, i.e. short-range intra-area connections, are not myelinated whereas most long axonal connections between brain areas are myelinated. This difference in the myelination level results to different axonal conduction speeds in intra- and inter-area connections. Moreover it is important to note that the resulting interaction delay between neurons may be similar in both intra-area and inter-area connections due to the different spatial length of the axons though the axonal speeds are different. For instance, intra-area connections exhibit conduction speeds of about 0.1 – 1m/s while inter-area connections show conduction speeds of about 1 – 10m/s and

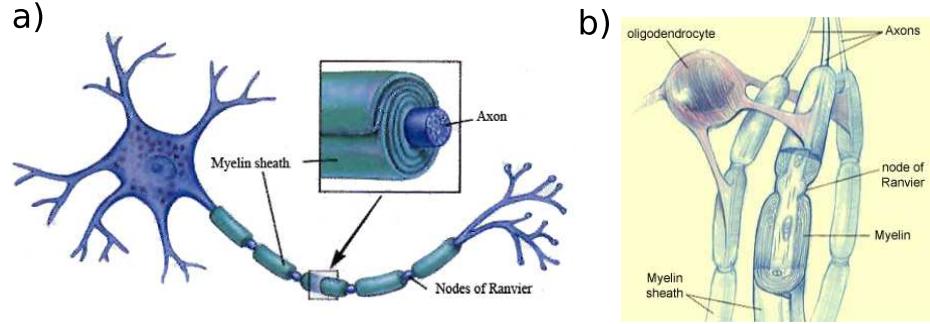


Figure 2.1: Myelination of axonal fibres. a) The myelin sheath wraps around the axon in regular sections, but leaves small gaps unwrapped. These gaps are called nodes of Ranvier. b) The myelin sheath is built by oligodendrocytes, which are neuroglia cells and stabilize the axonal fibre.

rarely up to 100m/s. Assuming the reasonable axonal lengths of $500\mu\text{m}$ and 5mm in intra-area and inter-area connections, respectively, the corresponding interaction delay is 5ms in both axonal connection types (Braitenberg and Schütz, 1998; Koch, 1999). This delay is similar to the time scales of chemical synapses indicating a considerable effect of axonal delays on the dynamics of neural networks.

Moreover, there are various types of delayed axonal connections in the brain. Figure 2.2 illustrates two major cases. The intra-area connections represent a spatial distribution of axonal fibres whose delays are proportional to the distance $|x - y|$ between two spatial locations x and y in the spatial area under study. Such transmission delays are natural in spatial systems, and they are also called propagation delays since the interaction between two elements takes a certain time proportional to their distance. In contrast, the feedback connections exhibit a spatial distribution of connections between two spatial locations, while the corresponding delay is constant. For instance, delayed feedback loops from the cortex via the thalamus may be modeled by such connections while neglecting the thalamus dynamics.

Summarizing, the transmission delays depend on the distance $|x - y|$ between spatial locations x and y and is given by $|x - y|/c$ for transmission speeds c while the feedback delay is constant, say τ . In the presence of a single axonal transmission speed and a single feedback delay, the evolution equation is extended to (Atay and Hutt, 2005; Hutt et al, 2003a)

$$\begin{aligned} \hat{L}\bar{V}(x,t) = & \alpha \int_{\Omega} K(d(x,y))S\left[\bar{V}\left(y,t - \frac{d(x,y)}{c}\right)\right] dy \\ & \beta \int_{\Omega} F(d(x,y))S[\bar{V}(y,t - \tau)] dy + I(x,t). \end{aligned} \quad (2.4)$$

Here, $F(x)$ is the probability density of feedback connections and β is the global synaptic gain of such connections.

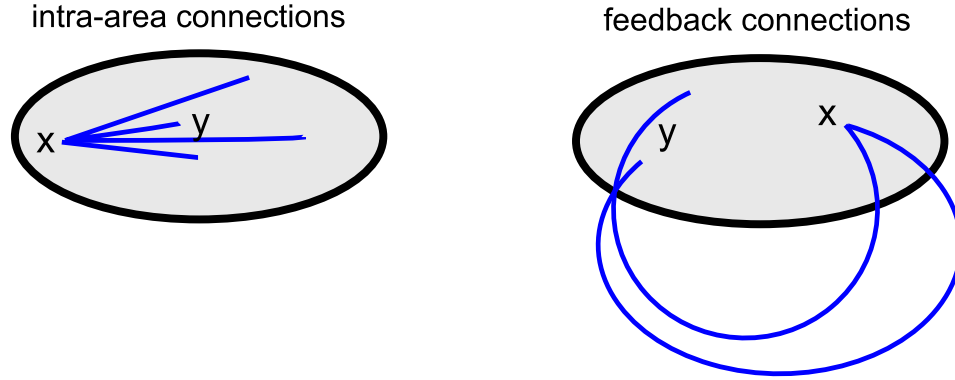


Figure 2.2: Illustration of two connection topologies under study.

Most studies of equations of the type (2.4) consider a one-dimensional spatial domain implying periodic boundary conditions, i.e. the domain is a circle. Such boundary conditions stipulate the periodicity of spatial distances and, hence, the kernel function $K(x-y)$. More specifically let $L = |\Omega|$ be the length of the circle, then the distance $d(x,y)$ between two points x, y on the circle is not unique and may be larger or smaller than $L/2$. Since periodic boundary conditions are reasonable in abstract models only, such as in models of visual orientation tuning (Somers et al, 1995; Wennekers, 2001), it is necessary to define the distance function $d(x,y)$ additionally. It is reasonable to assume the shortest distance between two points and hence the distance function reads $d(x,y) = L/2 - |L/2 - |x-y||$ according to rules in circular statistics (Mardia and Jupp, 1999).

Moreover, there is experimental evidence, that the transmission speed and the feedback delays obeys a distribution (Girard et al, 2001; Bringuier et al, 1999). Then the evolution equation of the neural population is of the type

$$\begin{aligned} \hat{L}\bar{V}(x,t) &= \alpha \int_0^\infty g(c) \int_\Omega K(x-y) S \left[\bar{V} \left(y, t - \frac{|x-y|}{c} \right) \right] dy dc \\ &\quad + \beta \int_0^\infty f(\tau) \int_\Omega F(x-y) S[\bar{V}(y, t - \tau)] dy d\tau + I(x,t). \end{aligned} \quad (2.5)$$

with the distribution functions $g(c)$ and $f(\tau)$ of the axonal transmission speed and the feedback delays, respectively (Hutt and Atay, 2006; Atay and Hutt, 2006).

2.1.3 Relation to partial differential equations

The spatial interactions in neural populations based on the axonal branching system is non-local in nature, i.e. the probability of connections may be larger at distant locations than at closer locations. Such so-called patchy connections are found e.g. in certain layers in the human Bressloff (2001); Swindale (1996) and monkey visual cortex (Horton and Hubel, 1981; Lund et al, 2003) and monkey

prefrontal cortex (Levitt et al, 1993; Gutkin et al, 2000). Moreover, other cortical layers may exhibit more local connections, where the largest probability of connections is at close locations (Hellwig, 2000). The integral differential equation (IDE), i. e. Eq. (2.3) or (2.5), considers both local and global topographies naturally by the corresponding choice of the kernels. In recent years, equivalent formulations in terms of partial differential equations (PDE) have attracted much attention (Coombes et al, 2007; Liley et al, 1999; Coombes, 2010; Laing and Troy, 2003; Owen et al, 2007). To illustrate the bridge between the two model types, let us assume a one-dimensional infinite spatial domain and re-write the integral term as (Hutt, 2007; Hutt and Atay, 2005)

$$\int_{-\infty}^{\infty} K(x-y)S[V(y)] dy = \sum_{n=1}^{\infty} \frac{(-1)^n}{n!} K_n \frac{\partial^n}{\partial x^n} S[V(x)] \quad (2.6)$$

with the kernel moments

$$K_n = \int_{-\infty}^{\infty} x^n K(x) dx .$$

For instance, let us assume a symmetric exponential decreasing probability density function of axonal connections $K(x) = \exp(-|x|/\sigma)$, as has been found experimentally (Hellwig, 2000). Here σ represents the spatial range. Then the density function enjoys the moments $K_n = n!\sigma^n, n$ even, and $K_n = 0, n$ odd. Assuming a linear transfer function for simplicity $S[V(x)] = V(x)$ in addition, the integral in Eq. (2.6) reads (Hutt, 2007; Hutt and Atay, 2005)

$$\begin{aligned} \int_{-\infty}^{\infty} K(x-y)V(y) dy &= \sum_{n=1}^{\infty} \sigma^{2n} \frac{\partial^{2n}}{\partial x^{2n}} V(x) \\ &\approx V(x) + \sigma^2 \frac{\partial^2 V(x)}{\partial x^2}. \end{aligned}$$

In the last step, the infinite series has been truncated after the second term, which is a valid approximation for small interaction ranges σ , see (Hutt, 2007) for a more general discussion. We observe that the integral includes a diffusion term for a short spatial interactions.

More generally, PDEs represent inverted IDEs in the sense that the differential operator in the PDE is the inverse of the integral operator in the IDE (Coombes et al, 2007), i.e.

$$\begin{aligned} U(x) &= \int_{-\infty}^{\infty} K(x-y)S[V(y)] dy = \hat{I}S[V(x)] \\ \leftrightarrow \hat{I}^{-1}U(x) &= \hat{\mathcal{D}}U(x) = S[V(x)] \end{aligned}$$

with the partial derivative operator $\hat{\mathcal{D}} = \hat{\mathcal{D}}(\frac{\partial}{\partial x})$. Although this is a strong relation between the IDE and the PDE, it is important to point out that the inverse $\hat{I}^{-1} = \hat{\mathcal{D}}$ does not exist for all spatial kernels $K(x,y)$. Since the spatial kernel is easy to choose for all axonal topologies, the IDE formulation appears a natural model choice and exists for all spatial kernels. The sections below show several properties of the IDEs and illustrate analytical tools to extract dynamical features of this integral model.

2.1.4 Numerical simulation of IDEs

After having introduced the evolution equation and its relation to more general neural field models, it is necessary to discuss the numerical simulation of the IDE (2.4). Some numerical studies of the neural field PDE-model have applied the standard scheme for numerical simulations of PDEs (Coombes et al, 2007), while the numerical integration scheme for the IDE is much more complex, especially in higher dimensions. This complexity results mainly from the numerical effort to store the memory of delayed activity at each spatial location. This storage is memory intensive, especially if a good spatial resolution is requested. Moreover, numerical methods for PDEs assume a spatial grid and consider few neighbours at each spatial element, while the IDE-methods have to take into account all elements on the grid. Hence the numerical computation of spatial interactions is more time-consuming in IDEs than in PDEs.

To attack this problem, few numerical schemes exist for the transmission delay case. Since the numerical computation of the space integral deserves most attention, the subsequent paragraphs discuss computation schemes of the integral. All described methods assume periodic boundary conditions and consider an explicit numerical scheme for the time integration of the evolution equation, such as the Euler-forward scheme or the Runge-Kutta scheme of fourth order.

At first, let us discuss the integration schemes in one spatial dimension on a regular spatial grid with number of intervals N . All methods store the delayed field activity up to a maximum delay of L/c .

1. The simplest approach is the rectangular summing rule (Atay and Hutt, 2005). The error of this sum is proportional to the second derivative of the integrand and $(L/N)^2$. Hence the integral is well approximated for a large number of intervals N , smooth activity $V(x,t)$ and smooth kernels $K(x)$. This method fails in the presence of highly irregular activity, such as noise.
2. A more advanced algorithm divides the integration region into subintervals, and on each iteration the subinterval with the largest estimated error is bisected. Each interval is integrated according to the 61-point GaussKronrod rules (Hutt and Atay, 2005) considering the suitable stored delay terms. It improves the computation of irregular activity compared to the rectangular rule.
3. Another method takes into account the boundary conditions specifically. To this end, the discussion of periodic boundary conditions in sub-section 2.1.2 allows to write the integral in

Eq. (2.4) as (Hutt et al, 2003a)

$$\begin{aligned} & \int_{\Omega} K(d(x,y))S\left[V(y,t - \frac{d(x,y)}{c})\right] dy \\ &= \int_0^L (A(x-y,t-y/c) + A(x+y,t-y/c))K(u) du \\ &= \int_0^L G(x,y,t)K(y) dy \end{aligned} \tag{2.7}$$

(2.8)

with the functional $A(x,t) = S[V(x,t)]$. Introducing a regular spatial discretization with $y_n = n\Delta y$, $n = 1, \dots, N$ and large N , $G(x,y,t)$ approximates to

$$G(x,y,t) \approx G(x,y_n,t) + \frac{G(x,y_{n+1},t) - G(x,y_n,t)}{\Delta y}(y - y_n), \quad y_n \leq y \leq y_{n+1}.$$

Inserting this result into (2.7) yields a good approximation scheme for smooth field functionals $A(x,t)$.

4. More advanced integration rules take into account the kernel properties. The VEGAS algorithm is a Monte-Carlo integration algorithm in combination with importance sampling (Lepage, 1978; Gough, 2003). The algorithm samples points from a probability function to be integrated, i.e. the integrand in our problem. Hence the sample points are concentrated in the regions that make the largest contribution to the integral. In the simulations, a certain number of sampling calls are applied for a single Monte-Carlo integration, which is repeated several times. Essentially the average of the gained results is considered Atay and Hutt (2006). This method is much more accurate than the latter ones and less sensitive to irregular activity.

To extend the study of neural fields to two spatial dimensions, one may implement some of the previous methods in two spatial dimensions, see e.g. the work of Faye and Faugeras (2010). However, such methods are not numerically efficient. The additional difficulty in two dimensions compared to one spatial dimension results from the larger number of calculations N^4 in methods 1, 2 and 3 compared to the number of computations N^2 in 1D and the much larger number of necessary samples in method 4. To cope with this problem, one may take a close look onto Eq. (2.4) and recognizes that the integral is a convolution for an infinite transmission speed c . Since convolutions may be treated efficiently in numerics, e.g. by the application of a Fast Fourier Transform, it is desirable to re-write the integral in a convolution form. In fact, this can be done according to (Hutt and Rougier, 2010)

$$\begin{aligned} & \int_{\Omega} K(|\mathbf{x} - \mathbf{y}|)S\left[V\left(\mathbf{y}, t - \frac{|\mathbf{x} - \mathbf{y}|}{c}\right)\right] d^2y \\ &= \int_{\Omega} \int_0^{\tau_{max}} L(|\mathbf{x} - \mathbf{y}|, t - \tau)S[V(\mathbf{y}, \tau)] d\tau d^2y, \end{aligned} \tag{2.9}$$

where Ω denotes the two-dimensional domain, τ_{max} represents the maximum delay in the field and the new space-time kernel L is defined as $L(\mathbf{x}, t) = K(\mathbf{x})\delta(|\mathbf{x}|/c - \tau)$ with the delta-distribution $\delta(\cdot)$. The double integral in Eq. (2.9) is a convolution in space and an integral in time both connected by the space-time kernel L . Figure 2.3 illustrates that L represents a superposition of delay rings and each ring has the radius $c\tau$. The re-formulation of the integral as a

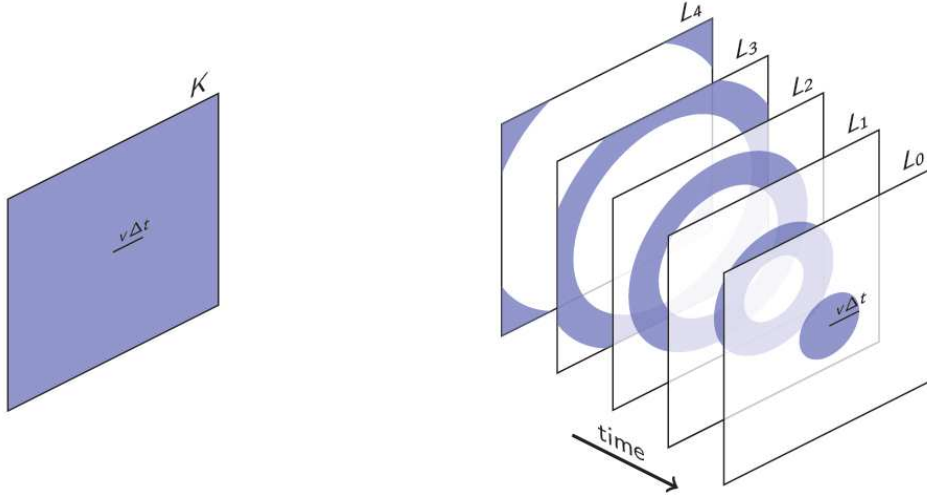


Figure 2.3: Illustration of the space-time kernel $L(\mathbf{x}, t)$ introduced in Eq. (2.9). For a certain kernel function K (left panel), L exhibit rings of radius $v\tau$ if v is the transmission speed. The kernel function L is a linear superposition of such rings. Figure is provided by N. Rougier.

convolution according to (2.9) allows to implement numerically a Fast Fourier Transform and speeds up the computation dramatically. An equivalent method has been mentioned briefly in the work of Coombes et al (2003) and Venkov (2009) for one-dimensional neural fields. Figure 2.4 shows the response of a two-dimensional neural field involving transmission delays to a local stimulus.

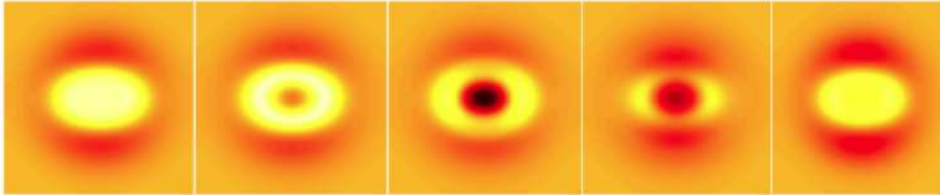


Figure 2.4: Breathers in two dimensions evoked by an anisotropic local input in the presence of a finite transmission speed (Hutt and Rougier, 2010).

Synchronous and asynchronous computation

The numerical methods above are explicit in time and are synchronous in space in the sense that the update of *each* spatial element x_i at a certain time point t_k is based on the other elements in the field x_j at the same time point. Moreover, most neural field studies aim to compute numerical solutions to compare their results to analytical solutions or choose an optimal numerical algorithm to ensure the accordance of numerical results to solutions of the equation under study.

In contrast to such synchronous methods, one may update a *single* element x_i chosen randomly at time t_k considering the other elements x_j and then proceed to the next update. This procedure is well-known in the theory of cellular automata (Fates, 2008), in computational biology (Stark and Hughes, 2000) and ecology (Dieckmann et al, 2000). Moreover, the asynchronous procedure knows two variants: (i) either all elements are chosen randomly from the spatial domain without choosing an element twice or (ii) the choice of elements is unrestricted (Rougier and Hutt, 2010; Taouali et al, 2009). The first method variant (i) is called asynchronous uniform and the latter asynchronous non-uniform. In two studies (Rougier and Hutt, 2010; Taouali et al, 2009), we find that the asynchronous computation scheme introduces random fluctuations to the system and, hence, yields spatio-temporal phenomena different to synchronous effects. For instance, in synchronous computation identical stimulus bumps at different spatial locations induce two activity bumps in neural fields, while the asynchronous method may result to an activity bump at a single location (Rougier and Hutt, 2010) subjected to the time discretization step. Moreover the stability condition of fixed points is identical to the condition in synchronous computation and reducing the time discretization step let the asynchronous computation approach the synchronous computation. Consequently, asynchronous computation represents a random variant of numerical algorithms.

2.2 Linear response theory in neural fields

After introducing neural fields in the previous section, this section presents analytical and numerical results on neural fields involving transmission delay and/or feedback delay. The methods applied represent basic analytical tools to study other similar or more complex networks. At first, stationary solutions and their linear stability are studied revealing various types of emerging spatio-temporal patterns at the stability threshold. Then the following paragraphs discuss more generally the linear response theory in neural fields. Finally, two applications to real neural systems illustrate the power of the analytical tools.

The following sections consider a single transmission speed and a single feedback delay only, but most analytical studies have been done for distributed transmission speeds and distributed delays as well. This focus on the non-distributed case is reasonable since the speed and delay distributions do not introduce effects different to the ones found for single speed and delay. Moreover, all studies assume a one-dimensional spatial domain Ω and periodic boundary conditions and the distance

function is $d(x, y) = |x - y|$ which represents the shortest distance between two points, cf. subsection 2.1.2.

2.2.1 The stationary state and its stability in the absence of noise

For constant external inputs $I(x, t) = I_0$, Eq.(2.4) has a constant stationary state V_0 determined by the implicit equation $L(0)V_0 = (\alpha + \beta)S(V_0) + I_0$, cf. (Hutt and Atay, 2005). Hence the stationary state depends on the external input I_0 which may serve as the control parameter of the system.

Considering small deviations $u(x, t) = \tilde{V}(x, t) - V_0$ from the stationary state, the linear evolution equation reads

$$\begin{aligned} \hat{L}u(x, t) &= s' \alpha \int_{\Omega} K(|x - y|) u \left(y, t - \frac{|x - y|}{c} \right) dy \\ &\quad s' \beta \int_{\Omega} F(|x - y|) u(y, t - \tau) dy. \end{aligned} \quad (2.10)$$

with the nonlinear gain $s' = \delta S[V] / \delta V, V = V_0$.

Transmission delay is equivalent to distributed delays

An equivalent expression to (2.10) may be achieved by the spatial Fourier transform of $u(x, t)$ leading to an equation of the type

$$\hat{L}\tilde{u}(k, t) = \int_0^{\infty} n(k, \tau') \tilde{u}(k, t - \tau') d\tau' + m(k) \tilde{u}(k, t - \tau). \quad (2.11)$$

with the Fourier transform $\tilde{u}(k, t)$ of $u(x, t)$, the time-dependent kernel function $n(k, t)$ and the time-independent function $m(k)$ which are proportional to the Fourier transforms of the corresponding kernels. Equation (2.11) reveals that transmission delays in location space are equivalent to distributed delays in Fourier space, while the delay distribution is defined by the wavenumber and the spatial kernel K (Hutt and Frank, 2005; Hutt and Atay, 2007). In contrast, feedback delays remain unchanged.

The wave ansatz $u(x, t) = u_0 e^{ikx + \lambda t}$ with wavenumber $k \in \mathcal{R}$ and Lyapunov exponent λ inserted into (2.10) yields an implicit characteristic equation (Hutt and Atay, 2005; Atay and Hutt, 2005; Hutt and Atay, 2006; Atay and Hutt, 2006; Hutt, 2007, 2008b; Hutt and Atay, 2007; Hutt and Frank, 2005) of the type

$$L(\lambda) = s' \int_{\Omega} \alpha K(z) e^{-ikz - \lambda|z|/c} + \beta F(z) e^{-ikz - \lambda\tau} dz. \quad (2.12)$$

for general spatial homogeneous kernels K and F . Here again the transmission delay contribution is $|z/c|$, i.e. space-dependent, while the feedback delay τ remains unchanged.

Asymptotic stability for general transmission speeds and delays

The system loses stability if $Re(\lambda) = 0$. For instance, $\lambda = i\omega$, $\omega \neq 0$ reflects an oscillatory instability which does not emerge under certain conditions. Assuming distributed transmission speeds, then the mean transmission delay reads

$$\tau_p = \underbrace{\int_0^\infty \frac{g(c)}{c} dc}_{1/\bar{c}} \underbrace{\int_\Omega |xK(x)| dx}_\xi$$

with the mean inverse of the transmission speed $1/\bar{c}$ and the mean interaction range ξ . Then the following theorem holds:

Theorem 1. *Suppose that the synaptic response function is bi-exponential and hence $L(\lambda) = \lambda^2 + \gamma\lambda + \rho$, $\gamma, \rho > 0$. If*

$$\alpha\tau_p + \beta \int_0^\infty \tau f(\tau) d\tau < \gamma,$$

then Eq. (2.10) does not have oscillatory solutions of the type $u(x, t) = u_0 \exp(i\omega t + ikx)$.

See (Hutt and Atay, 2006) for the proof.

The importance of kernel Fourier moments for the instability threshold

For large transmission speeds and small feedback delays, this characteristic equation may be approximated to (Atay and Hutt, 2006)

$$L(\lambda) = s' \sum_{n=0}^N \frac{(-1)^n \lambda^n}{n!} \left(\frac{1}{c^n} \hat{K}_n(k) + \tau^n \hat{F}(k) \right) \quad (2.13)$$

with the kernel Fourier moments

$$\hat{K}_n(k) = \int_\Omega |x|^n K(x) e^{-ikx} dx \quad (2.14)$$

introduced first in (Atay and Hutt, 2005). Since the kernels represent probability density functions, $\hat{K}_n(0)$ for n even are the statistical moments of order n of the spatial interaction characterizing the axonal spatial spread. Moreover, $\hat{K}_0(k)$ is the spatial Fourier transform. The term $\hat{F}(k)$ is the Fourier transform of the feedback kernel $F(x)$. For distributed transmission speeds and delays, the corresponding characteristic equation resembles Eq. (2.13) by replacing $1/c^n$ by $\int g(c)/c^n dc$ and τ^n by $\int f(\tau) \tau^n d\tau$.

To gain some more insight into the stability and the possible types of instabilities at the stability threshold, let us consider the case $N = 2$. Then one distinguishes the case of stationary instabilities with $\lambda = 0$, such as spatially-periodic non-oscillating patterns, and oscillatory instabilities with $\lambda =$

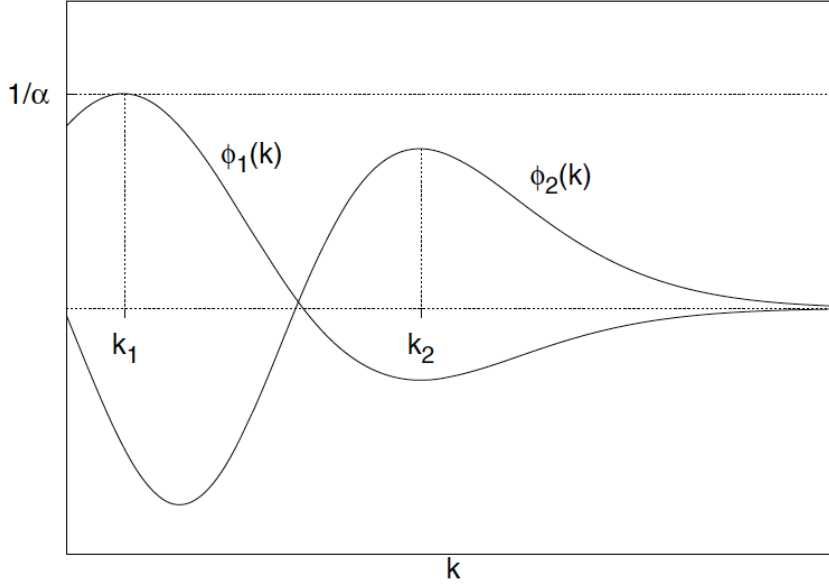


Figure 2.5: Schematic diagram of the competition between stationary and oscillatory bifurcations for vanishing feedback. The curves $\phi_1(k) = s' \hat{K}_0(k)/\rho$ and $\phi_2(k) = -s' \hat{K}_1(k)/\gamma c$ are motivated in the text. As the bifurcation parameter α is increased from zero, the horizontal line $1/\alpha$ becomes tangent to one of the curves. The tangency with ϕ_1 is equivalent to a stationary bifurcation, while the tangency with ϕ_2 is equivalent to an oscillatory bifurcation. Since these tangencies depend only on the maxima of the curves, located at the wave numbers k_1 and k_2 , respectively, the type of bifurcation is determined by the maximum between $\phi_1(k_1)$ and $\phi_2(k_2)$, see the work of Atay and Hutt (2006) for more details.

$i\omega$ and angle frequency ω , e.g. traveling and standing waves. Assuming a bi-exponential synaptic response function of the type h_2 in Eq. (2.1), the polynomial $L(\lambda)$ is of the type $\lambda^2 + \gamma\lambda + \rho$ with constants $\gamma, \rho > 0$ and the corresponding instability criteria read

$$\begin{aligned} \rho/s' &= \alpha \hat{K}_0(k_c) + \beta \hat{F}(k_c) && \text{(stationary instability)} \\ \gamma/s' &= -\frac{\alpha}{c} \hat{K}_1(k_c) - \beta \tau \hat{F}(k_c) && \text{(oscillatory instability)}. \end{aligned}$$

Figure 2.5 illustrates the criterion in the absence of feedback, i.e. $\beta = 0$: the instability with the largest maximum value is selected first while increasing the synaptic gain s' . This is a rule-of-thumb for spatio-temporal instabilities (Atay and Hutt, 2005, 2006). Since s' depends strongly on the external stimulus I_0 , the change of the external stimulus, e.g. an externally injected current, may evoke spatio-temporal instabilities.

2.2.2 The stability in the presence of external stimuli

Now let us discuss the effect of random fluctuations on the dynamics of neural populations. Several previous studies showed that randomness may be beneficial to the information processing in the brain (Masuda et al, 2007; Doiron et al, 2003; Longtin et al, 1991; Destexhe and Contreras, 2006). The origin of spontaneous fluctuations in the living brain, i.e. fluctuations unrelated to external stimuli, is poorly understood though there is evidence for stochastic ion channel dynamics in the cell membrane and spontaneous activity failure in synapses Koch (1999). The latter two examples of fluctuations represent random changes of neuron properties over space and time. Since most of these properties are formulated mathematically as variables multiplied to the activity variable in the model, the spontaneous random fluctuations yield so-called multiplicative noise. Besides these spontaneous or internal fluctuations one may consider external fluctuations, which may originate from other neural populations or from external stimuli (Masuda et al, 2007; Doiron et al, 2003). The following paragraphs consider the stability of a stationary state involving this type of fluctuations. At first let us neglect delay effects which are discussed in the last paragraphs.

In the previous section 2.2.1, we have determined the stationary state constant in space and time and studied the Lyapunov exponent of the linearized problem about the stationary state. At a first glance this approach does not apply here since the system is time-dependent for all times due to the external random fluctuations. Hence the question arises how one can define a stationary state in this case. At first let us recall the definition of stability. Several definitions of stability exist Kozin (1969), such as asymptotic stability considered in the previous section or the mean-square stability: if the deviation about a system state is $u(x,t)$ and $\langle |u(x,t)|^2 \rangle < \delta$ holds for a $\delta > 0$, then this system state is called mean-square stable. If in addition $\lim_{t \rightarrow \infty} \langle |u(x,t)|^2 \rangle \rightarrow 0$, then the state is called asymptotically mean-square stable. Hence, in simple words, a system state may be called stable if the system evolves in a small neighborhood of this state. Consequently the stable state might be equivalent to the deterministic stable stationary state V_0 and the system evolves in a small neighborhood about V_0 due to the external random fluctuations.

In the beginning let us neglect delays and consider, for simplicity reasons, the single-exponential synaptic response function h_1 in (2.1), i.e. $\hat{L} = \partial/\partial t + 1$ leading to the evolution equation

$$\frac{\partial V(x,t)}{\partial t} = -V(x,t) + \alpha \int_{\Omega} K(x-y) S[V(y,t)] dy + I(x,t). \quad (2.15)$$

In contrast to the previous section, now the external input $I(x,t)$ is the sum of a constant input I_0 and random Gaussian fluctuations $\xi(x,t)$, i.e., $I(x,t) = I_0 + \xi(x,t)$ with $\langle \xi(x,t) \rangle = 0$ where $\langle \cdot \rangle$ denotes the ensemble average. The subsequent paragraphs assume Gaussian-distributed random fluctuations

$$\langle \xi(x,t) \xi(x',t') \rangle = Q \delta(x-x') \delta(t-t') \quad (2.16)$$

which are uncorrelated in space and time and have the variance Q .

Further presuming the fluctuation variance Q being small may yield small deviations from the stationary state $u(x,t) = V(x,t) - V_0 \ll V_0$ and we obtain

$$\frac{\partial u(x,t)}{\partial t} = -u(x,t) + s' \alpha \int_{\Omega} K(x-y)u(y,t) dy + \xi(x,t) \quad (2.17)$$

with $s' = \delta S / \delta V$ computed at $V = V_0$. In the following sections, s' serves as the control parameter.

Theorem 2. *If the Lyapunov exponents $\{\lambda_n\}$ of the deterministic part in equation (2.17), i.e. $\xi(x,t) = 0$, are bounded to the left hand side of the complex axis, i.e. $Re(\lambda_n) < 0 \forall n$, then $\exists \delta > 0$ such that $\langle |u^2(x,t)| \rangle < \delta$ and the stationary state V_0 is mean-square stable.*

See (Hutt, 2010) for the proof.

Now let us consider the presence of transmission delays. The criteria for stability of delayed stochastic systems has been established in previous studies, e.g. by Gushchin and Kuechler (2000). The extension to transmission and feedback delay also holds:

Theorem 3. *The stationary state V_0 of Eq. (2.4) subjected the stochastic input $I(x,t) = I_0 + \xi(x,t)$ is mean-square stable, i.e. $\exists \delta > 0$ such that $\langle |u^2(x,t)| \rangle < \delta$, $u(x,t) = V(x,t) - V_0$, if the Lyapunov exponents $\{\lambda_n\}$ of Eq. (2.10) are bounded to the left complex plane.*

See (Hutt and Atay, 2007; Hutt and Frank, 2005) for the elements of the proof.

We conclude that the linear mean-square stability of small deviations about the (deterministic) stationary state V_0 of Eq. (2.4) in the presence of external additive fluctuations is given by the Lyapunov exponents deretmined from the deterministic case. This result allows to study the characteristics of the small deviations as shown in the next section discussing the linear response. However, further results on the non-linear response (section 2.3.1) elucidates that larger deviations show different characteristics then linear deviations.

2.2.3 General response theory

Considering small deviations $u(x,t)$ about the stationary state V_0 and small external stimuli the linear evolution equation reads

$$\begin{aligned} \frac{\partial u(x,t)}{\partial t} = & -u(x,t) + s' \alpha \int_{\Omega} K(x-y)u\left(y,t - \frac{|x-y|}{c}\right) dy \\ & + s' \beta \int_{\Omega} F(x-y)u(y,t - \tau) dy + \xi(x,t) . \end{aligned} \quad (2.18)$$

By virtue of the finiteness of the domain and the periodic boundary conditions, the membrane potential may be expanded into a discrete Fourier series with the corresponding Fourier projections

$u_n(t) \in \mathcal{C}$, $u_n = u_{-n}$ yielding

$$\frac{d\tilde{u}_m(t)}{dt} = \int_0^\infty N_m(\tau') \tilde{u}_m(t - \tau') d\tau' + M(k) \tilde{u}_m(t - \tau) + \tilde{\xi}_m(t) \quad , \quad -\infty < m < \infty. \quad (2.19)$$

similar to Eq. (2.11) with corresponding kernel functions N, M . The terms $\tilde{\xi}_m$ are proportional to the Fourier transform of the external stimulus $\xi(x, t)$.

Then linear response theory gives the general solution of (2.19) by

$$\tilde{u}_m(t) = \tilde{u}_{m,h}(t) + \int_{-\infty}^\infty dt' G_m(t - t') \tilde{\xi}_m(t'). \quad (2.20)$$

Here $u_{m,h}(t)$ represents the homogeneous solution of (2.19) and $G_m(t)$ is the Greens function of the Fourier mode m . Applying standard techniques in linear response theory finally leads to

$$G_m(t) = \frac{1}{2\pi} \int_{-\infty}^\infty d\omega \frac{e^{-i\omega t}}{-i\omega - \int_0^\infty N_m(\tau') e^{i\omega\tau'} d\tau' - M_m e^{i\omega\tau}}. \quad (2.21)$$

This integrand can be computed, e.g. by the application of the residue theorem as shown in (Hutt and Atay, 2007). The denominator of the integrand is the characteristic equation defining the stability conditions as outlined in section 2.2.1.

The response function

To illustrate the response of the system to an external spatio-temporal stimulation, Figure 2.6 shows the response (2.20) to a block stimulation $\tilde{\xi}_m(t) = H(t) - H(T - t)$ of duration T . Here the system under consideration exhibits a finite axonal transmission speed, non-local intra-area connections and no nonlocal feedback. The response depends on the wave number $k = k_n$ of the spatial Fourier mode n of the external stimuli. The plot shows the systems strongest response to spatially constant inputs ($k = 0$), which decays most slowly, while inputs with larger spatial frequency evoke weaker responses and are damped much faster. The shape of the response curve is fully determined by the kernel Fourier moments defined in section 2.2.1, the finite transmission speed and the synaptic response function (2.1).

The correlation function and power spectrum

The solution of (2.18) reads

$$u(x, t) = \tilde{u}_h(x, t) + \frac{1}{\sqrt{\Omega}} \int_0^t \sum_{n=-\infty}^\infty \sum_{l=1}^{m_n} e^{\lambda_{l,n}(t-t')} \tilde{\xi}_n(t') r_{l,n} e^{ik_n x} dt', \quad (2.22)$$

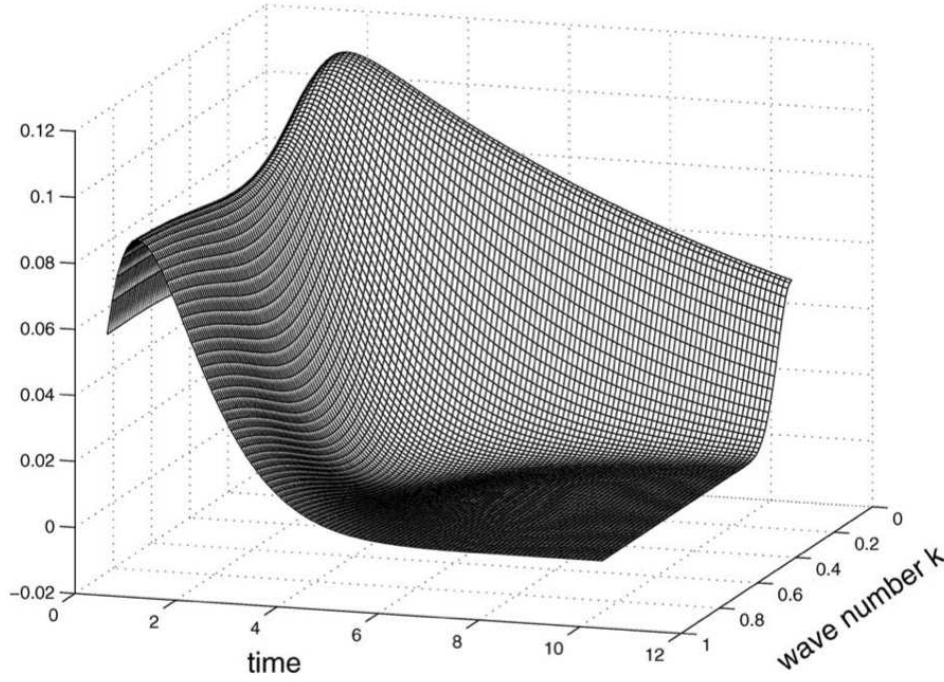


Figure 2.6: An example for the response function (2.20) to an external block stimulus of finite length (Hutt and Atay, 2007).

assuming the initial time $t = 0$, $r_{l,n}(k)$ are constants defined by the residues at the l th root $\Omega_{l,n}$ of the integrand denominator in (2.21), $\lambda_{l,n} = i\Omega_{l,n}$ and m_n is the number of roots of mode n . Now, for simplicity, the external stimulus $\xi(x, t)$ is chosen to Gaussian uncorrelated random fluctuations. Then their Fourier transform are also Gaussian and satisfy $\langle \tilde{\xi}_m(t) \rangle = 0$, $\langle \tilde{\xi}_n^*(t) \tilde{\xi}_m(t') \rangle = Q \delta_{m,n} \delta(t - t')$ with the noise variance Q . This leads to the auto-correlation function $C(x, \tau) = \langle u^*(x, t) u(x, t - \tau) \rangle$ at spatial location x and the corresponding power spectrum $S^2(\nu)$ with frequency ν (Hutt and Frank, 2005):

$$C(x, \tau) = Q \sum_{n=-\infty}^{\infty} \sum_{l=1}^{m_n} P_{nl} e^{\lambda_{l,n}^* |\tau|}, \quad P_{nl} = - \sum_{k=1}^{m_n} \frac{r_{l,n}^* r_{k,n}}{\lambda_{l,n}^* + \lambda_{k,n}}$$

$$S^2(\nu) = \frac{Q}{\sqrt{\pi/2}} \sum_{n=-\infty}^{\infty} \sum_{l=1}^{m_n} P_{nl} \frac{\lambda_{l,n}^*}{\lambda_{l,n}^{*2} + 4\pi^2 \nu^2}$$

These results show that both the auto-correlation function and the power spectrum represent linear superpositions of single contributions, that reflect the responses of single Fourier modes (sum over n) involving several different time scales (sum over l). This is the typical signature of linear responses. The contributions of the Fourier modes are weighted by the factor P_{nl} . In this context, it is interesting

to note that this superposition of time scales facilitates so-called $1/f^\alpha$ -power spectra widely found in spatially-extended systems (Dutta and Horn, 1981). This $1/f^\alpha$ -power behavior has also been found theoretically close to spatio-temporal instability in neural fields (Hutt and Frank, 2005). Moreover, it is interesting to note that at large frequencies $\nu \rightarrow \infty$ the system shows the signature of Brownian motion or, equivalently, normal diffusion with $S^2(\nu) \rightarrow \sum_{n,l} c_{n,l}/\nu^2$ with a constant factor $c_{n,l}$.

The previous sections considered the evolution equation (2.4) to illustrate how to extract information on its spatio-temporal dynamics in principle. The subsequent paragraphs focus on the analytical treatment of neural fields reflecting physiological neural structures and illustrates the application of the methods presented in the previous sections. Since most experimental studies report on measured neural activity by the plot of its power spectrum, the subsequent theoretical studies present theoretical results on the power spectrum of neural field activity. The first example application considers the power spectrum of the membrane potential in weakly-electric fish subjected to spatially-correlated external noise. The subsequent example application shows first results on the stability of stationary solutions in cortical areas during general anesthesia, followed by the power spectrum study of fluctuations about this state reflecting EEG-activity.

2.2.4 Application: Induction of oscillations in certain frequency bands by external stimuli

From experiments, it is known that neural populations oscillate in certain frequency bands dependent on the experimental conditions. Such frequency bands allow a classification of underlying neural processes and permit an interpretation of stages of information processing. Especially, the switches between activated frequency bands have attracted some attention since they might reveal underlying interactions between different neuron populations. For instance, Buonviso et al (2003) showed that the respiratory cycle in rats switches the rhythms in the olfactory system between the β - ($\sim 15\text{Hz}$) and the γ - ($\sim 40\text{Hz}$) band in the presence of odours. This switch may be caused by the different input strength and different input patterns during inhalation and expiration. The underlying mechanism of this switch is unknown.

Another example are frequency activations subjected to external input signals in certain weakly-electric fish, such as the *Apteronotus leptorhynchus*. Such species live in muddy water and emit weak electric waves at their tails. Such waves are received on the skin of the emitting fish and are amplitude modulated by objects in the surrounding. The corresponding electro-receptors on the skin of the fish generate spiking activity sent to the primary sensory area called the electric line lobe (ELL), see (Berman and Maler, 1999). The ELL projects to other neural structures, of which some project back to the ELL with a certain time delay. Previous *in-vivo* studies (Doiron et al, 2003) on the spike activity in the ELL demonstrated that the inter-spike interval distribution of neurons in the ELL depend strongly on the spatial correlation of random fluctuations generated experimentally on the fish skin: while stimulating the skin receptors by spatially uncorrelated noise one observes a 100Hz-

rhythm, while the stimulation by strongly correlated spatial noise adds a firing pattern of a frequency of $\sim 35\text{Hz}$. It was also shown experimentally in the work of Doiron et al (2003), that the induced additional rhythm vanishes after blocking a specific delayed global feedback pathway. Hence, the spatial correlation of external stimulation tunes the oscillation frequencies in the system (Chacron et al, 2005; Masuda et al, 2007; Lindner et al, 2005) by the delayed feedback.

Taking this phenomenon as an example for the induction of frequency bands, the question arises how the spatial range of the feedback from the ELL via other areas correlates to the spatial correlation of the external stimulation and how the feedback delay affect the induced frequency. To this end, a previous work (Hutt et al, 2008b) developed a neural field model involving the intra-area and feedback topology of the primary sensory system to study the power spectrum of neural population activity in the ELL, cf. Fig. 2.7. The spatio-temporal input $I(x,t)$ drives the ELL via excitatory synapses. The ELL projects topologically to the area Np via axonal connections with spatial connectivity kernel $K_{ne}(x)$, and the area Np projects back topologically with the axonal connectivity kernel $K_{en}(x)$. This topology reflects the physiological structure in weakly-electric fish while the topographic connections resemble the concept of receptive fields, e.g. known from the mammalian visual system. The axons from the ELL to the Np terminate at excitatory synapses and the axons from Np to ELL terminate at inhibitory synapses. The axonal delay along the ELL-Np and Np-ELL connection is τ_1 and τ_2 , respectively. Moreover, neurons in the ELL and Np do not exhibit intra-area

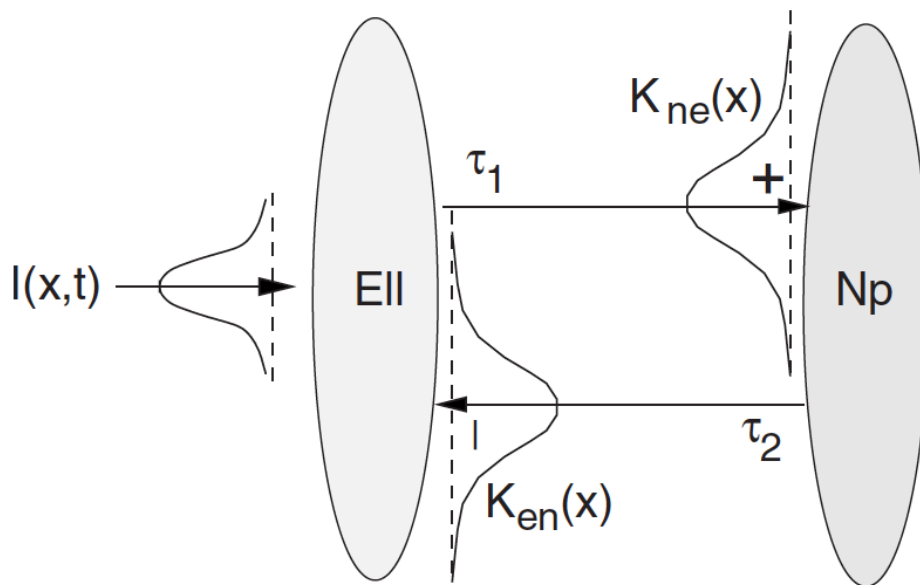


Figure 2.7: Topology of the network of neural fields reflecting the physiological structure of the primary feedback system in weakly-electric fish (Berman and Maler, 1999).

connections, but just communicate indirectly via the axonal feedback. Essentially, the evolution equation of the two neural fields read (Hutt et al, 2008b)

$$\begin{aligned}\tau_{in} \frac{\partial E(x,t)}{\partial t} &= -E(x,t) - g_{in} \int_{\Omega_n} K_{en}(x-y) S_n [N(y,t - \tau_2)] dy + I(x,t) \\ \tau_{ex} \frac{\partial N(x,t)}{\partial t} &= -N(x,t) + g_{ex} \int_{\Omega_e} K_{ne}(x-y) S_e [E(y,t - \tau_1)] dy\end{aligned}\tag{2.23}$$

with the membrane potential in the ELL (E) and the Np (N), the time constants of excitatory and inhibitory synapses τ_{ex} and τ_{in} , resp. Moreover, g_e , g_i are the corresponding synaptic gains and S_e and S_i represent the transfer functions of neurons in the ELL (e) and Np (i), respectively. In addition Ω_e and Ω_i denote the one-dimensional spatial domains of the ELL and the Np, respectively.

After linearization about a stationary state constant in space and time, cf. section 2.2.2, linear deviations about the stationary state may be expressed by the deviations in the ELL $u(x,t)$ which obey the single time-dependent integral-differential equation

$$\hat{L}u(x,t) = -\frac{g}{\tau_{ex}\tau_{in}} \int_{\Omega_e} F(x-y)u(y,t - \tau_d) dy + I(x,t).$$

Here, $g = (\delta S_e / \delta E)(\delta S_n / \delta N)g_{ex}g_{in}$, the total axonal delay is $\tau_d = \tau_1 + \tau_2$, the temporal operator is defined to $\hat{L} = \partial^2 / \partial t^2 + (1/\tau_{ex} + 1/\tau_{in})\partial / \partial t + 1/\tau_{ex}\tau_{in}$ and the effective connectivity kernel reads

$$F(x-y) = \int_{\Omega_n} K_{en}(x-z)K_{ne}(z-y) dz.$$

This effective feedback kernel is the convolution of the receptive field kernels in the system and resembles the effective kernel in optical systems involving several lenses. Finally let us assume spatially correlated random input fluctuations with $\langle I(x,t) \rangle = 0$, $\langle I(x,t)I(y,T) \rangle = Q\delta(t-T)C(x-y)$ with the spatial correlation function $C(x) = \sigma \mathcal{N}(0, \sigma_i^2)$ and the effective feedback kernel $F(z) = \mathcal{N}(0, \sigma_f^2)$, where \mathcal{N} denotes the Gaussian normal distribution. Then the power spectrum reads (Hutt et al, 2008b)

$$S^2(\nu) = Q \int_{-\infty}^{\infty} \frac{\hat{C}_0(l)}{A(\nu) + B(\nu)\hat{F}_0(l) + D\hat{F}_0^2(l)}$$

with the constant D , the functions $A(\nu), B(\nu)$ dependent of the frequency ν and the kernel Fourier moments of 0th order $\hat{C}_0(l)$, $\hat{F}_0(l)$ dependent of the dimensionless wavenumber l (recall the definition of the kernel Fourier moments given in section 2.2.1). The specific choice of $C(x)$ guarantees that the input intensity $\langle I^2(x,t) \rangle$ is independent of the spatial correlation variance σ_i^2 in accordance to the experimental setup in the work of Doiron et al (2003). Explicitly, it is $\hat{F}_0 = \exp(-\eta^2 l^2 / 2)$ implying the relation of the spatial range of the feedback and the input correlation $\eta = \sigma_f / \sigma_i$.

Figure 2.8 shows the power spectrum for two values of η and reveals an induced power peak at about 40Hz for $\eta = 1/40$, i.e. a much larger spatial input correlation than feedback correlation.

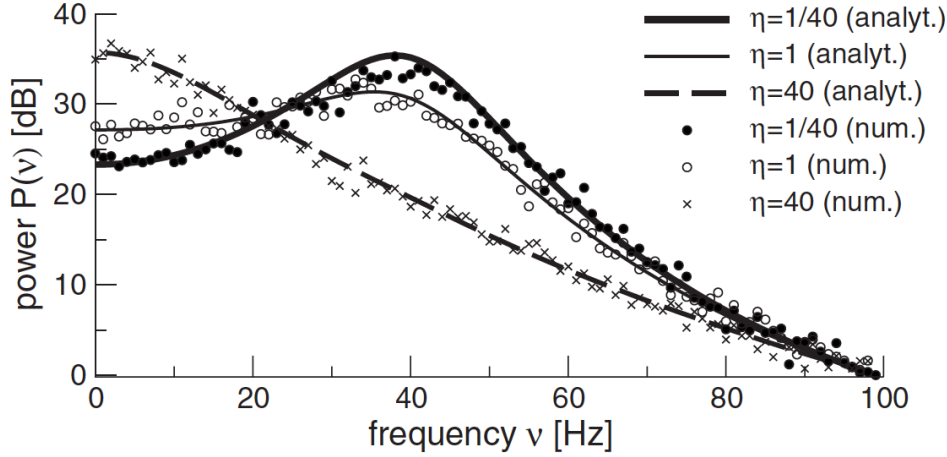


Figure 2.8: Power spectrum $P(\nu) = S^2(\nu)$ of $u(x, t)$ subjected to the parameter η . Taken from (Hutt et al, 2008b).

This result shows good qualitative accordance to the experimental finding in (Doiron et al, 2003). Moreover, it extends previous studies on the effect of spatial correlations in feedback systems, e.g. (Chacron et al, 2005; Masuda et al, 2007; Lindner et al, 2005), by considering the receptive field concept.

To learn more on the underlying mechanism, let us investigate further the borders of the activated frequency band. Detailed analytical calculations reveal, that the power spectrum is split in several frequency bands $\nu_m < (1 + 2m)/4\tau_d < \nu_{m+1}$, $m \in \mathcal{L}_0$ and the borders depend on the effective delay τ_d and the synaptic time constants τ_{ex} , τ_{in} . The frequency bands of activation (deactivation) of oscillations are given by $m = 0, 2, \dots$ ($m = 1, 3, \dots$). Hence, long-range spatial correlations induce oscillation frequencies about $1/4\tau_d$, $5/4\tau_d, \dots$. For instance, assuming the reasonable physiological time delay $\tau_d = 6\text{ms}$, the lowest activated frequency band occurs at $\sim 42\text{Hz}$, i.e. in the γ -frequency band.

The latter findings allow the interpretation, that the external stimulus selects internal oscillation modes present in the feedback system. The selection parameter is the spatial correlation of the noisy input. This activation mechanism is found in much simpler physical systems, like the guitar. There, the strings allow for many oscillation modes and a certain grip and tapping of the strings fixates and activates a certain oscillation mode, i.e. generating the tone. This mechanism may serve as a general model in spatially extended neural feedback systems showing the induction of certain frequency bands subjected to different experimental conditions.

2.2.5 Application: Model for EEG in general anaesthesia

General anaesthesia during surgery is a constant part of everyday hospital practice. It ensures that the patient is immobile during the operation, does not feel any pain during surgery (analgesia), loses consciousness or awareness (hypnosis) and does not remember subconsciously any details (amnesia). To guarantee the emergence of the latter elements, today the anaesthetist controls the state of the patient by observing the brain potential on the scalp of the patient during the surgery, i.e. the EEG. For instance, a prominent EEG-marker of the loss of consciousness is the spectral change of the EEG: the EEG of the aware subject exhibits strong α -activity, i.e. oscillations about 10Hz, whereas the unconscious subject shows a drop of the major frequency in the EEG to the δ - or θ -band, i.e. 2 – 8Hz. For certain anaesthetics, there is even an increase of the most prominent frequency to the β -band, i.e. 12 – 20Hz, while increasing the anaesthetic concentration before the neuronal oscillations drop to the low frequencies. This spectral change is called *biphasic*. Several so-called EEG-monitors have been developed to extract a number from the EEG power spectrum to indicate the state of consciousness of the subject by that index. If the index remains in a certain value range, the surgery proceeds.

Although the spectral properties of the EEG under general anaesthesia is important during surgery, it is poorly understood why the EEG spectrum changes from high frequencies to low frequencies while increasing the anaesthetic concentration. This section proposes a neural field model to explain the EEG power spectrum change with varying anaesthetic concentration.

Several previous studies of neural populations have investigated the effect of anaesthetics on the EEG and most have applied a PDE-model to describe the neural field activity (Steyn-Ross and Steyn-Ross, 1999; Bojak and Liley, 2005; Molaee-Ardekani et al, 2007). A recent work (Hutt and Schimansky-Geier, 2008; Hutt and Longtin, 2009) considered excitatory and inhibitory synapses, pyramidal (excitatory) neurons and interneurons (inhibitory neurons), axonal connections, finite axonal transmission delay and external random input and introduced a system of integral-differential equations

$$\begin{aligned} \hat{L}_e(V_e(x,t) - V_r) = & \\ a_e \int_{\Omega} K_E(x-y) S_E \left[V_e(y, t - \frac{|x-y|}{c}) - V_i(y, t - \frac{|x-y|}{c}) - \Theta_E \right] dy + I(x,t) & \\ & (2.24) \\ \hat{L}_i(p)(V_i(x,t) - V_r) = & \\ a_i f(p) \omega_0^2(p) \int_{\Omega} K_I(x-y) S_I \left[V_e(y, t - \frac{|x-y|}{c}) - V_i(y, t - \frac{|x-y|}{c}) - \Theta_I \right] dy . & \end{aligned}$$

These equations define the spatio-temporal evolution of the post-synaptic potential of excitatory and inhibitory synapses $V_e(x,t)$ and $V_i(x,t)$, respectively. The parameter V_r denotes the resting potential of the neurons and the external $I(x,t)$ represents the random fluctuations from other brain areas. Moreover the parameter p reflects the concentration of the anaesthetics in the neuron population.

Assuming the application of the anaesthetic *propofol*, increasing the anaesthetic concentration, i.e. increasing the value of p (Hutt and Longtin, 2009), increases the decay phase of the synaptic response function h of inhibitory GABAergic synapses, cf. Eq. (2.1). Figure 2.9 illustrates the effect of p on the response function. Moreover, the prologation of the response decay phase affects the

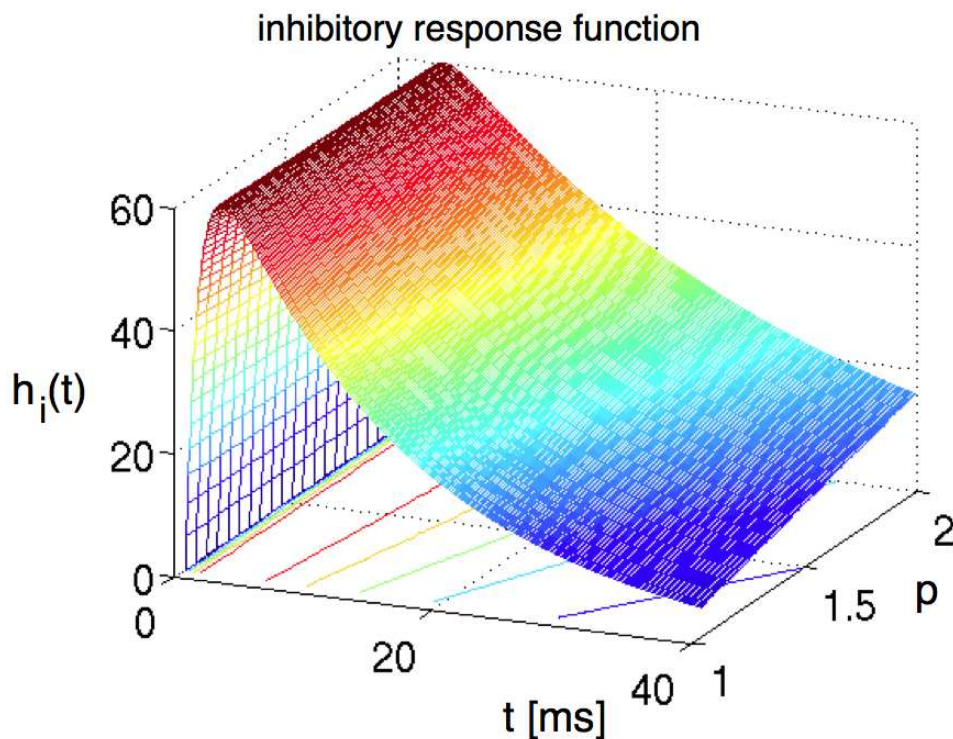


Figure 2.9: Effect of the model parameter p on the synaptic response function of GABAergic synapses. Taken from (Hutt and Longtin, 2009).

charge transfer in the inhibitory synapses by the factor $f(p)$. Considering experimental data, in good approximation this factor is $f(p) = r^{-r/(r-1)}(rp)^{rp/(rp-1)} \approx p$, $r \approx 8.5$. The initial value $p = 1$ represents the case of zero concentration of propofol and $p > 1$ reflects non-zero propofol concentration.

To gain the power spectrum of the population activity, at first it is necessary to compute the constant stationary state \bar{V}_- and its stability. First analytical studies of the stationary solutions show that it is sufficient to consider the effective stationary membrane potential $\bar{V}_- = \bar{V}_e - \bar{V}_i$ with the stationary states \bar{V}_e , \bar{V}_i . The study of \bar{V}_- reveals two cases subjected to system parameters (Hutt and Schimansky-Geier, 2008; Hutt and Longtin, 2009). In the so-called triple solution case increasing p renders the system bi-stable for some values of p , while the single solution case exhibits a single

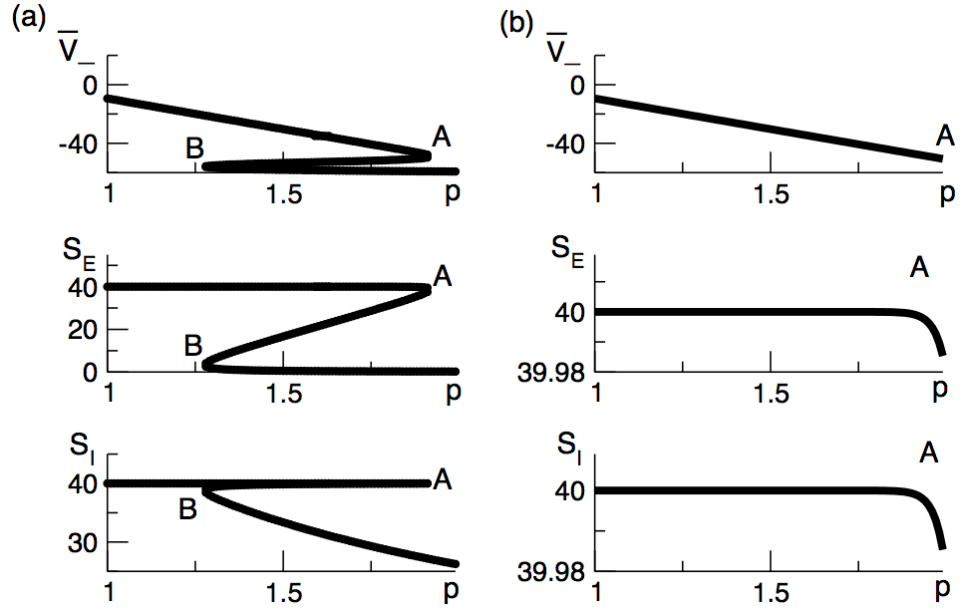


Figure 2.10: Stationary states \bar{V}_- of Eqs. (2.24) and the corresponding population firing rates S_E , S_I for the triple solution case (a) and the single solution case (b). Taken from (Hutt and Longtin, 2009)

stationary solution for all p . Figure 2.10 shows the stationary states \bar{V}_- and the corresponding firing rate functions S_E and S_I for excitatory and inhibitory neurons, respectively, in both solution cases. The triple solution case (panels (a)) exhibits a single stationary state for small and large values of p and shows three stationary solutions for medium values. Stability studies reveal that the centre branch of the three solutions is unstable, and the top and bottom branch are stable for wavenumbers $k = 0$, i.e. these states do not lose stability via spatially constant instabilities. The single stationary solution shown in Figure 2.10(b) is stable in its constant mode $k = 0$. It is interesting to note, that the top and bottom branch in (a) and the single solution in (b) may lose stability for $k \neq 0$ in a non-oscillatory manner and for all k in an oscillatory manner.

Now considering small deviations about the stationary state, specifying the excitatory external input $\Gamma(x, t)$, and taking into account the equivalence of the temporal differential operators $\hat{L}_{e,i}$ and

the temporal integral kernels $h_{e,i}(t)$ by $\hat{L}_{e,i}h_{e,i}(t) = \delta(t)$, Eqs. (2.24) read

$$u_e(x,t) = a_e \delta_E \int_{-\infty}^t d\tau h_e(t-\tau) \quad (2.25)$$

$$\times \int_{\Omega} dy K_e(x-y) \left(u_e(y, \tau - \frac{|x-y|}{c}) - u_i(y, \tau - \frac{|x-y|}{c}) \right) + \Gamma(x,t)$$

$$u_i(x,t) = a_i \delta_I f \omega_0^2 \int_{-\infty}^t d\tau h_i(t-\tau) \quad (2.26)$$

$$\times \int_{\Omega} dy K_i(x-y) \left(u_e(y, \tau - \frac{|x-y|}{c}) - u_i(y, \tau - \frac{|x-y|}{c}) \right)$$

with the nonlinear gains $\delta_{E,I} = \delta S_{E,I} / \delta V$ computed at the stationary state. The variables $u_e(x,t) = V_e(x,t) - \bar{V}_e$ and $u_i(x,t) = V_i(x,t) - \bar{V}_i$ denote the deviations from the stationary states \bar{V}_e and \bar{V}_i and depend linearly on the evoked currents in the membrane, that are present in the dendritic tree and its surrounding. These evoked currents propagate along the dendritic branch towards and away from the trigger zone at the neuron soma and essentially generate the electric activity on the scalp measured as EEG signals. The external input at excitatory synapses reads

$$\Gamma(x,t) = \int_{-\infty}^t d\tau h_e(t-\tau) \xi(x,\tau) \quad (2.27)$$

with the synaptic response function $h_e(t)$ and the random fluctuations $\xi(x,t)$ uncorrelated in space and time, i.e. $\langle \xi(x,t) \rangle = 0$, $\langle \xi(x,t) \xi(y,t') \rangle = Q \delta(x-y) \delta(t-t')$. Then the power spectrum reads

$$S^2(\nu) = \frac{Q}{\sqrt{2\pi}} |\tilde{G}(\nu)|^2 |\bar{h}_e(\nu)|^2 \quad (2.28)$$

with the fluctuation strength Q and the Fourier transform of the Greens function

$$\tilde{G}(\nu) = \frac{1}{\sqrt{2\pi}} \left(1 - \sum_{n=0}^{\infty} \mathcal{L}_n(\nu) (-2\pi i \nu)^n \right)^{-1} \quad (2.29)$$

$$\mathcal{L}_n(\nu) = \frac{1}{n!} \left(-\frac{1}{c} \right)^n \int_0^{\infty} dt (a_e \delta_E h_e(t) \hat{K}_e^n - a_i \delta_I f(p) 4\pi^2 v_0^2 h_i(t) \hat{K}_i^n) e^{2\pi i \nu t},$$

$$\hat{K}^n = \int_{\Omega} dz K(z) |z|^n, \quad \bar{h}_e(\omega) = \int_0^{\infty} dt h_e(t) e^{i\omega t}.$$

Equation (2.28) represents the power spectrum of the EEG measured on the scalp. The advantage of this detailed mathematical formulation is the possibility of an analytical study of the power spectrum behavior. This study has been performed in a recent work (Hutt and Longtin, 2009) and conditions for the occurrence of the bi-phasic spectrum have been derived analytically. Considering these conditions, it is possible to extract parameter sets leading to the bi-phasic power spectrum shown in Fig. 2.11. The figure confirms that the two equations (2.24) represents a sufficient model to reproduce bi-phasic power spectra subjected to anaesthetic concentrations.

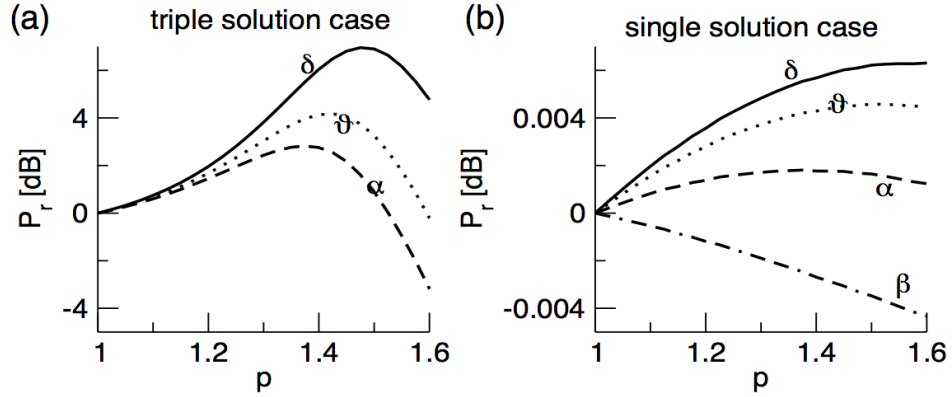


Figure 2.11: Bi-phasic power spectra (a) in the triple solution case on the top branch and (b) the single solution case. The frequencies bands are defined in the intervals [0.1Hz;4Hz] (δ -band), [4Hz;8Hz] (θ -band), [8Hz;12Hz] (α -band) and [12Hz;20Hz] (β -band). Modified from (Hutt and Longtin, 2009).

2.3 Non-linear response in neural fields

After the linear study of small deviations about a stationary state, the present section focusses on larger deviations from the stationary state and considers the nonlinear dynamics of neural fields. At first, the subsequent paragraphs discuss the effects of additive noise on the stability of a stationary state in a neural field. Then traveling fronts are discussed, which link globally two stationary states to a moving object.

2.3.1 Additive noise tunes the stability of stationary states

The theory of linear response assumes that the external input is small and evokes small deviations about the stationary state. Moreover the theory implies that the input does not modify the stationary state or its stability, i.e. adding a small input to the system just induces fluctuations about the stationary state. These assumptions raise the question what happens if the external input is not small and the deviations about the stationary state are large and nonlinear interactions may come into play, i.e. the response of the system is non-linear. Much work has been devoted to the investigations to such nonlinear effects. For instance, Tuckwell (2008b,a) showed how the nonlinear FitzHugh-Nagumo system responds to external noise and quantified the contributions of nonlinear interactions to the statistical moments of the activity. Most previous studies assume that the stationary state remains the same and its stability is not changed. However, there is an exception: it is well-known that parametric driving affects the stability of systems. Specifically, the stochastic variation of a system parameter is known to induce instabilities by rendering the stability conditions dependent on the

noise strength (Horsthemke and Lefever, 1984).

In contrast to the standard view, the present section shows that additive external fluctuations may change the stability of the stationary state of nonlinear systems close to the instability point. Consequently additive noise may affect the firing characteristics in neural models, in addition to the contribution of nonlinear interactions. In order to illustrate the nonlinear behaviour near the bifurcation point, the subsequent paragraphs discuss the Turing instability in neural fields neglecting transmission and feedback delays.

Expanding Eq. (2.15) to cubic nonlinear order in V about V_0 and introducing the variable $\xi(x, t) = I(x, t) - I_0$ yields

$$\frac{\partial u(x, t)}{\partial t} = \int_{\Omega} dy K_1(x-y) u(y, t) + K_2(x-y) u^2(y, t) + K_3(x-y) u^3(y, t) + \xi(x, t) \quad (2.30)$$

with $K_1(x) = -\delta(x) + s' \alpha K(x)$, $K_2(x) = s'' \alpha K(x)/2$, $K_3(x) = s''' \alpha K(x)/3!$, cf. (Hutt and Atay, 2005; Hutt et al, 2008a). The constants s'' and s''' are the functional derivatives of S of second and third order, respectively, computed at the stationary state $V = V_0$. The following discussion considers external random fluctuations uncorrelated in time and constant in space, i.e. $\xi(x, t) = \xi_0(t)$. Such random fluctuations are called *global fluctuations* in the following. This rather artificial specific choice simplifies the mathematical analysis, while it still illustrates the importance of additive noise on the stability of a stationary state. First extensions of this choice to more general spatially correlated noise show additional effects (not shown).

Now expanding u into its Fourier series yields the infinite set of stochastic differential equations

$$\begin{aligned} du_n(t) = & \alpha_n u_n(t) + \beta_n \sum_l u_l(t) u_{n-l}(t) + \gamma_n \sum_{l,m} u_l(t) u_m(t) u_{n-l-m}(t) \\ & + \eta \delta_{n,0} dW(t) \quad , \quad -\infty < n < \infty \end{aligned} \quad (2.31)$$

with the Fourier transform $u_n(t)$ of $u(x, t)$ and the constants $\alpha_n = \tilde{K}_1(k_n) \in \mathfrak{R}$, $\beta_n = \tilde{K}_2(k_n)/\sqrt{|\Omega|} \in \mathfrak{R}$, $\gamma_n = \tilde{K}_3(k_n)/|\Omega| \in \mathfrak{R}$. The terms $\tilde{K}_l(k_n)$ denote the Fourier transform of the kernel function $K_l(x)$ and $dW(t)$ represents the differential of a Brownian process with $\langle dW(t) \rangle = 0$, $\langle dW(t) dW(T) \rangle = 2\delta(t-T) dt dT$ with the fluctuation strength η . In addition, k_n is the wave number of Fourier mode n .

Re-calling the stability study in sections 2.2.1, 2.2.2 and assuming that the constant stationary state V_0 is stable for a certain control parameter, i.e. $\alpha_n < 0 \forall n$, the change of the control parameter may render the stationary state unstable. Then the maximum value of α_n crosses the imaginary axis for certain critical wave numbers k_c , while other non-critical $\alpha_{n \neq c} \neq 0$ with $\alpha_0, \alpha_c \gg \alpha_{2c}, \alpha_{3c}, \dots$. Hence, near the instability threshold the system exhibits a Turing instability with wave number k_c if $\alpha_c \Rightarrow 0$.

If the system evolves on the threshold, i.e., $\alpha_c = 0$ and $\alpha_i < 0$, $i \neq c$, the stochastic center manifold theorem applies (Boxler, 1989; Xu and Roberts, 1996) and the stable modes $u_{i \neq c}$ depend on

time and u_c , i.e., $u_i(t) = u_i(u_c, t) = g_i(u_c, t)$. For large times, this relation allows to compute the functions $g_i(u_c, t)$ and, hence, the dynamics of the stable modes $u_{i \neq c}(t)$. Inserting g_i into the differential equation of u_c yields a one-dimensional differential equation for the dynamics whose solution gives the functions g_i .

Summarizing this reasoning, the stable modes obey the dynamics of the critical modes on the center manifold just around the stability threshold, while they evolve faster than the critical modes. In physical terms, the slow critical modes enslave the fast stable modes, which in turn obey the dynamics of the critical modes. This dependence is also called the slaving principle and the circular dependence is known as the circular causality (Schoener and Haken, 1986; Haken, 2004).

Moreover, $g_i(u_c, t)$ depend on the external fluctuations and may introduce multiplicative noise terms into the differential equations of u_c . Consequently, additive noise in the evolution equation of stable modes may introduce multiplicative noise into the critical modes close to the stability threshold and, hence, trigger noise-induced phase transitions as outlined above.

Now, assuming an order of scales with $u_c \sim O(\varepsilon^{1/2})$, $\alpha_c \sim O(\varepsilon)$, $\eta \sim O(\varepsilon)$ and $\alpha_{n \neq c}, \beta_n, \gamma_n \sim O(1)$ (Hutt and Atay, 2005; Hutt et al, 2008a; Hutt, 2010, 2008a; Hutt et al, 2007), and considering terms up to $O(\varepsilon^{5/2})$, the system (2.31) may be approximated to

$$du_c = (\alpha_c + bu_0u_c + 2\gamma_cu_c^3 + 3\gamma_cu_cu_0^2) dt \quad (2.32)$$

$$du_0 = (\alpha_0u_0 + 4\beta_0u_c^2 + \beta_0u_0^2 + 2\gamma_0u_0u_c^2) dt + \eta dW(t). \quad (2.33)$$

To obtain some insight into the possible solutions of Eq. (2.32), (2.33), let us neglect the random fluctuations for the moment. Then the analysis of (2.32), (2.33) reveals a stable solution $u_c = 0$ for $\alpha_c < 0$ and a stable solution $u_c = \pm \sqrt{\alpha_c/a}$ for $\alpha_c > 0$ with $a = 2\gamma_c - 8\beta_0\beta_c/\alpha_0 - 8\beta_{2c}\beta_c/\alpha_{2c} > 0$. The positivity of the constant a guarantes that the linearly unstable solutions for $\alpha_c > 0$ remain bounded. This instability type is called a pitchfork bifurcation.

Now considering the external fluctuations, the stochastic center manifold analysis (Hutt et al, 2008a; Hutt, 2010) yields the final Fokker-Planck equation for the critical mode u_c

$$\frac{\partial P(u_c, t)}{\partial t} = -\frac{\partial}{\partial u_c} \left[(\alpha_c - \alpha_{\text{th}}(\eta))u_c + Cu_c^3 + Du_c^5 \right] P(u_c, t) \quad (2.34)$$

with

$$\alpha_{\text{th}}(\eta) = \eta^2 \left(\frac{\beta_0 b}{\alpha_0^2} - 3 \frac{\gamma_c}{|\alpha_0|} \right) \quad (2.35)$$

and the constants C, D . The term $P(u_c, t)$ denotes the probability density of the critical mode u_c . Since no diffusion term is present in Eq. (2.34), the order parameter u_c obeys the deterministic equation

$$\dot{u}_c = (\alpha_c - \alpha_{\text{th}}(\eta))u_c + Cu_c^3 + Du_c^5, \quad (2.36)$$

where $\alpha_c - \alpha_{th}$ defines the new stability threshold, which now depends on the fluctuation strength η and thus reflects noise-induced transitions. Equation (2.36) reveals that the noise retards (advances) the emergence of the instability with increasing α_c for $\alpha_{th} > 0$ ($\alpha_{th} < 0$) and thus stabilizes (destabilizes) the neural field Hutt et al (2008a).

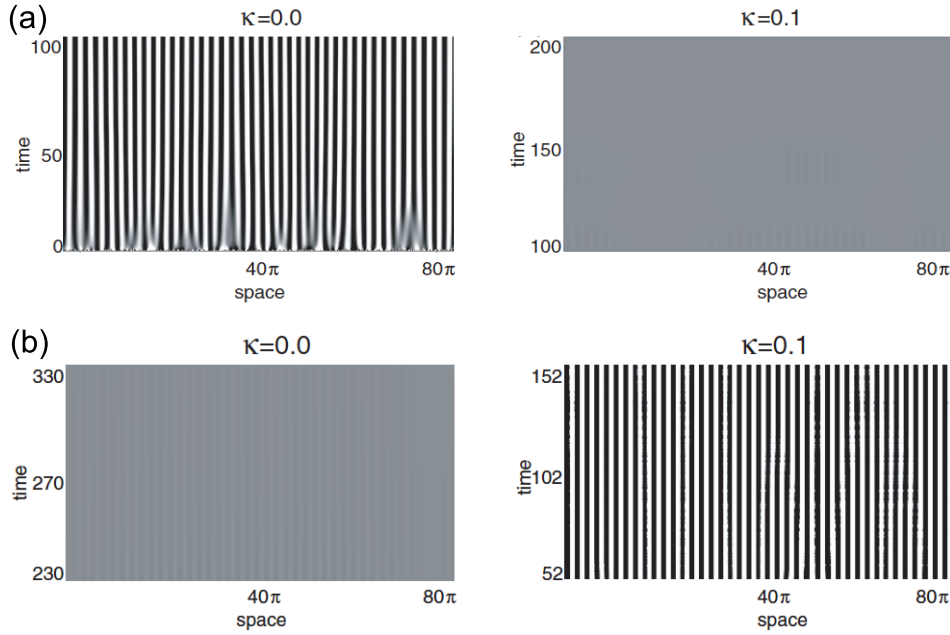


Figure 2.12: Spatio-temporal solutions of the extended Swift-Hohenberg equation subjected to additive global fluctuations (Hutt, 2008a). (a) Turing instability without additive noise, i.e. $\kappa = 0$, which is destroyed in the presence of fluctuations ($\kappa = 0.1$). (b) No Turing instability in the absence of external fluctuations ($\kappa = 0$) but Turing instability in the presence of the global fluctuations ($\kappa = 0.1$).

Consequently, additive global fluctuations change the stability of the stationary state dependent on the system parameters (Hutt and Atay, 2005; Hutt et al, 2008a; Hutt, 2010, 2008a; Hutt et al, 2007). Since the neural field equation generalizes pattern forming systems, as discussed in section 2.1.3, this effect can be observed in other systems as well, e.g. which are described by partial differential equations. Figure 2.12 shows the space-time activity of a stochastic Turing instability in the absence and presence of global fluctuations in a systems described by the extended Swift-Hohenberg equation (Hutt, 2008a; Hutt et al, 2007). The Turing instability may be destroyed or induced by the additive global fluctuations dependent on the system parameters.

Concluding, additive global fluctuations change the stability of the neural population via specific nonlinear coupling schemes and thus affect the neural processing. This finding reveals that the linear

response theory in section 2.2.3 may be valid only if the noise level η is very small and, hence, the possible stability shift by α_{th} is negligible.

2.3.2 Traveling fronts

Neural structures are complex systems, in the sense that it involves several interacting subunits on a microscopic scale (neurons) building mesoscopic structures or units reflecting the major dynamics of the subunits (neuronal populations). Mesoscopic units represent coarse-grained models taking into account some microscopic features while neglecting others. The most important question in this context is the definition of the major microscopic property elements that should be taken into account. For instance, neural fields take into account that neurons are excitable systems, i.e. become active for specific inputs. This excitability results from the intrinsic activity threshold of neurons. Hence excitable systems are nonlinear. Moreover, it can be shown easily that neural fields share this property (Hutt, 2009): an external spatially localized input exceeding a certain size may induce traveling fronts. Consequently neural fields may respond nonlinearly to external stimuli by travelling fronts. To learn more about this nonlinear action, previous studies have investigated the uniqueness and existence of travelling fronts in the presence of distributed transmission speeds and distributed feedback delays (Atay and Hutt, 2006). These results hold for spatially homogeneous populations. Moreover, the question arises whether traveling fronts exist in spatially inhomogeneous neural fields, which are more realistic models of neural structures. Such inhomogeneous neural fields relax the condition that the spatial connectivity just depends on the distance and is identical at all spatial locations. Some previous studies have investigated the spatio-temporal dynamics in such neural fields, e.g. by Qubbaj and Jirsa (2009) and Bressloff (2001). Schmidt et al (2009) show the nonlinear analysis of such fronts and derive conditions for front propagation and front propagation failure. Figure 2.13 illustrates the propagation of such a front in a neural field perturbed by spatially periodic inhomogeneities.

2.4 Multivariate signal analysis

The previous sections show in detail the analysis of mathematical models describing the spatio-temporal activity of neural populations. The motivation of such models is based on experimental findings. For instance, the neural field model introduced in section 2.1 was originally motivated by intracranially measured activity in cortical structures (Wilson and Cowan, 1972). Early experimental studies on the orientation tuning of neurons in the visual system exhibited certain visual stimuli constant in time (Hubel and Wiesel, 1963; Ben-Yishai et al, 1995). The gained experimental results were stationary over time and motivated the investigation of stationary solutions of theoretical models, such as neural fields. Moreover, the most important experimental quantity extracted was the stationary amplitude of the neural activity.

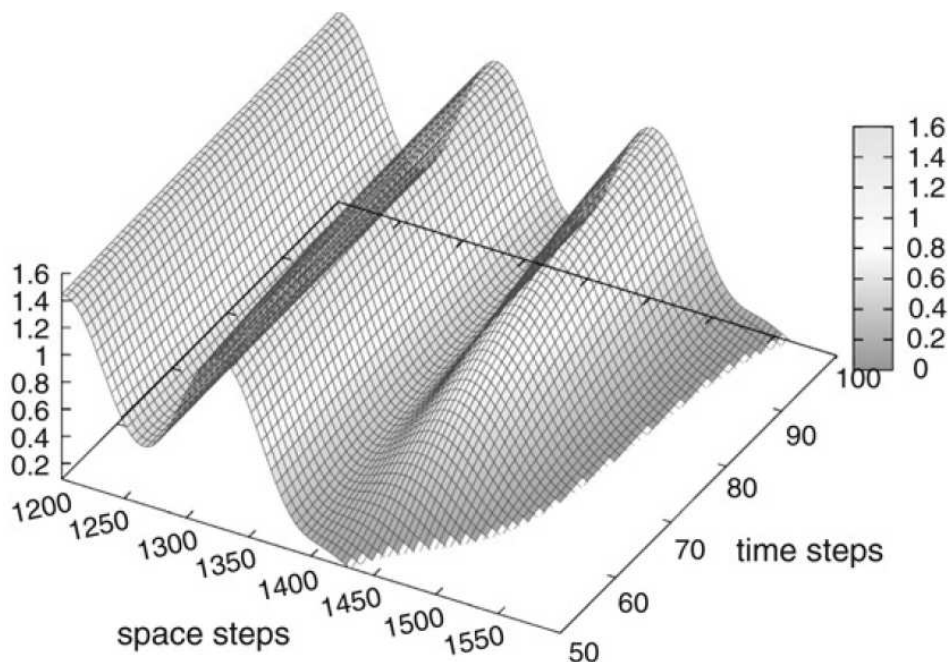


Figure 2.13: Space-time evolution of a traveling front in a neural field involving a spatially periodic inhomogeneity. Taken from (Schmidt et al, 2009).

Today most experimental setups exhibit a stimulus changing over time, which then yields non-stationary neural activity. Hence today's most experimental data, such as the electroencephalogram (EEG) or the Local Field Potentials (LFP), shows activity which is transient in time and space. Novel concepts such as the instantaneous synchronization (Pikovsky et al, 2001; Lachaux et al, 1999) or chaotic itinerancy (Kay, 2003; Breakspear and Friston, 2001; Freeman, 2003) formalizes the transient behaviour and propose analysis techniques to quantify signal features, such as time-dependent amplitudes or phases. In turn the transient experimental data stipulates the study of non-stationary dynamics in theoretical models. The subsequent paragraphs discuss briefly recent advances in the analysis of multivariate brain signals and illustrate the corresponding problems.

In neuropsychological experiments, the subject may perform a cognitive task which generates so-called evoked potentials in the EEG. Such potentials are amplitude peaks which occur at several electrodes. One says that the activity in the electrodes is synchronized in the amplitude, i.e. one observes signal components with an increase and decrease of amplitude in most of the time series. Typically, such potentials emerge as prominent signal features after the time-locked average of several time series over different trials (Hutt, 2004; Hutt and Riedel, 2003). Another feature in brain signals are transient oscillations common in time series of different electrodes. These oscillations

exhibit certain frequencies with transient amplitude increases and/or transient phase relations.

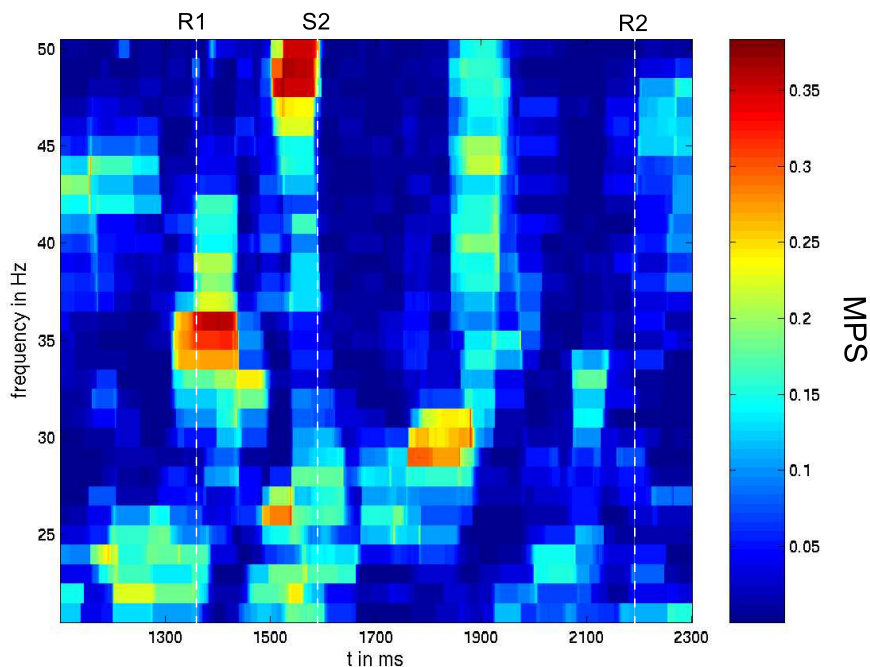


Figure 2.14: The panel shows the global phase synchronization index (MPS) in a selected time window for a single trial in a visuo-motor experiment with monkeys (Hutt and Munk, 2006). The horizontal and vertical axis gives the time and the frequency, respectively. The vertical white lines indicate the time onset of a motor responses (R1 and R2) and the time onset of a visual stimulus (S2). We observe strong synchronization in the γ -band close to the motor response onset and the visual stimulus onset. Figure taken from the work of Hutt and Munk (2006).

The phase relations are typically studied between single pairs and have been shown to play an important role in the interaction between brain areas (Castelo-Branco et al, 1998; Engel et al, 1991). In addition, phase synchronization is supposed to explain how the brain binds together different features of sensory input to a single representation (Singer and Gray, 1995; Singer, 1999). By virtue of the oscillatory properties of phase-synchronized signals, one may lose the phase information of signals while averaging over trials as for evoked potentials. Consequently it is necessary to extract the phase synchronization in single trials and compute statistical measures based on the results gained from single trials. Such an analysis is feasible by clustering of the experimental data. Previous detailed clustering studies (Hutt et al, 2003b; Hutt and Munk, 2006, 2009) have taken into account all electrodes in the dataset to compute a corresponding synchronization quantity. Figure 2.14 shows the

global phase synchronization in a single trial during an invasive visuo-motor experiment in monkeys and we observe strong phase synchronization close to stimulus onset and offsets.

Although the results obtained allow for first interpretations of the neural processing, the gained synchronization quantity reflects the synchronization in the data very well only if most electrodes are synchronized, i.e. in the case of global synchronization.

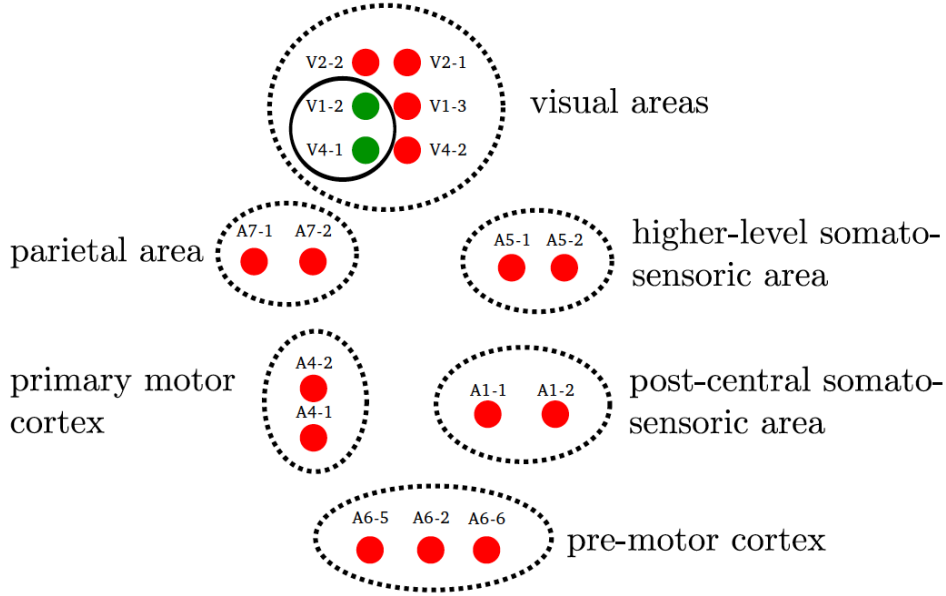


Figure 2.15: Detected subnetwork in Local Field Potentials obtained experimentally from monkeys, cf. Fig. 2.14. The dots denote electrodes positioned in different brain areas (dashed circles). As one first result, the partial synchronization method detected a prominent subnetwork of two channels in the visual cortex (green), while the remaining electrodes (red) are independent from this subnetwork but do not show any substructure itself. The green subnetwork occurs in early times in the trials under investigation and evolves in the γ -frequency band. Figure taken from (Rio et al, 2011).

However, a more realistic situation exhibits just few electrodes of synchronized activity, while the other electrodes are silent or show random fluctuations. In this case, the global synchronization quantity does not reflect well the real synchronization pattern. To put it differently: the global analysis assumes a single synchronized network, whereas in the presence of multiple synchronized sub-networks interacting with each other single sub-networks may be synchronized independently. Hence in the latter case the system may not show global synchronization, but rather so-called *partial synchronization* in a subset of elements.

To detect such sub-networks, i.e. partial synchronization, it is necessary to re-consider the notion of synchronization. Re-call that synchronization means, in general sense, common behaviour of

certain elements. A recent work considers oscillations at specific frequencies and the synchronized elements are their corresponding amplitudes. Moreover, the common behavior, i.e. the classifier for synchronization, is the increase and decrease of amplitudes similar to the evoked potentials discussed above. To analyse a multi-variate time series such as EEG in practice, at first the method developed extracts the amplitudes of single time series at each time point in narrow frequency bands by a continuous wavelet transformation. Then, at each time point and in each frequency band, the multivariate data reduces to a set of amplitude values embedded in a space whose dimension coincides with the number of time series. A subsequent clustering technique applied to the amplitude values detects subsets of time series which reflect the underlying sub-networks (Rio et al, 2011). Figure 2.15 illustrates the clustering result extracted from the LFPs of Fig. 2.14. Summarizing, the latter method detects sub-networks which (i) exhibit global synchronization in a set of time series and (ii) which oscillate in a not too wide frequency band.

Chapter 3

Research perspective

The latter chapter discusses previous studies on spatio-temporal dynamics in neural populations and multivariate analysis techniques of experimental data. These studies apply to rather general models and general experimental data extracting a diverse range of different properties and phenomena. For instance, the investigations of neural fields considered both stationary patterns and traveling waves oscillating with a single frequency. Moreover, the neural population model describes the neural activity on a single mesoscopic scale. In contrast, future work will focus on oscillatory systems which exhibit a broad spectrum of oscillation frequencies. Moreover, the work will study in detail how the power spectrum of such systems depends on internal system parameters or the properties of external inputs. The work will also consider the properties of neural activity on different spatial scales. This multi-scale approach is essential for the understanding of macroscopic oscillations.

The following section discusses oscillations of neural populations in the primary sensory area of weakly electric fish. These oscillations are subjected to the correlation structure of the external input. Then section 3.2 considers neural population oscillations in the olfactory bulb in mammals, which depend strongly on the odour applied and which are tuned by the breathing cycle. Both latter systems, i.e. the sensory system in weakly-electric fish and the olfactory system in mammals, involve delayed feedback loops and external inputs. Since delayed feedback loops are present in most neural structures, the understanding of the underlying mechanism in these systems will indicate a more general coding concept in neural structures. The last section will discuss the dynamics of neural populations in the human cortex during general anaesthesia. Since anaesthetics affect synaptic receptors at the microscopic level and modifies the electroencephalogram on the macroscopic level, the development of a successful model stipulates the study on each description level in between. The results from the first two sections may provide deeper insight in the human feedback system.

3.1 Generation of oscillations in weakly-electric fish

As described in section 2.2.4, the network oscillations in the primary sensory area of weakly-electric fish (ELL) depend strongly on the spatial correlation of the spatio-temporal random input. Experimental studies (Doiron et al, 2003, 2004) extracted the histogram of the inter-spike interval (ISI) of single neurons in the ELL. Since the neurons in the ELL are not connected to each other, this ISI histogram also reflects the population firing activity of the neurons. If the incoming random input is spatially uncorrelated, then the ISI histogram shows a single maximum at about 5ms. However, if the spatial correlation of the input increases, then an additional maximum in the histogram occurs at about 25ms.

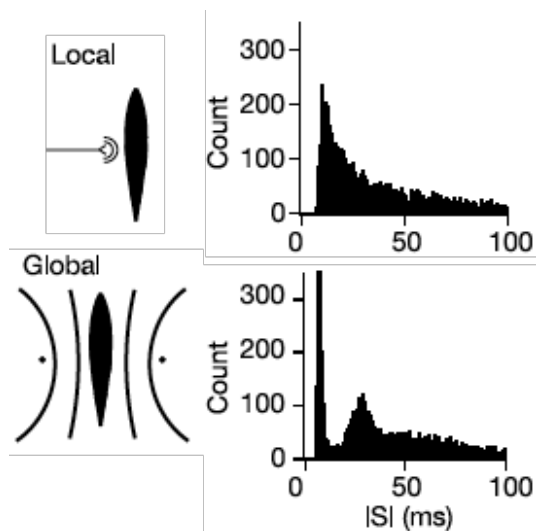


Figure 3.1: Strong spatial correlations of external noisy inputs generates *in-vivo* spike rhythms in the primary sensory area of weakly-electric fish. Top row: spatially localized random stimuli on the skin of the fish (left cartoon) leads to spiking activity in the ELL with a single peak in the inter-spike-interval (ISI) histogram and a long histogram tail (right panel). Bottom row: globally correlated random stimuli (left cartoon) generates an additional spiking rhythm with a peak in the corresponding ISI histogram at larger ISIs (right panel). Figure modified from Doiron et al (2003).

Hence, the increased spatial correlation of the input is responsible for the additional oscillation rhythm. The same experimental studies also show that this additional oscillation occurs only in the presence of an internal delayed feedback in the sensory system. Previous theoretical studies based on spiking neurons were able to reproduce the generation of the additional rhythm. However, these studies do not take into account the spatial connectivity structure in the primary sensory system which is supposed to play an important role in the decoding of incoming sensory signals. Future

work will study the generation of the additional oscillation rhythm by explaining the ISI histogram by a nonlinear neural field model involving the axonal connection topology. This analysis examines the population firing rate in the ELL and extends the previous study discussed in section 2.2.4 which just takes the experimental results as a motivation for a studies of membrane potentials.

The work aims to reproduce the ISI histogram. Since the ISI histogram reflects the population firing statistics (the neurons in the ELL are not coupled), it represents the inverse population firing rate which in turn is modeled by the nonlinear transfer function in neural fields. The corresponding model is given by the two equations (2.23) and the ISI in the ELL is given by $1/S_e$. A first analysis step will consider constant connectivity kernels, i.e. neglects spatial effects, and stationary states will be studied. Then a nonlinear analysis utilizing the moment expansion technique (see e.g. (Valenti et al, 2006)) may allow to extract the effect of spatial input correlations onto the dynamics of the system. Computing the distribution of values of the nonlinear transfer function $S_e = 1/ISI$, cf. (2.23), will give the ISI histogram subjected to the input correlation. This nonlinear study extends the linear approach as described in section 2.2.4 that does not study ISI histograms in particular. The study proposed will indicate whether neural fields may also allow to reproduce ISI histograms besides the study of membrane potentials, what is not explored until now. In addition, the study will reveal the mechanism how external inputs generates oscillations in the ELL. This knowledge will be valuable for the next study.

3.2 Frequency switch in the mammalian olfactory system

The spatio-temporal dynamics in the olfactory system has attracted much attention in recent decades, from both experimental (Wehr and Laurent, 1996; Sachse and Galizia, 2002; Friedrich and Laurent, 2001; Buonviso et al, 2003) and theoretical (Rabinovich et al, 2008; Freeman, 2000) perspectives. Most of the previous studies investigated the response of the neural population to an odour stimulus of finite temporal duration. Recent in-vivo studies have investigated the oscillatory dynamics in the mammalian olfactory bulb during the breathing cycle (Buonviso et al, 2003; Cenier et al, 2009) in the constant presence of an odour. It has been shown experimentally by measurements of Local Field Potentials in the olfactory bulb, that the change between inhalation and expiration during breathing induces switches between oscillation frequencies in the beta-band (12 – 20Hz) and the gamma-band (20 – 60Hz), cf. 3.2.

To understand this switch, it is necessary to consider more closely the physiology of the olfactory bulb, cf. Fig. 3.3. The odour activates the olfactory receptors which send their activity to the glomerulus projecting onto the olfactory bulb. The glomerulus is a complex of densely-packed neurons exhibiting mainly dendro-dendritic connections. The respiratory cycle oscillates in the delta-band (~ 2 Hz) and modulates the glomerulus activity, which then in turn modulates the stimulation of the bulb and the involved bulb cells.

Future work will aim to reproduce the experimental data by a detailed study of the neural popu-

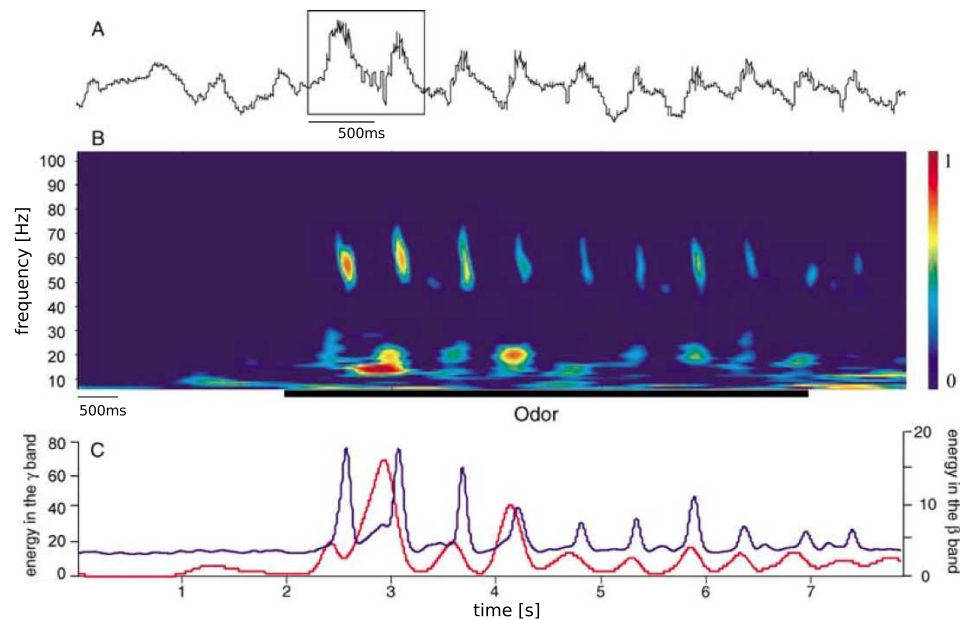


Figure 3.2: The Local Field Potentials measured in the olfactory bulb in rats during a respiratory cycle in the presence of an odour. A) The measured raw signal exhibits the slow breathing rhythm with a frequency of 1.6Hz (two breathing periods in inset) and the overlaid oscillatory beta- and gamma-rhythms. B) The scalogram shows clearly the switch between beta- and gamma activity during a respiratory cycle. C) The instantaneous energy of the beta-(encoded in red) and gamma-oscillations (encoded in violet). Figure modified from Buonviso et al (2003).

lation activity in the olfactory bulb. To this end, the work will develop a neural field model involving the detailed physiological properties of the synapses, neurons and connections in the olfactory bulb. The mathematical study will focus on the linear response of the population activity subjected to changing stimulus properties. The changes of the stimulus result from the respiration which may change the spatial correlation of the bulb input from the glomerulus or the stimulus amplitude similar to the weakly-electric fish in the previous section. Moreover, the study will consider the knowledge gained previously from the linear and nonlinear studies in weakly electric fish. The reproduction of the corresponding change in the power spectrum, i.e. the change of amplitudes of the the oscillation frequencies in the LFP, will elucidate either another different mechanism of oscillation frequency tuning in neural systems, or affirm one of the previous results in the weakly-electric fish. If the modifications of the power spectrum may be explained by the same mechanism in both the ELL and the olfactory bulb, the common mechanism would represent a basic principle in neural oscillation tuning and, more generally, control of neural information flow in neural structures.

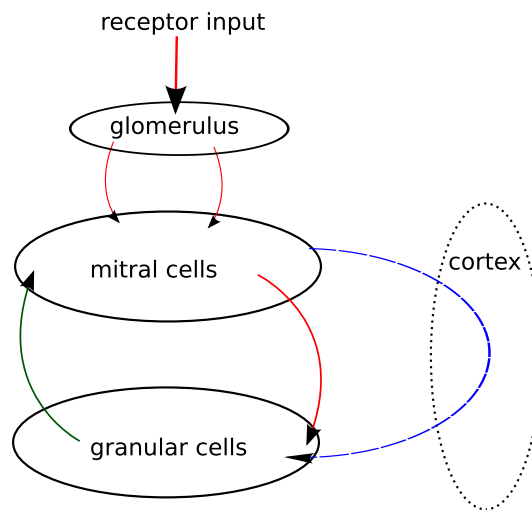


Figure 3.3: The topography of the mammalian olfactory bulb. An applied odour activates receptor neurons (not shown), which stimulate the glomerulus. The neurons in the glomerulus project to the mitral cells (pyramidal cells). These cells project to the granular cells (interneurons), in turn inhibiting the mitral cells via synaptic complexes. The additional feedback from the mitral cells to the granular cells via the olfactory cortex is inhibitory but indirect, i.e. the mitral cells project to the cortex which projects back to the granular cells. This feedback is assumed to be delayed but more details on the physiology and function are not known until today. The arrows in the figure denote functional connections with excitatory (red-colored) and inhibitory (green-coloured) synaptic connections. The blue feedback connection is delayed and excitatory, but indirect passing through the cortex.

3.3 Frequency tuning during general anaesthesia

General anaesthesia (GA) is an important tool in today's hospital surgery. The anaesthetist in the hospital administers the anaesthetic drug before and during surgery to prevent the patient to wake up during surgery (loss of consciousness or awareness), that the patient does not feel any pain (analgesia), does not move (immobility) and does not remember any details (amnesia). It is known that these different features of GA probably originate from different locations in the brain and body. For instance, analgesia results mainly from a block of neurons in the spinal cord, while amnesia is supposed to originate in the prefrontal cortex. One of the most important features in GA is the loss of consciousness (LOC), i.e. the lack of awareness to external stimuli. This loss of consciousness marks the so-called end point of anaesthetic drug administration and hence defines the maximum anaesthetic drug concentration. Since some patients may be sensitive to a too high dose of anaesthetics, this end point is very important in anaesthesia practice.

Although general anaesthesia works well in most operations, cases have been reported in which, e.g., patients have woken up and have observed surgeons, but without feeling pain or being able to move. Such a partial return from the anaesthetized state may be dangerous for the patient, but are far from being understood. Moreover, today the choice of the anaesthetics and its concentration applied is based on medical experience, but the on-site concentration of the anaesthetic in the neural structures is not known and under constant discussion in clinical research. Hence the molecular effect of the anaesthetics at the neural receptor sides has attracted much research activity in the recent decades, and is well understood. However, it is not understood how the microscopic effect at receptors affect the mental state of the patient, the end point of drug concentration increase and, e.g. the LOC.

To monitor the optimal anaesthetics concentration, modern anaesthesia methods may obtain experimentally the brain signals on the patients scalp during surgery, i.e. the EEG. The power spectrum of the EEG allows to estimate the end point of the drug administration. Consequently, the understanding of the power spectrum is one of the most important aims in general anaesthesia. The increase of the anaesthetic drug concentration induces a characteristic change of the power spectrum in the measured EEG. Typically, this change of power spectrum emerges as follows: during the increase of the anaesthetics concentration the power in the theta-, alpha-, beta- and gamma frequency band (4 – 60Hz) decreases. In the same time, the patient loses consciousness. Hence, the anaesthetic concentration tunes the major oscillation frequency of the EEG and controls the loss of consciousness. When subjects return to consciousness, the power changes are reversed. In addition, some studies show that the anaesthetic concentration at the LOC and the return of consciousness (ROC) is different, which indicates a hysteresis in the system. This hysteresis hypothesis is still under debate, see Project 4 below.

To this end, it is necessary to understand how microscopic effects at receptor sites affect the electric activity on the scalp. As a working hypothesis, future studies will consider cortical structures

only, since their activity is known to represent the electromagnetic source of the EEG. The cortical structures respond to the incoming activity from subcortical structures. Such structures may be part of the ascending arousal system (Magoun, 1952) including the brain stem and the hippocampus. The thalamus also drives the cortex as a gateway of sensory inputs. However, research in the close future will consider the subcortical activity as an external input to cortical systems for simplicity, while extensions to detailed subcortical models is always necessary.

The cortex is a complex structure involving several layers of sub-populations. Hence this model approach of an externally driven network of sub-networks, i.e. layers, resembles the studies on weakly-electric fish and the mammalian olfactory bulb. Consequently, the extracted knowledge on the induction of frequencies from both previous studies may be helpful in the context of GA.

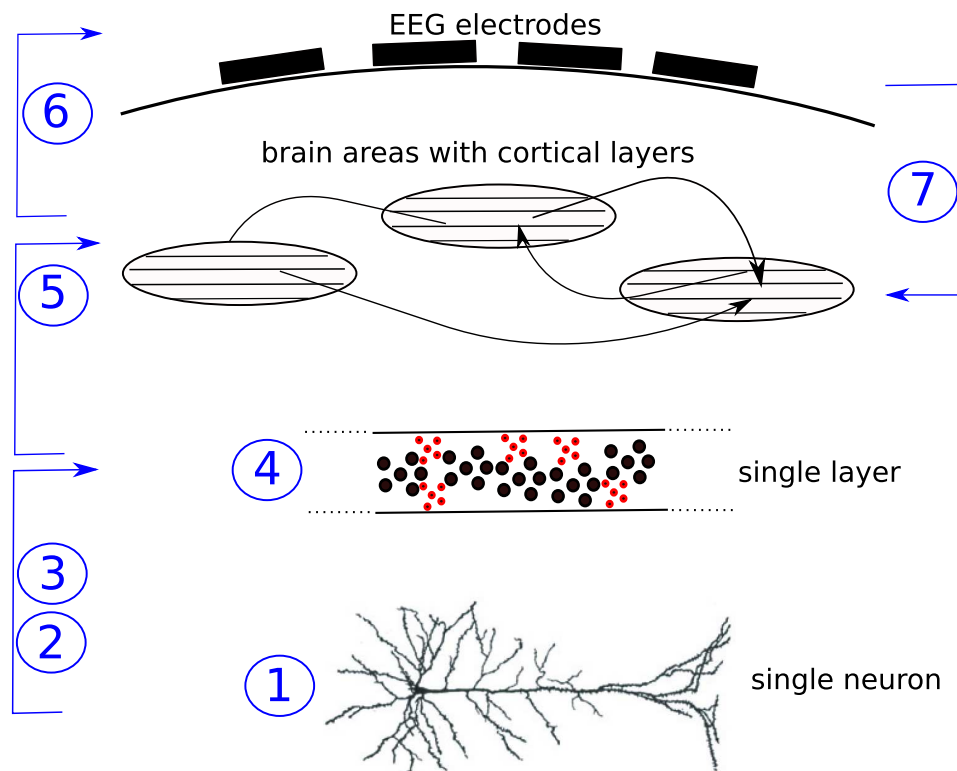


Figure 3.4: Project structure of the future work studying the multi-scale topology of the brain. The encircled numbers denote the Projects outlined in the subsequent sections. Project 1 to 6 investigate theoretical models on a certain description level or build the bridge from descriptions on smaller spatial scales to models on larger scales. Project 7 considers experimental EEG-data and aims to deduce conditions on underlying networks of neural populations.

Figure 3.4 illustrates the various modeling steps. Future work will develop mathematical models

describing the effect of anesthetics on receptor dynamics, which affect the dendritic activity of a single neuron, see Project 1. The next step considers the results of anaesthetics on the dendritic activity and develops neural population models assuming population rate coding (Project 2) and time-coding aspects (Project 3). The resulting population rate model describes the dynamics in a certain cortical layer. Project 4 studies in detail this rate model subjected to the anaesthetic effects on the receptors in single neurons. Moreover, in Project 5 the work will study the network dynamics of interacting neural populations in two spatial dimensions taking into account the spatial interactions of cortical layers. To understand the experimental data and compare it to the theoretical results finally, it will be necessary to study in some detail the electromagnetic generation of EEG based on the neural population activity. This modeling approach is described in Project 6. Essentially, Project 7 considers the multivariate data analysis of experimental EEG data and aims to extract signal features from the data, that may reflect underlying neural population dynamics.

Project 1: Analysis of dendritic activity subject to the anaesthetic action of propofol on GABA_A-receptors

Cortical dendrites exhibit various receptor types. For instance, synaptic receptors are located close to synaptic bulbs which emit neurotransmitters and activate the close receptors. Single incoming action potentials may activate the synaptic bulb to emit neurotransmitters and hence activate the close receptors to generate a so-called *phasic* response potential in the cell membrane. The rate of neurotransmitter emission depends on the activation of the synaptic bulb by incoming action potentials. If the rate of incoming action potentials are high, many neurotransmitters are spilled over the location of the synapse and not all transmitters may bind to the corresponding close synaptic receptors. The left over neurotransmitters diffuse into the synaptic surrounding and may activate other receptors of close-by synapses. The cloud of neurotransmitters also may hit extra-synaptic receptors which are not located close to synapses (Kopanitsa, 1997). Since such extra-synaptic receptors are de-located from synapses, they do not respond directly to incoming action potentials but respond rather by a *tonic* activation caused by an ambient neurotransmitter level, e.g. resulting from the increased concentration of neurotransmitters in the surrounding.

This tonic activation at extra-synaptic receptors may also originate from anaesthetic agents. For instance, some anaesthetics open ion channels of GABA_A receptors and induce a permanent current through the membrane at the receptor location. This tonic activation changes the membrane conductivity close to the receptor and hence modifies the propagation of currents on the dendrite. Previous experimental studies (Farrant and Nusser, 2005) have shown that this tonic activation induced by anaesthetics strongly affects the sedation effect in general anaesthesia (Orser, 2006).

The project will focus on the mathematical modeling of the effect of anaesthetics on the current propagation on passive dendritic trees. The anaesthetics will be specified to *propofol*, which is widely-used in hospital practice. Moreover propofol affects solely inhibitory synaptic and extra-synaptic GABA_A receptors. Since the tonic activation at extra-synaptic synapses increases the membrane conductivity and shifts the reversal potential towards the resting potential of the neurons membrane, the total effect of propofol is similar to shunting inhibition. Recall that shunting inhibition assumes an identical reversal potential of the inhibitory receptor and the membrane resting potential, whereas the tonic inhibition just let the reversal potential approach the resting potential. The work will study analytically and numerically the passive cable equation for dendrites (Mel, 1994; Tuckwell, 1988; Timofeeva et al, 2008) involving excitatory receptor dynamics and inhibitory synaptic and extra-synaptic dynamics. More detailed, after a first analytical study of the passive activity spread of excitatory (EPSP) phasic post-synaptic potentials and in the presence of tonic inhibition (IPSP) each generated at different locations, the work will study analytically the correction term to the sum of EPSPs and IPSP depending on the tonic inhibition. This correction term is known to depend nonlinearly of the EPSP and the IPSP (Tuckwell, 1988) for identical receptor reversal potentials and resting potentials. Previous studies on shunting inhibition either simplified the

synaptic response function to a Dirac-function or a Heaviside function or performed extensive numerical studies. In contrast, the proposed work will apply analytical techniques considering more realistic synaptic response functions, such as exponential decaying functions or the alpha-function, cf. Eq.(2.1).

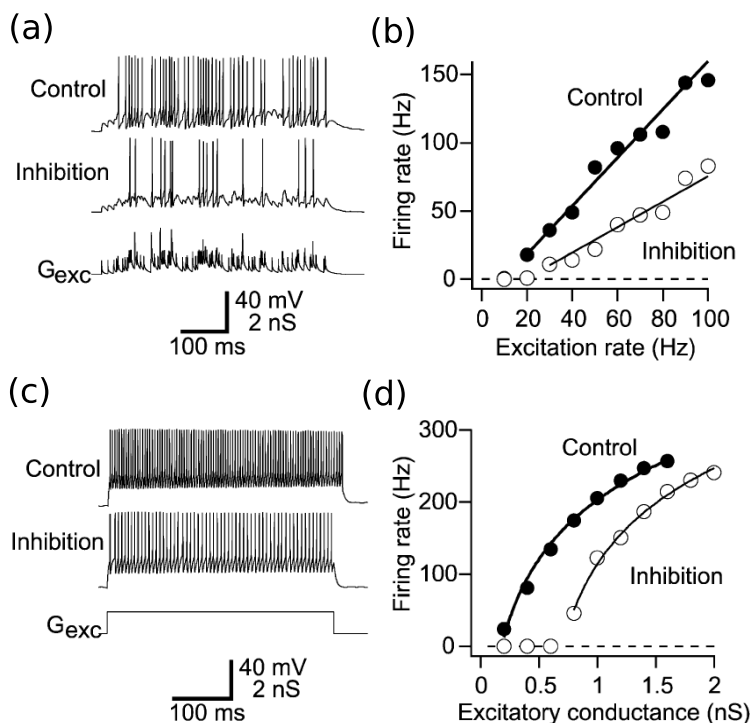


Figure 3.5: Tonic inhibition affects the firing rate in granular cells in rat cerebellum slices subjected to the excitatory stimulation. (a) Four independent 50Hz Poisson trains of transient excitatory synaptic conductance (G_{exc}) for control conditions and during 1nS tonic shunting inhibition. (b) Output firing rate-input frequency relationships for synaptic excitation for control (closed circles) and during tonic inhibition (open circles). The results reveal a divisive effect of tonic shunting. (c) Injection of a step of 1nS tonic excitatory conductance (G_{exc}) for control and with 1nS of tonic inhibition. (d) Output firing rate as a function of tonic excitatory conductance amplitude for control (closed circles) and with tonic inhibition (open circles). The results reveal a subtractive effect of tonic shunting. Taken from (Mitchell and Silver, 2003)

Moreover, the study will take into account the spatial distribution of the receptors on the dendritic tree gaining a realistic model of the anaesthetic effect on activity on spatially extended dendrites. This spatial distribution depends on the dendritic branching structure and the physiological properties of the corresponding branches rendering the analytical treatment rather complex for gen-

eral dendritic trees. To my best knowledge, this study has not been done before and it will give some insights how to extract the effects of anaesthetics on dendritic activity in general. To test the theoretical results, we will try to obtain experimental data on the spatial distribution of synaptic and extra-synaptic receptors. This would give us the possibility to achieve more realistic results. Finally, the last analysis step is a numerical simulation of the dendritic activity considering realistic synaptic structures. This simulation will be performed by the application of standard software tools, such as NEURON (Carnevale and Hines, 2006) or BRIAN (Goodman and Brette, 2009).

The result of this study will yield analytical expressions for the anaesthetic action on the neuron firing activity, e.g. quantified by the firing rate and the nonlinear gain. It is known that shunting inhibition has a divisive effect on the subthreshold amplitude of excitatory post-synaptic potentials, i.e. changes the slope of the rate-amplitude curve (Carandini and Heeger, 1994), or a subtractive effect on the firing rate by shifting the transfer function by a constant value (Holt and Koch, 1997). Moreover, the study of Mitchell and Silver (2003) on tonic inhibition points out that divisive and subtractive effects on the firing rate depend on the statistical properties of the applied excitatory synaptic stimulation, cf. Fig. 3.5. Since the tonic anaesthetic inhibition shifts the reversal potential towards the resting potential but may not reach it, the result may not be identical to the shunting inhibition case, but similar. Hence, the major quantities under study will be the resulting firing rate and its nonlinear gain subjected to the anaesthetic concentration.

Project 2: Novel population rate-model based on anaesthetic action on single neurons

The achievement of Project 1 is the understanding how anaesthetic action affects the firing activity of a single neuron. Now considering a population of neurons, the question arises how the anaesthetic effect on a single neuron translates into the neural population activity. This neural population describes the activity in a specific cortical layer of neurons receiving inputs from other cortical layers and/or non-cortical structures.

In this project, we will assume population firing rates, i.e. neglect the time-coding of single neurons, and assume the embedding of the network in a two-dimensional spatial domain. The assumption of population coding is reasonable for sensory inputs in primary sensory areas, such as the primary motor cortex (Georgopoulos et al, 1992) and the primary visual cortex (Hubel and Wiesel, 1963). The work will follow a mean-field approach according to a previous study (Hutt and Atay, 2005). This approach considers the ensemble (population) firing rate of a neural population in a very short time window, i.e. the number of spikes emitted in the population in a time window of few milliseconds. It takes into account the probability distribution of membrane potentials at the soma in each neuron and the distribution of firing thresholds in the neuron population. The resulting model does not consider the transfer function of single neurons, but just the distribution of the firing thresholds. Moreover, the approach involves the response of neurons to incoming spiking activity by a single synaptic response function for each single receptor type (excitatory or inhibitory receptors). It also neglects more specific receptor effects, such as shunting inhibition, which however may play an important role in the neural information processing. In addition to the properties of single neurons, the model involves the spatial distribution of axonal fibers and the corresponding axonal transmission delay, but neglects the spatial extension of dendritic structures.

To improve this standard model and consider more specific dynamics of the dendritic activity and the firing dynamics, the new model will additionally take into account the probability distribution of single neuron parameters, such as the firing threshold and the slope of the nonlinear gain. Since these single neuron properties depend of the anaesthetic action on inhibitory synapses, the new neural population model involves the anaesthetic action. The extension will be possible by a new analytical derivation of the model equations now considering the dependence of the firing threshold and the nonlinear gain of the anaesthetic action. Consequently the new model will represent a population firing rate model considering effects similar to shunting inhibition.

The novel single-layer population model is spatially extended and might exhibit axonal transmission delays between neurons. Since the major task is the understanding of the cortical activity, we will consider realistic spatial extensions of single cortical areas and certain cortical layers. Good candidates for such cortical brain regions are the mesial parietal cortex, the posterior cingulate cortex and the precuneus which play in an important role in the loss of consciousness (Kaisti et al, 2002; Alkire et al, 2008). If the spatial dimensions suggest a too small transmission delay, the population

model will not include them. Moreover, the real spatial distribution of axonal connections in cortical layers will be investigated. The work will involve these distributions in accordance to experimental findings to gain a realistic population model.

To validate the resulting population model, extended numerical simulations of both the network of single neurons and the neural population model will be performed and compared. To this end, it will be necessary to find, or develop, an abstract single neuron model which allows to reproduce the firing dynamics subjected to specific choices of inhibitory reversal potentials and their distribution, i.e. with the specific firing rate and nonlinear gain statistics derived previously. With the help of this model, it will be possible to simulate a network of single neurons and compute the population firing rate in this network.

After the successful derivation of the population model, it will be necessary to investigate its dynamical dynamics. To this end, at first we will determine the stationary state of the system and study the spatio-temporal oscillatory dynamics subjected to the anaesthetic action about this state. The work will achieve this goal by a detailed analysis of the linear response as presented in section 2.2. This analysis allows to compute the power spectrum of the linear activity. This is one of the major tasks in the project, since the work aims to extract the change of the power spectrum subjected to changing microscopic receptor dynamics. A comparison of the gained power spectrum results to previous studies (Hutt and Longtin, 2009) and experimental data will be elusive concerning the novel systems properties. The results will reveal the importance of shunting inhibition effects on the spatio-temporal dynamics of the neural population. Moreover, the analysis will apply the oscillation activation schemes found in sections 3.1, 3.2 and investigate whether they may explain the frequency shift found in EEG during GA.

Since external additive random fluctuations may affect the stability of the system as shown in section 2.3.1, the work will also investigate the nonlinear response of the system to external random fluctuations. This study will be demanding due to the expected increased complexity of the model. However it is necessary to gain a full picture of the possible dynamical effects of the anaesthetics.

Project 3: Novel population time-coding model based on a single neuron model

The previous project aims to derive a novel population model based on the neural firing rates of single neurons while neglecting the timing of single spikes emitted by the single neurons. However, some neural structures decode incoming activity according to the neural inter-spike interval and utilize temporal coding, such as in retinal ganglion cells (Van Rullen and Thorpe, 2001). A large number of studies in the recent decades have elucidated the importance of temporal coding (Deco et al, 2008; Van Rullen et al, 2005). Especially the dynamical adaption of synaptic strength found in many systems (Markram et al, 1997; Bi and Poo, 1998) have been studied successfully in networks, see e.g. (Siri et al, 2008; Cessac et al, 2009). An additional coding mechanism is the time-coding in populations, that has been found in motor cortex as a additional coding variant (Fetz, 1997; Riehle et al, 1997). Consequently, an extension of the population rate model in Project 2 to a population time-coding model renders the population model more realistic.

To achieve this goal, the project will investigate the Lighthouse model developed recently by Haken (Haken, 2002). This hybrid model of networks considers the generation of spikes in a single neuron k based on an instantaneous firing rate function S by introducing an abstract phase ϕ_k which obeys

$$\frac{d\phi_k(t)}{dt} = S \left[\sum_m c_{km} \psi_m(t) + p_{ext,k}(t) - \theta \right].$$

The phase rotates with the speed of the firing rate function and the neuron fires if the phase obeys $\phi_k \bmod 2\pi = 0$. In addition, the variables ψ_m denote the dendritic current induced at synapse m on the dendritic dendrite of neuron k wheighted by the factor c_{km} . The function $p_{ext,k}$ denotes an external driving current and θ is the firing threshold.

Assuming an exponential synaptic response function, the dendritic currents obey

$$\frac{d\psi_m(t)}{dt} = -\gamma\psi_m(t) + \sum_k a_{mk} P_k(t)$$

with the synaptic response decay rate γ , the incoming pulse train $P_k(t)$ from neuron k and the wheights a_{mk} . The pulse train is given by the sum of Dirac-functions

$$P_k(t) = \sum_{n=-\infty}^{\infty} \dot{\phi}_k(t) \delta(\phi_k(t) - \phi_k(t_n))$$

with $\phi_k(t_n) = 2\pi n$ and $\dot{\phi} = d\phi/dt$. In contrast to some other spiking neuron model, the Lighthouse model involves the output firing rate of neurons while taking into account dendritic activity and synaptic responses subjected to incoming spikes. In the context of the present task, the former aspect allows to take into account the anaesthetic action since the shunting inhibition-like effect of anaesthetics defines the output firing rate of the neuron. Hence, Project 1 delivers the firing rate function of the Lighthouse model. Moreover, the axonal connectivity matrix with elements a_{mk}

in a network of Lighthouse neurons may be chosen according to connectivity structures found in experiments. Moreover, The original work of Haken does not embed the neurons in a metric space. Future work will take into account the spatial embedding corresponding to a recent study of Chow and Coombes (Chow and Coombes, 2006). The spatial connection topology will also decide whether it is necessary to include axonal transmission delays in the model or not.

Summarizing, the work will take into account the anaesthetic action of propofol and aims to map the corresponding effects to model elements, such as the firing rate function S , in the Lighthouse model. The analysis steps investigate both the interspike-interval dynamics (ISI) and the dendritic current dynamics (Local Field Potentials), since typical experiments extract these quantities. The study will investigate the oscillatory activity of a network of such neurons in the linear regime subjected to the action of propofol. A comparison of the gained results, the results from Project 2, previous results in a population rate-coding model (Hutt and Longtin, 2009) and experimental data will elucidate the importance of the time coding aspects.

Project 4: Nonlinear analysis of neural fields subjected to external inputs

After the development of neural population models in Projects 2 and 3, this project will study these models in the nonlinear domain in the presence of external input.

Since the neural origin of loss of consciousness (LOC) during under anaesthesia is not understood, various cortical population rate models have been developed to gain further insight into the underlying neural mechanism (Bojak and Liley, 2005; Steyn-Ross and Steyn-Ross, 1999; Hutt and Longtin, 2009). Some models claim that linear interactions in the system are sufficient to explain the change of the EEG-power (Bojak and Liley, 2005). Such models explain the power spectrum change, but do not give explanations of the LOC and return to consciousness (ROC) and do not consider the hysteresis aspect. Another theoretical model (Steyn-Ross and Steyn-Ross, 1999; Steyn-Ross et al, 2004) claim that the LOC and the ROC represent non-linear stochastic phase transitions of first order, which explain the hysteresis and the EEG-power spectrum change by the critical fluctuations occurring close to phase transitions, cf. Fig. 3.6. In addition this theory explains the LOC by the jump from an active population to a population with almost vanishing neural activity. Consequently this model suggests that unconsciousness represents low neural activity. This approach gives a nice and clear explanation of the loss of consciousness (loss of consciousness = loss of neural activity). However, the mathematical description of this model is linear though the phase transition is a strongly non-linear effect.

Since the evidence for a nonlinear effect at LOC is strong, future studies will investigate the phase transition hypothesis by a detailed nonlinear mathematical treatment of the population models in Project 2 and 3. This study will include the anaesthetic effect represented by a specific parameter reflecting the anaesthetic concentration. This parameter will serve as a control parameter in the system, i.e. at a critical control parameter value the phase transition occurs. Moreover, the model describes the activity of a single layer in the cortex and will assume external deterministic and random inputs from other brain areas. The deterministic input may originate from the thalamus, that typically exhibits regular tonic or bursting behaviour which may be interpreted as periodic or quasi-periodic in time and unspecific in space. The random inputs are supposed to reflect uncorrelated input in space and time from other cortical or sub-cortical areas. Essentially, the project will study the nonlinear dynamics of the system showing jumps between two stationary states driven by the external noise and the deterministic driving.

The project will answer the question whether the jumps between the two stationary states in the neural population activity are the origin of the characteristic power spectrum change under anaesthesia. The theoretical results will give analytical expressions for the expected nonlinear power spectrum and thus predicts the measured activity, see the detailed description of the mathematical tools below. In a final step, the work will perform a final search for physiological parameters to reproduce experimental EEG-power spectra. Only if reasonable physiological parameters have been found, then the phase transition theory holds. In contrast, if the study does not find reasonable

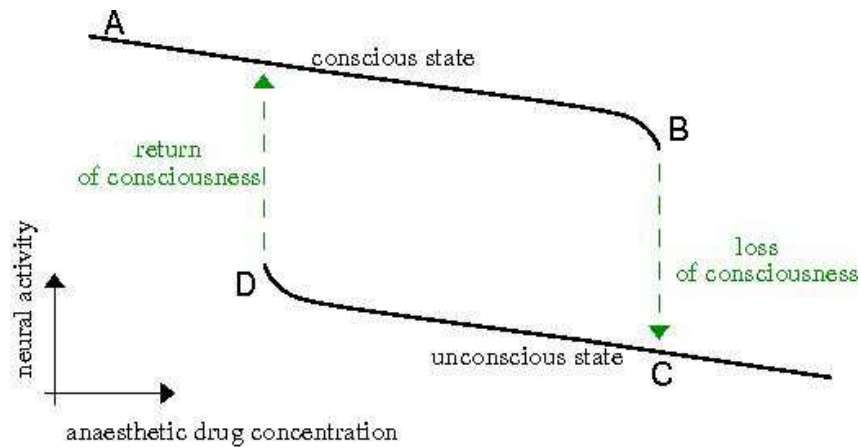


Figure 3.6: Sketch of the phase transition approach. Before the administration of the anaesthetics, the neural population exhibits high activity (point A) and the subject is awake. Now increasing the anaesthetics concentration let the system move on the top branch of high activity up to point B. For larger anaesthetics concentration no state exists anymore at high neural activity and the activity drops to a much lower activity level (loss of consciousness at point C), where it remains for further concentration increase. After the administration of the anaesthetics stopped, the subjects body catabolizes the drug and the anaesthetics concentration decreases at a low neural activity level up to point D. Since a further concentration decrease yields no state at low activity, the activity jumps back to the upper branch of high activity (return of consciousness) and the subject awakes.

physiological parameters that allow to reproduce the experimental power spectrum, the anaesthetic effect is no purely cortical effect and it is necessary to involve the anaesthetic effect of subcortical structures as well.

Since the neural population rate model may be viewed as a template for a more general pattern forming system, the non-linear analysis of the model may be applicable to other systems as well. In general terms, the mathematical study makes it necessary to develop novel mathematical techniques to investigate stochastic effects in delayed and non-delayed spatially extended systems that are driven by external stochastic and periodic forces. Expected effects are *coherence resonance* neglecting external periodic driving and *stochastic resonance* involving external periodic driving.

a) Local nonlinear analysis

As a first analysis step and to reveal possible nonlinear effects of the system dynamics, the work will assume small deviations about a single stationary state but taking into account higher nonlinear terms of the small deviations, e.g. of quadratic or cubic order. Previous studies (cf. section 2.3.1 and Bloemker (2007)) have shown that additive external inputs may modify the stability of stationary

states subjected to the input strength. Hence the first analysis step will investigate the nonlinear power spectrum of the system subjected to the anaesthetic concentration.

To this end, at first the population model neglects axonal transmission delays. This is a reasonable approximation if the spatial spread of the population is small enough. For instance, the action potential propagation along an axonal fibre of length 1mm with the typical speed of 0.5m/s may yield a delay of 2ms, which may be negligible compared to synaptic response times of several tens of milliseconds. Moreover, initially we may analyse the system assuming a constant spatial interaction kernel. This choice renders the dynamics of the system space-independent. A recently developed analytical perturbation approach (Tuckwell, 2008b,a) allows to compute the nonlinear power spectrum of the system. A comparison of this nonlinear power spectrum to the linear power spectrum (cf. section 2.2.3) and experimental findings will indicate whether it is sufficient to include the small nonlinear corrections to explain the experimental effects. Then analytical investigations for non-constant spatial kernels will reveal additional spatio-temporal dynamics resulting into corrections of the nonlinear power spectrum, cf. section 2.2.3. After the non-delayed study, we will extend the perturbation approach introduced in Tuckwell (2008b,a) for the non-delayed case to the transmission delays. This case may occur if the brain region under study is rather large or contains long-range axonal interactions, e.g. cortico-cortical connections of typical length of 10mm, with small propagation speeds, e.g. of 2m/s. Since the largest contributions to the power spectrum are close to instability points, future work will investigate the non-linear power spectrum close to instabilities of the linear system. To this end, a time-dependent center manifold theory for delayed systems will be developed close to instability points to derive an equivalent evolution equation without delays., see (Lefebvre et al, 2011) for a first successful example. This non-delayed equation permits to extract the nonlinear power spectrum corresponding to the non-delayed case described above. The comparison of the gained result to the non-delayed case will reveal the importance of the transmission delay for the explanation of the experimental data.

b) Global nonlinear analysis

The previous analysis assumes that the system remains close to a stationary state and the external stimulation is not strong enough to repel the activity from the vicinity of the stationary state. However, strong enough stimulation by the external fluctuations or the deterministic driving input may induce jumps of the system between the stationary states. Then the corresponding mathematical treatment becomes much more complicated and it is not sufficient anymore to treat nonlinear terms in lower orders. Different mathematical methods are necessary to apply. The work will utilize the methods developed in the context of stochastic resonance (Gammaitoni et al, 1998). In general terms, the problem considered in stochastic resonance is the statistical description of stochastic jumps between stationary states while the system is driven by a deterministic force. The transition rates between simple stationary states may be computed analytically which allows for the calculation of spectral quantities, such as the power spectrum of the activity, the signal-to-noise ratio of the

activity and the distribution of the residence time in the vicinity of a certain stationary state. These quantities are also interesting in the context of neural cortical activity, since they may be accessible experimentally (Wilson et al, 2010). Though stochastic resonance has been studied mathematically in detail in low-dimensional systems for decades, its study in spatially extended systems is less developed (Gammaitoni et al, 1998). Moreover, only few studies, e.g. (Tsimring and Pikovsky, 2001), consider delays in the system and to our best knowledge no study investigates stochastic resonance in spatially-extended systems involving transmission delay. The future work will try to develop methods to treat jumps between stationary jumps in neural populations. To this end, a first extensive literature study on spatial systems will reveal the already developed mathematical tools for stochastic resonance. These methods may be applied to the non-delayed neural population model at first, before its extension to the delay case along the lines of previous work on low-dimensional systems (Tsimring and Pikovsky, 2001). Such studies will yield analytical expressions, e.g. for the power spectrum, which may be compared to experimental data.

Project 5: Cortical layer network of neural populations

The previous projects investigated a single neural population. Such a population may exist in a single cortical layer in a single brain area. However, the cortex exhibits 6 different layers in each brain area and these layers are strongly interconnected to each other, cf. Fig. 3.7.

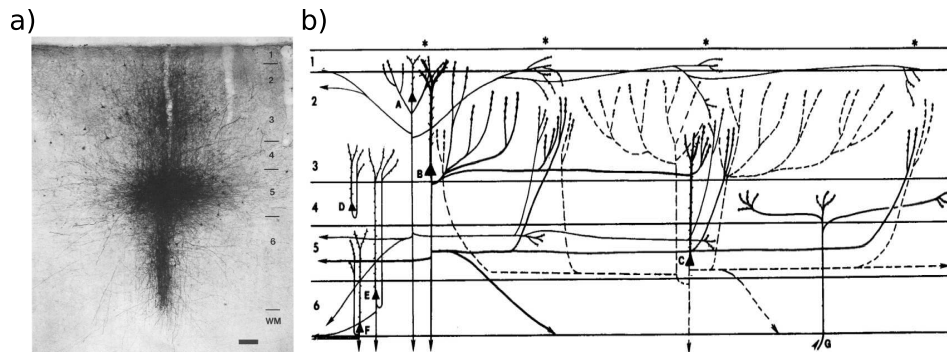


Figure 3.7: Example for the cortical layer structure: intrinsic connections in visual area V4 in macaque monkeys. a) The photomicrograph shows a biocytin injection into layer 5 revealing single pyramidal cells (in layers 2, 3, 5 and 6) and connecting fibres between different layers. Horizontally spreading fibers are seen predominantly in layers 3 and 5. Scale bar has a length of $100\mu\text{m}$. b) Diagram of intrinsic pyramidal neuron projections suggested on the basis of patterns of biocytin labeling. Taken from (Yoshioka et al, 1992).

Moreover, different brain areas are connected by cortico-cortical axonal paths linking specific layers in the brain areas. Hence, to come closer to a realistic cortical structure, an improved model includes a network of connected layers and a network of such networks. Recent mathematical studies have been able to derive stability conditions for such a model (Faugeras et al, 2009). Since the study of such a complex model is very difficult, at first the work will try to infer analytically the multi-layer network dynamics from the single-layer model and apply the same analysis steps to this network model as in the single-layer model. To this end, at first a linear stability analysis will be performed. It is expected that standard techniques may be sufficient to study the corresponding linear network dynamics. Additional analysis steps, such as the nonlinear investigations as in Project 4, will make necessary the development of new mathematical tools.

To learn more about the spatio-temporal dynamics of the multi-layer model, it will be necessary to integrate numerically the evolution equations. Since the cortical layers are two-dimensional sheets in a good approximation, the project will extend the simulation techniques mentioned in section 2.1.4 for scalar models to vector models. The new techniques have to be optimised with respect to speed and memory allocation due to the complexity of the model.

Project 6: Linking neural populations and EEG by an electromagnetic forward solution

The neuronal activity in cortical layers is the neural source of the EEG (Nunez and Srinivasan, 2006; Niedermeyer and Lopes da Silva, 2004). To explain the EEG based on neuronal population activity in the cortical layers, the work will compute the electromagnetic forward solution, i.e. the electric activity on the scalp dependent on the neural population activity in the cortex. The following paragraphs explain the theory, the corresponding difficulties and ways to solve the problems.

Action potentials (AP) propagate along axonal trees and terminate at synapses. The work will consider chemical synapses, though electric synapses, i.e. gap junctions, may also play a role in neural processing. The APs induce ion currents at synapses and the laws of electromagnetism tells us that the current flow in or out of the cell at the synapse induces a closed current loop (Nunez and Srinivasan, 2006). In more physical terms, the synaptic response to an AP generates a current field that extends spatially in the vicinity of the synapse, see Fig. 3.8.

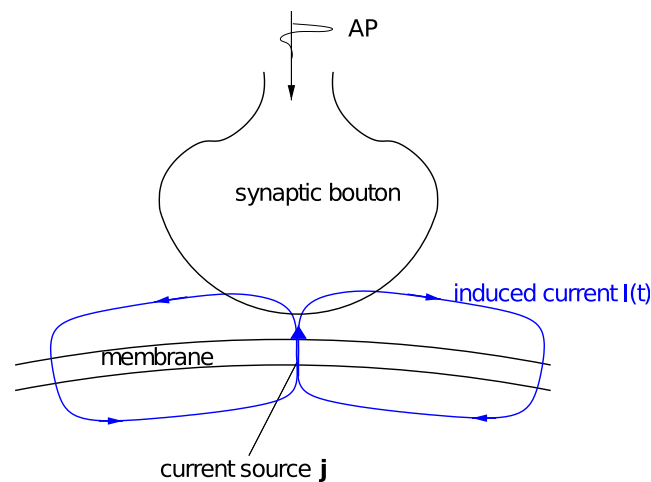


Figure 3.8: An incoming AP induces a PSP in the membrane that represents a current source \mathbf{j} with a closed current loop. The sketch gives an example of an inhibitory synapses where the induced current points out of the membrane.

Moreover synapses populate densely the dendritic tree of a single neuron. For instance, experimental studies in rats (Megias et al, 2001) revealed that a single pyramidal cell in the hippocampus receives inputs from ~ 30.000 excitatory and ~ 1700 inhibitory synapses in average. Considering all synapses and the corresponding currents, it is in principle possible to compute the resulting current field in good approximation as a linear superposition of the current fields of the individual synapses. However, the synapse positions are difficult to detect and the geometry of the dendritic branches and thus the spatial orientation of the current source and sinks is rather complex. Consequently in

practice it is almost impossible to compute the exact synaptic current field close to a single neuron.

Physiological experiments may apply electrodes directly to the membrane of a single neuron and measure the trans-membrane potential or may apply the electrodes to the tissue outside the neurons and extract the extracellular potential, the so-called Local Field Potentials (LFP). Now let us assume that we know the exact synaptic current field close to a neuron. Then the laws of electromagnetism gives us the related electric potential. In the absence of free charges, the current field $\vec{J}(x, t)$ at spatial location x and time t has no source or sink and thus its divergence vanishes, i.e.

$$\vec{\nabla} \cdot \vec{J} = 0 \quad (3.1)$$

where $\vec{\nabla}$ represents the three-dimensional differential vector operator $\vec{\nabla} = (\partial/\partial x, \partial/\partial y, \partial/\partial z)$. Assuming a purely resistive linear medium, the current field may involve ohmic currents $\sigma \vec{E}$ proportional to the electric field \vec{E} and currents originating from sources \vec{J}_s , i.e.

$$\vec{J}(x, t) = \sigma(x) \vec{E}(x, t) + \vec{J}_s(x, t) . \quad (3.2)$$

Here $\sigma(x)$ is the spatially dependent conductivity tensor. Inserting Eq. (3.2) into Eq. (3.1) and applying the relation of \vec{E} to the electric potential $\vec{E} = -\vec{\nabla} \Phi$, we find

$$\vec{\nabla} \cdot [\sigma(x) \vec{\nabla} \Phi(x, t)] = -s(x, t) \quad , \quad s(x, t) = -\vec{\nabla} \cdot \vec{J}_s(x, t) \quad (3.3)$$

with the electric potential $\Phi(x, t)$. The term $s(x, t)$ may be interpreted as the volume current source density of the electric potential Φ that is generated by the induced synaptic currents $\vec{J}_s(x, t)$. Consequently the solution $\Phi(x, t)$ of Eq. (3.3) is the electric potential outside a single neuron and $\Phi(x, t) - \Phi(x_r, t)$ represents the LFP measured in the neural tissue at spatial location x with the reference electrode at x_r .

Now let us discuss the link to the experimental EEG. It represents electric activity on the scalp and is found experimentally to be strongly correlated to the brain activity (Regan, 1989). Figure 3.9 shows a dataset of experimental EEG measurements and illustrates the spatial distribution of activity and its temporal evolution. Detailed studies in the last decades on the origin of the EEG revealed that it originates from the top layer of the brain (Jirsa et al, 2002; Nunez and Srinivasan, 2006), i.e. the neo-cortex. The EEG electrodes on the scalp have a diameter of about ~ 1 cm and detect the potential difference between them and a reference electrode. In addition re-calling the small spatial scale of neural activity sources (~ 1 mm and below), their spatial extension in the neural tissue and their underlying complexity, the EEG electrodes detect the activity of a large number of neural sources and thus it appears very difficult to explain the origin of the EEG by single sources. Nevertheless the concept of neural dipoles represent a promising approach to model EEG.

Neural dipoles reflect the mean-field activity of neurons in spatial patches, i.e. small spatial volumes. This mean-field activity results from the network interaction of the single neurons. Corresponding to the paragraphs above, where we have introduced the current sources \vec{J}_s in a single neuron,

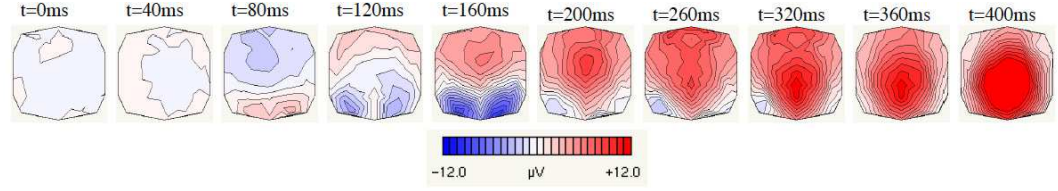


Figure 3.9: Example of an EEG measurement taken during a visualization task experiment (Herrmann et al, 1999). At $t = 0\text{ms}$, a visual stimulus has been applied. The maps show the electric potential difference on the scalp seen from above, where the nose is on the top side and the back of the head is on the bottom side. The potential difference is taken between various spatial locations on the scalp and a fixed base electrode, e.g. the ear or the nose. The data shown has been obtained with 64 electrodes distributed over the head, the activity is interpolated between the spatial locations of electrodes and the measured electric activity has been averaged over subjects and experimental trials. The lower scale gives the encoding of the measured voltage.

here we consider a mesoscopic current dipole moment per unit volume $P(\vec{x}, t)$ of the spatial patch at spatial location \vec{x}

$$P(\vec{x}, t) = \frac{1}{W} \int_W \vec{w} s(\vec{x}, \vec{w}, t) d^3w, \quad (3.4)$$

see Fig. 3.10. In this formulation, $s(\vec{x}, \vec{w}, t)$ represents the volume current source density in Eq. (3.3)

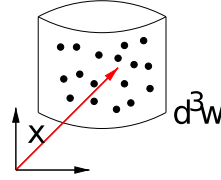


Figure 3.10: The spatial patch at location x is the integration volume d^3w to compute the mesoscopic current dipole moment \vec{P} , see Eq. 3.4. The dots represent the current sources which define the current source density $s(\vec{x}, \vec{w}, t)$ in Eq. (3.4).

at location \vec{w} in the volume element, which is located at \vec{x} . The volume element has the size of a macro-column, i.e. a side length of about 1mm or smaller. To compute the potential on the scalp from the current source density s , the standard theory of electromagnetism tells us to expand the potential into an infinite series of multipoles and compute all multipole moments (Jackson, 1998). Since it is very difficult to compute all multipoles, re-call that the electrodes on the scalp are far from the neural sources in the neo-cortex compared to the size of the spatial patches. Consequently high-order multipoles of the neural sources do not contribute much to the potential on the scalp and it is sufficient to consider the few lowest orders in the multipole expansion. Considering just the

lowest current multipole, i.e. the current dipole (3.4), the potential on the scalp reads

$$\Phi_{scalp}(\vec{r}, t) = \int_{neo-cortex} \vec{G}(\vec{r}, \vec{x}) \vec{P}(\vec{x}, t) d^3x. \quad (3.5)$$

This model assumes the brain as a volume conductor and the Greens function $G(\vec{r}, \vec{x})$ takes into account the electric and magnetic properties and the geometry of the brain, including the neural tissue, the skull and the scalp. It is important to mention that the potential Φ_{scalp} in Eq. (3.4) is not the same as in Eq. (3.3), which is the intracranial potential in the neural tissue.

Moreover, the integral equation (3.5) may also be formulated as the Poisson equation (Gramfort et al, 2010; Kybic et al, 2005)

$$\vec{\nabla} \left[\sigma(x) \vec{\nabla} \Phi_{scalp}(x, t) \right] = \vec{\nabla} \vec{J}_p(x, t). \quad (3.6)$$

Here, \vec{J}_p is the spatial density distribution of current dipoles. Most previous studies investigating electromagnetic forward solutions choose a distribution of current dipoles. However, most studies do not discuss how this dipole distribution is related to the population activity in certain layers, though this relation is crucial to understand the resulting EEG (Niedermeyer and Lopes da Silva, 2004). For instance, the experimental data in Fig. 3.9 shows occipitally a changing polarity between 80ms and 120ms, the so-called components P1 and N1, respectively. This change in polarity may be modeled by a localized dipole distribution inverting the orientation during the sequence from P1 to N1. However, physiologically this polarity change originates from the activation of synapses in different cortical layers (Niedermeyer and Lopes da Silva, 2004). Hence, a closer look to the physiological structure is necessary to link neural population activity and the potential on the scalp much better.

To illustrate further the relation of synaptic activity and the EEG, recall that the neo-cortex has 6 inter-connected horizontal layers of neurons and each layer exhibits a specific connection structure. In the subsequent simple example, we assume a spatial patch where the upper and lower layers contain excitatory and inhibitory synapses only, respectively, and the magnitude of the extracellular current in the top and bottom layers is I . Moreover, the extracellular current I is treated to be proportional to the neural population activity considered in the Projects 2 - 5. Then the current source density is proportional to I , i.e. $s(\vec{x}, \vec{w}, t) \sim \pm I$. Moreover the resulting extracellular current density \vec{J} and the current dipole moment $\vec{P} \sim -\vec{J}$ are directed along the axis of the patch in opposite directions, see Fig. 3.11. This simplified example illustrates well how the neural population activity generates the current dipole moment \vec{P} and, consequently, how to determine the electric potential on the scalp by Eq. (3.5). Hence, it is important to know the locations of excitatory and inhibitory synapses in the different layers to compute the corresponding scalp potential.

The major task of the project is the link of the physiological structure, the corresponding neural population activity and the EEG. To this end, the project will consider the population model developed in Project 5, derive a dipole distribution based on the physiological and functional structure

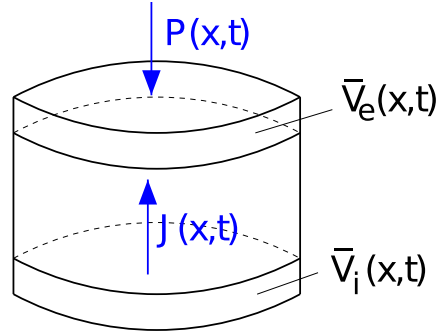


Figure 3.11: Illustrative example for a spatial patch containing neurons with excitatory (on top) and inhibitory (on bottom) synapses. The resulting extracellular current density $\vec{J}(x,t)$ is directed along the axis of the patch and in opposite direction to the current dipole moment $\vec{P}(x,t)$. The variables $\bar{V}_e(x,t)$ and $\bar{V}_i(x,t)$ represent the averaged membrane potentials of excitatory and inhibitory synapses, respectively, and are proportional to the extracellular synaptic currents.

of the cortex and map it to a dipole distribution generating the EEG. The specific cortical area under study may be the parietal cortex, cf. Project 2. Moreover, the electromagnetic forward solution will be computed by the application of the already developed software tool OPENMEEG developed at INRIA in Sophia-Antipolis (Gramfort et al, 2010). This tool computes the EEG based on an ensemble of current dipoles.

Project 7: Multivariate analysis of EEG obtained during general anaesthesia

In all projects given above, the work includes the comparison of the theoretical results to experimental data obtained during general anaesthesia. This comparison stipulates the frequency analysis of experimental data¹. For instance, the analysis of single electrode EEG activity in the context of GA includes the computation of the power spectrum or the bi-spectral indices (Miller et al, 2004). Moreover, the frequency analysis of multi-electrode EEG promises to provide deeper insights into neural dynamics during anaesthesia (Johnson et al, 2003; Gugino et al, 2001; John and Prichep, 2005; John et al, 2001).

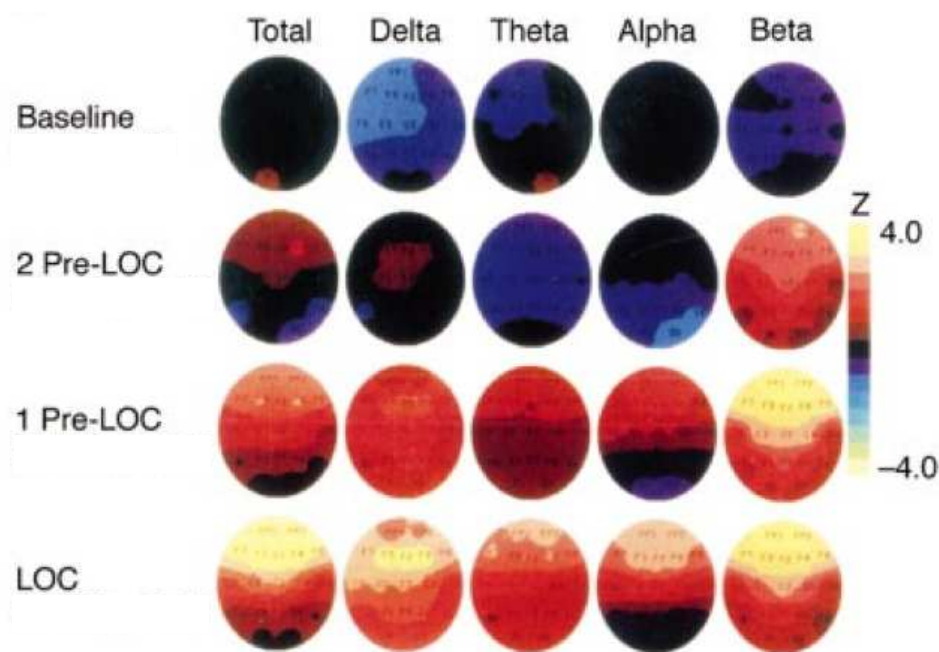


Figure 3.12: Example EEG activity under propofol/fentanyl anaesthesia. The spatial maps color-encode the Z-score transformed absolute power of oscillations within the delta-(1.5 – 3.5Hz), theta-(3.5 – 7.5Hz), alpha-(7.5 – 12.5Hz) and beta-(12.5 – 25Hz) band averaged over 16 subjects. The rows show the EEG activity for anaesthetic concentrations at baseline level, light sedation (denoted as 2 PRE-LOC), deeper sedation (denoted as 1 PRE-LOC) and at the loss of consciousness (denoted as LOC). Figure modified from (Gugino et al, 2001).

Figure 3.12 shows averaged EEG during propofol anaesthesia at different stages of consciousness. We observe a spatio-temporal change of electric activity on the scalp, which is specific for

¹Experimental data will be provided, .e.g. by the University of Auckland, New Zealand, and the Medical Faculty in Strasbourg, France.

each frequency band. For instance, oscillations in the alpha-band are stronger in the frontal areas than in the occipital areas after loss of consciousness. These results illustrate that the spatial activity distribution in EEG may play a role in the understanding of GA. Moreover future multivariate data analysis should consider the spatio-temporal dynamics of EEG-patterns in specific frequency bands separately. This analysis would reveal a sudden jump of the activity shown in Fig. 3.12 in the delta-band close to the loss of consciousness supporting the hypothesis of phase transition, cf. Project 4.

To gain deeper insight into the spatio-temporal dynamics of the underlying neural populations, an additional dynamic approach may shed some light on the data from another side. Let us consider the EEG-data with N electrodes, call it $\vec{s}(t) \in \mathcal{R}^N$ and decompose it into a finite sum of spatial patterns $\vec{v}_i \in \mathcal{R}^N, i = 1 \dots N$ evolving in time with amplitude $a_i(t)$, i.e.

$$\vec{s}(t) = \sum_{i=1}^N a_i(t) \vec{v}_i .$$

The fit of the temporal dynamics, i.e. of $\{a_i(t)\}$, to ordinary differential equations synchronous to the projection on spatial modes has been successful in the analysis of EEG during petit-mal epilepsie (Friedrich and Uhl, 1996), in event-related potentials (Uhl et al, 1998), early evoked potentials (Hutt and Riedel, 2003) and in the source localization of neural generators (Uhl et al, 2001). Figure 3.13 illustrates the separation in spatial modes and temporal amplitudes applied to evoked

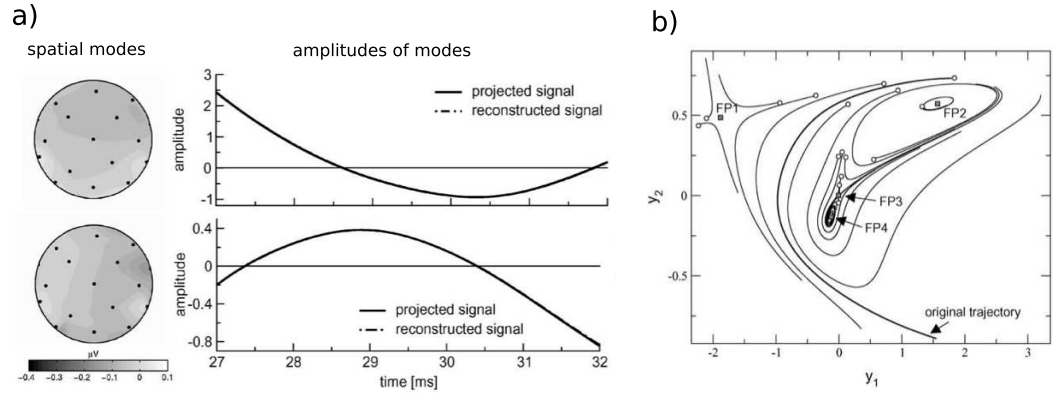


Figure 3.13: Optimal decomposition of the component P30 in 32-channel middle-latent auditory evoked potentials (averaged EEG) by synchronous fit of dynamical system. a) Optimal projection onto two spatial modes \vec{v}_1, \vec{v}_2 and their corresponding amplitudes $a_1(t), a_2(t)$. The reconstructed signal represents the solution of fitted ordinary differential equations fit to the projected signal. The fit to the original data is $\sim 92\%$. b) Trajectories of the determined dynamical system reveal the underlying topology of the fitted dynamical system. Figures modified from (Hutt and Riedel, 2003).

potentials. It also presents the topology of the dynamical system fitted to the amplitudes. This anal-

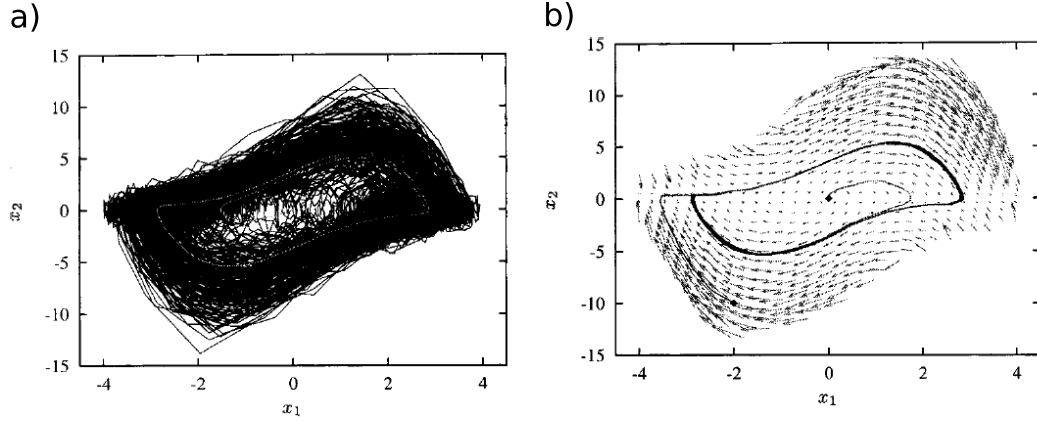


Figure 3.14: Illustration of the drift reconstruction of a stochastic process from simulated data (Gradisek et al, 2000). a) Stochastic time series $(x_1(t), x_2(t))'$ in two dimensions obeying a stochastic van der Pol oscillator model. b) Reconstructed drift coefficient $\vec{D}^{(1)}(x_1, x_2)$ shown as vector field which gives the topology similar to Fig. 3.13b) and two deterministic trajectories gained from the reconstructed topology by forward simulation. Figure modified from (Gradisek et al, 2000).

ysis technique, called Dynamical Systems Based Modeling (DSBM), works well for data with high signal-to-noise ratios.

Since, however, experimental data obtained during anaesthesia exhibit a high level of noise and a rather low signal-to-noise ratio, future work will extend the DSBM by fitting stochastic differential equations to the amplitudes $\{a_i(t)\}$. To this end, the time series of the spatial modes $a_i(t)$ will be considered as stochastic processes and the novel method computes the corresponding drift and diffusion coefficients (Siegert et al, 1998; Siefert et al, 2003)

$$D_i^{(1)}(\vec{x}, t) = \lim_{\tau} \langle a_i(t + \tau) - x_i \rangle_{\vec{a}(t) = \vec{x}}$$

$$D_{ij}^{(2)}(\vec{x}, t) = \lim_{\tau} \langle (a_i(t + \tau) - x_i)(X_j(t + \tau) - x_j) \rangle_{\vec{a}(t) = \vec{x}}$$

where $\vec{a}(t)$ is the multivariate stochastic projection amplitude. The drift coefficient $\vec{D}^{(1)}(x, t)$ reflects the topology of the underlying stochastic processes, whereas the diffusion coefficient matrix $\mathbf{D}^2(x, t)$ indicates the level of noise in the data. Figure 3.14 illustrates the extraction of the drift coefficient from stochastic data.

In the framework of EEG-analysis, the spatial modes of the EEG interact dynamically with each other according to the extracted topology, i.e. the drift, and the noise intensity. Now, such interactions are assumed to reflect interacting subnetworks in the neural population that generates the EEG. Consequently, the spatial EEG-maps may be interpreted to correspond to spatial subnetworks

in the neural population and the dynamical EEG-topology and noise intensity reflects the dynamics of underlying neural interactions, i.e. the dynamical topology of interacting subnetworks. This link of neural subnetworks to EEG-patterns is supported by the linear electromagnetic relation of neural source amplitude to electric activity on the scalp, cf. Project 6. Moreover the extracted topology of the EEG indicates functional interactions of subnetworks and constrains the neural population dynamics to specific interactions.

Summarizing, this inverse approach yields information on interacting subnetworks in neural populations and their functional interactions. This information represents a constraint which, in turn, may yield conditions for physiological parameters and may reject certain theoretical dynamical phenomena in neural populations.

Further perspectives

The previous Projects 1 to 7 represent just the backbone of a more general future work in general anaesthesia. The described projects may be extended in several ways. Project 1 focusses on the intravenous anaesthetic propofol, whereas medical procedures administer other anaesthetics as well, such as the volatiles and nitrous oxides. Moreover, today's general anaesthesia administers a combination of several drugs to guarantee the single anaesthetic actions. For instance, frequently propofol is applied in combination with remifentanyl to guarantee both the hypnotic and analgesic action. Hence future studies shall treat this combination in theoretical models as well according to Project 1, 2, 3 and 5.

The nonlinear analysis in Project 4 assumes a single cortical population driven by external stimuli, though the cortex is embedded in a delayed recurrent network of brain structures. More extended studies will consider the delayed cortico-thalamic connections, the thalamic activity and the delayed thalamo-cortical feedback. In addition, this closed loop is driven by other sub-cortical structures, such as the ascending arousal system. Since the most prominent activities of the thalamus are tonic spiking and bursting in single neurons, the first novel challenge will be the development of a population model taking into account these single neuron activity types in a population model.

Bibliography

- Alkire M, Hudetz A, GTononi (2008) Consciousness and anesthesia. *Science* 322:876–880
- Amit DJ (1989) Modeling brain function: The world of attractor neural networks. Cambridge University Press, Cambridge
- Atay FM, Hutt A (2005) Stability and bifurcations in neural fields with finite propagation speed and general connectivity. *SIAM J Appl Math* 65(2):644–666
- Atay FM, Hutt A (2006) Neural fields with distributed transmission speeds and constant feedback delays. *SIAM J Appl Dyn Syst* 5(4):670–698
- Baker BJ, Kosmidis EK, Vucinic D, Falk CX, Cohen LB, Djuricic M, Zecevic D (2005) Imaging brain activity with voltage- and calcium-sensitive dyes. *Cell Mol Neurobiol* 25(2):245–82
- Ben-Yishai R, Bar-Or R, Sompolinsky H (1995) Theory of orientation tuning in visual cortex. *Proc Natl Acad Sci* 92:3844–3848
- Berman NJ, Maler L (1999) Neural architecture of the electrosensory lateral line lobe: adaption for coincidence detection, a sensory searchlight and frequency-dependent adaptive filtering. *J Exp Biol* 202:1243–1253
- Bi GQ, Poo MM (1998) Synaptic modifications in cultured hippocampal neurons: dependence on spike timing, synaptic strength, and postsynaptic cell type. *J Neurosci* 18(24):10,464–10,472
- Billock VA, Tsou BH (2007) Neural interactions between flicker-induced self-organized visual hallucinations and physical stimuli. *PNAS* 104(20):8490–8495
- Bloemker D (2007) Amplitude equations for stochastic partial differential equations. World Scientific
- Bojak I, Liley D (2005) Modeling the effects of anesthesia on the electroencephalogram. *Phys Rev E* 71:041,902
- Boxler P (1989) A stochastic version of the center manifold theorem. *ProbThRelFields* 83:509–545

- Braitenberg V, Schütz A (1998) *Cortex : statistics and geometry of neuronal connectivity*, 2nd edn. Springer, Berlin - New York
- Breakspear M, Friston K (2001) Symmetries and itinerancy in nonlinear systems with many degrees of freedom. *Behav Brain Sc* 24:813–814
- Bressloff PC (2001) Traveling fronts and wave propagation failure in an inhomogeneous neural network. *Physica D* 155:83–100
- Bringuier V, Chavane F, Glaeser L, Fregnac Y (1999) Horizontal propagation of visual activity in the synaptic integration field of area 17 neurons. *Science* 283:695–699
- Buonviso N, Amat C, Litaudon P, Roux S, Royet J, Farget V, Sicard G (2003) Rhythm sequence through the olfactory bulb layers during the time window of a respiratory cycle. *Eur J Neurosci* 17:1811–1819
- Carandini M, Heeger DJ (1994) Summation and division by neurons in primate visual cortex. *Science* 264:1333–1335
- Carnevale NT, Hines ML (2006) *The NEURON Book*. Cambridge University Press, Cambridge, UK
- Castelo-Branco M, Neuenschwander S, Singer W (1998) Synchronization of visual response between the cortex, lateral geniculate nucleus, and retina in the anesthetized cat. *J Neurosci* 18(16):6395–6410
- Cenier T, David F, Litaudon P, Garcia S, Amat C, Buonviso N (2009) Respiration-gated formation of gamma and beta neural assemblies in the mammalian olfactory bulb. *Eur J Neurosci* 29(5):921–30
- Cessac B, Rostro H, Vasquez JC, Vieville T (2009) How gibbs distributions may naturally arise from synaptic adaptation mechanisms. *J Stat Phys* 136(3):565–602
- Chacron MJ, Longtin A, Maler L (2005) Delayed excitatory and inhibitory feedback shape neural information transmission. *PhysRevE* 72:051,917
- Chow CC, Coombes S (2006) Existence and wandering of bumps in a spiking neural network model. *SIAM Journal on Applied Dynamical Systems* 5:552–574
- Cohen D (1972) Magnetoencephalography: detection of the brain's electrical activity with a superconducting magnetometer. *Science* 175:664–66
- Coles AJ, Alastair D, Compston S, Selmaj KW, Lake SL, Moran S, Margolin DH, Norris K, Tandon PK (2008) Alemtuzumab vs. interferon beta-1a in early multiple sclerosis. *New Engl J Med* 359(17):1786–1801
- Coombes S (2010) Large-scale neural dynamics: Simple and complex. *NeuroImage* 52:731–739

- Coombes S, Lord G, Owen M (2003) Waves and bumps in neuronal networks with axo-dendritic synaptic interactions. *Physica D* 178:219–241
- Coombes S, Venkov N, Shiao L, Bojak I, Liley D, Laing C (2007) Modeling electrocortical activity through improved local approximations of integral neural field equations. *PhysRevE* 76:051,901–8
- Cruz-Martinez A, Gonzalez-Orodea JI, Lopez PR, Arpa J (2000) Disability in multiple sclerosis. the role of transcranial magnetic stimulation. *Electromyogr Clin Neurophysiol* 40(7):441–447
- Deco G, Jirsa VK, Robinson PA, Breakspear M, Friston K (2008) The dynamic brain: From spiking neurons to neural masses and cortical fields. *PLoS Comput Biol* 4(8):e1000,092
- Deco G, Jirsa VK, McIntosh AR (2011) Emergent concepts for the dynamical organization of resting-state activity in the brain. *Nat Rev Neurosci* 12(1):43–56
- Destexhe A, Contreras D (2006) Neuronal computations with stochastic network states. *Science* 314:85–90
- Deuschl G, Raethjen J, Lindemann M, Krack P (2001) The pathophysiology of tremor. *Muscle Nerve* 24(6):716–735
- Dieckmann U, Law R, Metz JAJ (eds) (2000) *The Geometry of Ecological Interactions: Simplifying Spatial Complexity*. Cambridge University Press, Cambridge
- Doiron B, Chacron M, Maler LM, Longtin A, Bastian J (2003) Inhibitory feedback required for network burst responses to communication but not to prey stimuli. *Nature* 421:539–543
- Doiron B, Lindner B, Longtin A, Maler LM, Bastian J (2004) Oscillatory activity in electrosensory neurons increases with the spatial correlation of the stochastic input stimulus. *PhysRevLett* 93:048,101
- Dutta P, Horn P (1981) Low-frequency fluctuations in solids: $1/f$ noise. *Rev Mod Phys* 53(3):497–516
- Engel A, Koenig O, Kreiter A, Singer W (1991) Interhemispheric synchronization of oscillatory neuronal response in cat visual cortex. *Science* 252:1177–1179
- Farrant M, Nusser Z (2005) Variations on an inhibitory theme: phasic and tonic activation of GABA receptors. *Nature Rev Neurosci* 6:215–229
- Fates NA (2008) Asynchronism induces second order phase transitions in elementary cellular automata. *J Cell Autom* 4(1):21–38

- Faugeras O, Veltz R, Grimbert F (2009) Persistent neural states: stationary localized activity patterns in nonlinear continuous n-population, q-dimensional neural networks. *Neural Comput* 21(1):147–187
- Faye G, Faugeras O (2010) Some theoretical and numerical results for delayed neural field equations. *Physica D* 239:561–578
- Fetz EE (1997) Temporal coding in neural populations? *Science* 278(5345):1901–1902
- Fisher R, van Emde BW, Blume W, Elger C, Genton P, Lee P, Engel J (2005) Epileptic seizures and epilepsy: definitions proposed by the international league against epilepsy (ILAE) and the international bureau for epilepsy (IBE). *Epilepsia* 46(4):470–472
- Freeman W (2000) *Neurodynamics: An Exploration in Mesoscopic Brain Dynamics (Perspectives in Neural Computing)*. Springer-Verlag, Berlin
- Freeman W (2003) Evidence from human scalp eeg of global chaotic itinerancy. *Chaos* 13(3):1069
- Freeman WJ (1975) *Mass Action in the Nervous System*. Academic Press, New York
- Friedrich R, Uhl C (1996) Spatio-temporal analysis of human electroencephalograms: Petit-mal epilepsy. *Physica D* 98:171
- Friedrich RW, Laurent G (2001) Dynamic optimization of odor representations by slow temporal patterning of mitral cell activity. *Science* 291(5505):889–94
- Gammaitoni L, Haenggi P, Jung P, Marchesoni F (1998) Stochastic resonance. *Rev Mod Phys* 70(1):223–287
- Georgopoulos AP, Ashe J, Smyrnis N, Taira M (1992) The motor cortex and the coding of force. *Science* 256:1692–1695
- Girard P, Hupe J, Bullier J (2001) Feedforward and feedback connections between areas v1 and v2 of the monkey have similar rapid conduction velocities. *J Neurophysiol* 85:1328–1331
- Goodman DF, Brette R (2009) The brain simulator. *Front Neurosci* 3(2):192–197
- Gough B (2003) *GNU Scientific Library Reference Manual, 2nd edn*. Network Theory Ltd
- Gradsiek J, Siebert S, Friedrich R, Grabec I (2000) Analysis of time series from stochastic processes. *Phys Rev E* 62(3):3146–3155
- Gramfort A, Papadopoulou T, Olivi E, Clerc M (2010) Openmeeg: opensource software for quasistatic bioelectromagnetics. *BioMedical Engineering Online* 45:9

- Gugino LD, Chabot RJ, Prichep LS, John ER, Formanek V, Aglio LS (2001) Quantitative EEG changes associated with loss and return of consciousness in healthy adult volunteers anaesthetized with propofol or sevoflurane. *Br J Anaesth* 87(3):421–428
- Gushchin A, Kuechler U (2000) On stationary solutions of delay differential equations driven by a lévy process. *Stochastic Proc Appl* 88:195–211
- Gutkin B, Ermentrout G, O’Sullivan J (2000) Layer 3 patchy recurrent excitatory connections may determine the spatial organization of sustained activity in the primate prefrontal cortex. *Neurocomputing* 32-33:391–400
- Haas LF (2003) Hans berger (18731941), richard caton (18421926), and electroencephalography. *J Neurol Psych* 74:9
- Haken H (2002) *Brain Dynamics*. Springer, Berlin
- Haken H (2004) *Synergetics*. Springer, Berlin
- Harmony T, Fernandez T, Silva J, Bernal J, Diaz-Comas L, Reyes A, Marosi E, Rodriguez M, Rodriguez M (1996) Eeg delta activity: an indicator of attention to internal processing during performance of mental tasks. *Int J Psychophysiol* 24(1-2):161 – 171
- Hellwig B (2000) A quantitative analysis of the local connectivity between pyramidal neurons in layers 2/3 of the rat visual cortex. *BiolCybern* 82:111–121
- Herrmann C, Mecklinger A, Pfeifer E (1999) Gamma response and ERPs in a visual classification task. *Clin Neurophysiol* 110:636–642
- Holt GR, Koch C (1997) Shunting inhibition does not act divisively on firing rates. *Neural Comput* 9:1001–1013
- Horsthemke W, Lefever R (1984) *Noise-induced transitions*. Springer Berlin
- Horton JC, Hubel DH (1981) Regular patchy distribution of cytochrome oxidase staining in primary visual cortex of macaque monkey. *Nature* 292(5825):762–764
- Hubel D, Wiesel T (1963) Receptive fields of cells in striate cortex of very young, visually unexperienced kittens. *J Physiol* 26:994
- Hutt A (2004) An analytical framework for modeling evoked and event-related potentials. *Int J Bif Chaos* 14(2):653–666
- Hutt A (2007) Generalization of the reaction-diffusion, Swift-Hohenberg, and Kuramoto-Sivashinsky equations and effects of finite propagation speeds. *Phys Rev E* 75:026,214

- Hutt A (2008a) Additive noise may change the stability of nonlinear systems. *Europhys Lett* 84:34,003
- Hutt A (2008b) Local excitation-lateral inhibition interaction yields oscillatory instabilities in non-locally interacting systems involving finite propagation delay. *PhysLettA* 372:541–546
- Hutt A (2009) Oscillatory activity in excitable neural systems. *Contemporary Physics* 51(1):3–16
- Hutt A (2010) Spatio-temporal instabilities in neural fields and the effects of additive noise. In: DASteyn-Ross, MLSteyn-Ross (eds) *Modelling Phase Transitions in the Brain*, Springer, New York, Springer Series in Computational Neuroscience, vol 4
- Hutt A, Atay F (2005) Analysis of nonlocal neural fields for both general and gamma-distributed connectivities. *Physica D* 203:30–54
- Hutt A, Atay F (2006) Effects of distributed transmission speeds on propagating activity in neural populations. *Phys Rev E* 73:021,906
- Hutt A, Atay F (2007) Spontaneous and evoked activity in extended neural populations with gamma-distributed spatial interactions and transmission delay. *Chaos, Solitons and Fractals* 32:547–560
- Hutt A, Frank T (2005) Critical fluctuations and $1/f$ -activity of neural fields involving transmission delays. *Acta Phys Pol A* 108(6):1021
- Hutt A, Longtin A (2009) Effects of the anesthetic agent propofol on neural populations. *Cogn Neurodyn* 4(1):37–59
- Hutt A, Munk M (2006) Mutual phase synchronization in single trial data. *Chaos and Complexity Letters* 2(2):6
- Hutt A, Munk M (2009) Detection of phase synchronization in multivariate single brain signals by a clustering approach. In: Wennberg R, Velazquez JLP (eds) *Coordinated Activity in the Brain: measurements and relevance to brain function and behaviour*, Springer, New York
- Hutt A, Riedel H (2003) Analysis and modeling of quasi-stationary multivariate time series and their application to middle latency auditory evoked potentials. *Physica D* 177:203
- Hutt A, Rougier N (2010) Activity spread and breathers induced by finite transmission speeds in two-dimensional neural fields. *Phys Rev E* in press
- Hutt A, Schimansky-Geier L (2008) Anesthetic-induced transitions by propofol modeled by nonlocal neural populations involving two neuron types. *J Biol Phys* 34(3-4):433–440

- Hutt A, Bestehorn M, Wennekers T (2003a) Pattern formation in intracortical neuronal fields. *Network: Comput Neural Syst* 14:351–368
- Hutt A, Daffertshofer A, Steinmetz U (2003b) Detection of mutual phase synchronization in multivariate signals and application to phase ensembles and chaotic data. *Phys Rev E* 68:036,219
- Hutt A, Longtin A, Schimansky-Geier L (2007) Additive global noise delays turing bifurcations. *Phys Rev Lett* 98:230,601
- Hutt A, Longtin A, Schimansky-Geier L (2008a) Additive noise-induced turing transitions in spatial systems with application to neural fields and the swift-hohenberg equation. *Physica D* 237:755–773
- Hutt A, Sutherland C, Longtin A (2008b) Driving neural oscillations with correlated spatial input and topographic feedback. *PhysRevE* 78:021,911
- Jackson JD (1998) *Classical Electromagnetism*. Wiley, New York
- Jirsa V, Jantzen K, Fuchs A, Kelso J (2002) Spatiotemporal forward solution of the EEG and MEG using network modelling. *IEEE Trans Med Imag* 21(5):493–504
- John E, Prichep L (2005) The anesthetic cascade : A theory of how anesthesia suppresses consciousness. *Anesthesiol* 102:447–471
- John ER, Prichep LS, Kox W, Valdes-Sosa P, Bosch-Bayard J, Aubert E, Tom M, di Michele F, Gugino LD (2001) Invariant reversible qeeg effects of anesthetics. *Conscious Cogn* 10(2):165–183
- Johnson BW, Sleight JW, Kirk IJ, Williams ML (2003) High-density eeg mapping during general anaesthesia with xenon and propofol: a pilot study. *Anaesth Intensive Care* 31(2):155–163
- Kaisti K, Metshonkala L, Ters M, Oikonen V, Aalto S, Jskelinen S, Hinkka S, Scheinin H (2002) Effects of surgical levels of propofol and sevoflurane anesthesia on cerebral blood flow in healthy subjects studied with positron emission tomography. *Anesthesiol* 96:1358–1370
- Kay L (2003) A challenge to chaotic itinerancy from brain dynamics. *Chaos* 13(3):1057–1066
- Koch C (1999) *Biophysics of Computation*. Oxford University Press, Oxford
- Koch M, Mostert J, Heersema D, De Keyser J (2007) Tremor in multiple sclerosis. *J Neurol* 254(2):133–145
- Kopanitsa MV (1997) Extrasynaptic receptors of neurotransmitters: Distribution, mechanisms of activation, and physiological role. *Neurophysiology* 29(6):448–458

- Kozin F (1969) A survey of stability of stochastic systems. *Automatica* 5:95–112
- Kringelbach ML, Jenkinson N, Owen SLF, Aziz TZ (2007) Translational principles of deep brain stimulations. *Nat Rev Neurosci* 8:623–635
- Kybic J, Clerc M, Abboud T, Faugeras O, Keriven R, Papadopoulo T (2005) A common formalism for the integral formulations of the forward eeg problem. *IEEE Transactions on Medical Imaging* 24:12–28
- Lachaux JP, Rodriguez E, Martinerie J, Varela F (1999) Measuring phase synchrony in brain signals. *Human Brain Mapp* 8:194–208
- Laing C, Troy W (2003) PDE methods for non-local models. *SIAM J Appl Dyn Syst* 2(3):487–516
- Lefebvre J, Hutt A, Longtin A, LeBlanc V (2011) Non-autonomous center manifold reduction in a model of delayed feedback. submitted
- Lepage G (1978) A new algorithm for adaptive multidimensional integration. *J Comput Phys* 27:192–203
- Levitt J, Lewis D, Yishioka T, Lund J (1993) Topography of pyramidal neuron intrinsic connections in macaque monkey prefrontal cortex (areas 9 and 46). *J Comp Neurol* 338:360–376
- Liley D, Cadusch P, Wright J (1999) A continuum theory of electrocortical activity. *Neurocomp* 26-27:795–800
- Lindner B, Doiron B, Longtin A (2005) Theory of oscillatory firing induced by spatially correlated noise and delayed feedback. *PhysRevE* 72:061,919
- Longtin A, Moss F, Bulsara A (1991) Time interval sequences in bistable systems and noise induced transmission of neural information. *Phys Rev Lett* 67:656–659
- Lund J, Angelucci A, Bressloff P (2003) Anatomical substrates for functional columns in macaque monkey primary visual cortex. *Cerebral Cortex* 13:15–24
- Magoun HW (1952) An ascending reticular activating system in the brain stem. *Am Arch Neurol Psych* 67(2):145–154
- Mardia K, Jupp P (1999) *Directional Statistics*. Wiley, New York
- Markram H, Lubke J, Frotscher M, Sakmann B (1997) Regulation of synaptic efficacy by coincidence of postsynaptic apss and epsps. *Science* 275(5297):213–215
- Masuda N, Okada M, Aihara K (2007) Filtering of spatial bias and noise inputs by spatially structured neural networks. *Neural Comp* 19:1854–1870

- Megias M, Emri Z, Freund T, Gulyas A (2001) Total number and distribution of inhibitory and excitatory synapses on hippocampal ca1 pyramidal cells. *Neuroscience* 102:527–540
- Mel BW (1994) Information processing in dendritic trees. *Neural Compu* 6:1427–1439
- Michels L, Bucher K, Luchinger R, Klaver P, Martin E, Jeanmonod D, Brandeis D (2010) Simultaneous eeg-fmri during a working memory task: modulations in low and high frequency bands. *PLoS One* 5(4):e10,298
- Miller A, Sleight J, Barnard J, Steyn-Ross D (2004) Does bispectral analysis of the electroencephalogram add anything but complexity? *BritJAnaesth* 92(1):8–13
- Mitchell SJ, Silver RA (2003) Shunting inhibition modulates neuronal gain during synaptic excitation. *Neuron* 38(3):433–334
- Molae-Ardekani B, Senhadji L, Shamsollahi M, Vosoughi-Vahdat B, EWodey (2007) Brain activity modeling in general anesthesia: Enhancing local mean-field models using a slow adaptive firing rate. *Phys Rev E* 76:041,911
- Moore-Ede MC, Sulzman FM, Fuller CA (1982) *The Clocks that Time Us: Physiology of the Circadian Timing System*. Harvard University Press, Cambridge, MA
- Niedermeyer E, Lopes da Silva F (2004) *Electroencephalography: Basic Principles, Clinical Applications, and Related Fields*. Lippincott Williams and Wilkins
- Nunez P (2000) Toward a quantitative description of large-scale neocortical dynamic function and eeg. *Behav Brain Sci* 23:371–437
- Nunez P, Srinivasan R (2006) *Electric Fields of the Brain: The Neurophysics of EEG*. Oxford University Press, New York - Oxford
- Orser B (2006) Extrasynaptic gabaa receptors are critical targets for sedative-hypnotic drugs. *J Clin Sleep Med* 2:S12–8
- Orser B (2007) Lifting the fog around anesthesia. *Scientific American* 7:54–61
- Owen MR, Laing CR, Coombes S (2007) Bumps and rings in a two-dimensional neural field: splitting and rotational instabilities. *New JPhys* 9:378
- Phibbs B (2007) *The human heart: a basic guide to heart diseases*. Lippincott Williams & Wilkins
- Pikovsky A, Rosenblum M, Kurths J (2001) *Synchronization: A Universal Concept in Nonlinear Science*. Cambridge University Press
- Qubbaj MR, Jirsa VK (2009) Neural field dynamics under variation of local and global connectivity and finite transmission speed. *Physica D* 238(23-24):2331–2346

- Rabinovich M, Huerta R, Laurent G (2008) Transient dynamics for neural processing. *Science* 321(5885):48–50
- Regan D (1989) *Human brain electrophysiology: Evoked potentials and evoked magnetic fields in science and medicine*. Elsevier, New York
- Riehle A, Grun S, Diesmann M, Aertsen A (1997) Spike synchronization and rate modulation differentially involved in motor cortical function. *Science* 278(5345):1950–1953
- Rio M, Hutt A, Munk M, Girau B (2011) Partial amplitude synchronization detection in brain signals using bayesian gaussian mixture models. submitted
- Rougier N, Hutt A (2010) Synchronous and asynchronous evaluation of dynamic neural fields. *JDifference Eqs Appl* in press
- Sachse S, Galizia CG (2002) Role of inhibition for temporal and spatial odor representation in olfactory output neurons: A calcium imaging study. *J Neurophysiol* 87:1106–1117
- Sadaghiani S, Hesselmann G, Friston KJ, Kleinschmidt A (2010) The relation of ongoing brain activity, evoked neural responses, and cognition. *Front Syst Neurosci* 4:20
- Schmidt H, AHutt, Schimansky-Geier L (2009) Wave fronts in inhomogeneous neural field models. *Physica D* 238(14):1101–1112
- Schoener G, Haken H (1986) The slaving principle for Stratonovich stochastic differential equations. *Z Phys B* 63:493–504
- Siefert M, Kittel A, Friedrich R, Peinke J (2003) On a quantitative method to analyse dynamical and measurement noise. *Europhys Lett* 61:466–472
- Siegel JH (2002) *The neural control of sleep and waking*. Springer, New York
- Siegert S, Friedrich R, Peinke J (1998) Analysis of data sets of stochastic systems. *Phys Lett A* 234:275–280
- Singer W (1999) Neural synchrony: A versatile code for the definition of relations ? *Neuron* 24:49–65
- Singer W, Gray C (1995) Visual feature integration and the temporal correlation hypothesis. *Ann Rev Neurosc* 18:555–586
- Siri B, Berry H, Cessac B, Delord B, Quoy M (2008) A mathematical analysis of the effects of hebbian learning rules on the dynamics and structure of discrete-time random recurrent neural networks. *Neural Comput* 20(12):2937–2966

- Somers D, Nelson S, Sur M (1995) An emergent model of orientation selectivity in cat visual cortical simple cells. *J Neurosci* 15(8):5448–5465
- Stark WR, Hughes WH (2000) Asynchronous, irregular automata nets: the path not taken. *Biosystems* 55(1-3):107 – 117
- Steyn-Ross M, Steyn-Ross D (1999) Theoretical electroencephalogram stationary spectrum for a white-noise-driven cortex: Evidence for a general anesthetic-induced phase transition. *Phys Rev E* 60(6):7299–7311
- Steyn-Ross M, Steyn-Ross D, Sleight J (2004) Modelling general anaesthesia as a first-order phase transition in the cortex. *Prog Biophys Molecul Biol* 85(2-3):369–385
- Swindale NV (1996) The development of topography in visual cortex: a review of models. *Network* 7:161–247
- Taouali W, Alexandre F, Hutt A, Rougier N (2009) Asynchronous evaluation as an efficient and natural way to compute neural networks. In: *NUMERICAL ANALYSIS AND APPLIED MATHEMATICS: International Conference on Numerical Analysis and Applied Mathematics 2009*, American Institute of Physics, AIP Conference Proceedings, vol 1168, pp 554–558
- Timofeeva Y, Cox SJ, Cox S, Josic K (2008) Democratization in a passive dendritic tree: an analytical investigation. *J Comput Neurosci* 25:228–244
- Tsimring LS, Pikovsky A (2001) Noise-induced dynamics in bistable systems with delay. *Phys Rev Lett* 87:2506,021–4
- Tuckwell H (1988) *Introduction to theoretical neurobiology: Volume 2*. Cambridge University Press, Cambridge, UK
- Tuckwell HC (2008a) Analytical and simulation results for the stochastic spatial fitzhugh-nagumo model neuron. *Neur Comp* 20(12):3003–3033
- Tuckwell HC (2008b) Nonlinear effects in white-noise driven spatial diffusion: General analytical results and probabilities of exceeding threshold. *Physica A* 387:1455–1463
- Uhl C, Kruggel F, Opitz B, von Cramon DY (1998) A new concept for eeg/meg signal analysis: detection of interacting spatial modes. *Human Brain Map* 6:137
- Uhl C, Hutt A, Kruggel F (2001) Improvement of source localization by dynamical systems based modelling(DSBM). *Brain Top* 13(2):219–226
- Valenti D, Schimansky-Geier L, Sailer X, Spagnolo B (2006) Moment equations for a spatially extended system of two competing species. *EurPhysJB* 50:199–203

- Van Rullen R, Thorpe SJ (2001) Rate coding versus temporal order coding: what the retinal ganglion cells tell the visual cortex. *Neur Comput* 13(6):1255–83
- Van Rullen R, Guyonneau R, Thorpe S (2005) Spike times make sense. *Trends in Neurosci* 28(1):1–4
- Venkov NA (2009) Dynamics of neural field models. PhD thesis, University of Nottingham
- Wehr M, Laurent G (1996) Odour encoding by temporal sequences of firing in oscillating neural assemblies. *Nature* 384(6605):162–6
- Wennekers T (2001) Orientation tuning properties of simple cells in area V1 derived from an approximate analysis of nonlinear neural field models. *Neural Comput* 13:1721–1747
- Wilson H, Cowan J (1972) Excitatory and inhibitory interactions in localized populations of model neurons. *Biophys J* 12:1–24
- Wilson MT, Barry M, Reynolds JN, Crump WP, Steyn-Ross DA, Steyn-Ross ML, Sleight JW (2010) An analysis of the transitions between down and up states of the cortical slow oscillation under urethane anaesthesia. *J Biol Phys* 36(3):245–259
- Wright J, Kydd R (1992) The electroencephalogram and cortical neural networks. *Network* 3:341–362
- Xu C, Roberts A (1996) On the low-dimensional modelling of Stratonovich stochastic differential equations. *Physica A* 225:62–80
- Yoshioka T, Levitt JB, Lund JS (1992) Intrinsic lattice connections of macaque monkey visual cortical area v4. *J Neurosci* 12(7):2785–2802

Part II

Dossier

Chapter 1

Curriculum Vitae

Personal details

affiliation: Charge de Recherche Premiere Classe (CR1), INRIA Nancy Grand Est, Team
CORTEX, 615 rue du Jardin Botanique, 54602 Villers-les-Nancy Cedex
email: axel.hutt@loria.fr
homepage: <http://www.loria.fr/~huttaxel/>

Academic Qualifications

1991-1997 Study of Physics at the University of Stuttgart, Germany
1997 Diploma in Physics
1997-2000 PhD-project at the Max Planck Institute of Cognitive Neuroscience in Leipzig, Germany
2000 Research Associate at the Max Planck Institute of Cognitive Neuroscience in Leipzig, Germany
PhD in Physics at the University of Stuttgart, Germany
2001-2002 Schloessmann Fellow at the Max Planck Institute for Mathematics in the Sciences in Leipzig, Germany
2002 Visiting Postdoc position at the Faculty of Human Movement Sciences, Vrije Universiteit Amsterdam, Netherlands (3 months)
2002-2004 Postdoctoral position at the Weierstrass Institute for Applied Analysis and Stochastics in Berlin, Germany
2004-2007 Wissenschaftlicher Assistent at the Department of Physics, Humboldt University Berlin, Germany
2006-2007 Research Associate at the Department of Physics at University of Ottawa, Canada (sabbatical)
2007- Chargé de Recherche (CR1) at INRIA Nancy

Active Cooperations outside the own group — Theoretical

- Dr. Evelyn Buckwar, Heriot-Watts University Edinburgh, UK: numerics of stochastic delay differential equations in neural systems
- Prof. André Longtin, Department of Physics, University of Ottawa, Ottawa, Canada: neural populations subject to delay and noise
- Prof. Linghai Zhang, Department of Mathematics, Lehigh University, Bethlehem, USA: effects of distributed axonal transmission speeds in neural systems

Active Cooperations outside the own group – Experimental

- Dr. Matthias Munk, Max Planck Institute for Biological Cybernetics, Tuebingen, Germany: data analysis and synchronization in Local Field Potentials
- Prof. Torsten Schubert, Department of Psychology, Ludwigs-Maximilians University Muenchen, Germany: modeling of priming effects in psychophysical experiments
- Prof. Jamie Sleight, University of Auckland, New Zealand: analysis of EEG obtained experimentally during anaesthesia

Grants and Awards:

1999	Summer School Fellowship in Cognitive Neuroscience, Dartmouth College, USA
2000	Schloessmann Postdoc Fellowship of the Max Planck Society, Germany (2 years)
2008	British Royal Society Incoming Visitor Grant INRIA-Explorateur Grant CORDI PhD-project grant (3 years)
2009-2010	International project CNRS Neuroinformatique with Chile. Topic: Neural correlations in the retina
2011-2015	ERC Starting Grant. Topic: Mathematical modeling of anaesthesia (MATHANA)

Reviewer and editorial activities

Journals	Physical Review Letters (since 2000), Visual Cognition (2000), Physical Review E (since 2002), Neurocomputing (2005), SIAM J. Applied Mathematics (since 2005). Since 2006: SIAM J. Applied Dynamical Systems, Europhysics Letters, Physica D, Physics Letters A, Computer Methods and Programs in Biomedicine. Since 2007 - 2008: New J. of Physics, Biological Cybernetics, J. of Biological Physics, PloS Computational Biology, J. Physics A. Since 2009 - 2010: Physica A, Journal Mathematical Biology, Neuroimage, Frontiers in Computational Neuroscience, Cognitive Neurodynamics, Nonlinearity, European Journal of Physics.
Conference	Neurocomp 2010, BMIC 2011
Societies	The Netherlands Organization for Scientific Research - NWO, Marsden Fund New Zealand
Editor	Review Editor for Frontiers in Chronobioneurology and Sleep Medicine (since 2010)

Teaching experience at universities

- 1993-1997 Tutor of lecture exercises in Theoretical Physics, Experimental Physics, Mathematics, and experimental laboratory at University of Stuttgart
- 1998-2001 Tutor of lecture exercises in Theoretical Physics at University of Leipzig
- 2003-2006 Tutor of lecture exercises in Experimental and Theoretical Physics at the Humboldt University Berlin
- 2005 Single lectures in basic courses in Experimental and Theoretical Physics at the Humboldt University Berlin
- Full lecture course *Dynamics in neural systems* for physicists at the Humboldt University Berlin (winter semester 2005/2006)

Workshop organization

- 1998 Assistant organizer of the international workshop *Analysis of Neurophysiological Brain Functioning* at the Max Planck Institute of Cognitive Neuroscience in Leipzig
- 2005 Co-organizer of a minisymposium on *Spatio-Temporal Dissipative Structures Induced by Non-Local Interactions* at the SIAM Conference of Applications on Dynamical Systems in Snowbird, USA
- Assistant organizer of the international conference *100 years of Brownian Motion* in Erice, Italy funded by the European Science Foundation
- 2007 Organizer of the workshop *Modeling of anesthesia and sleep by neuronal networks* at the Computational Neuroscience Meeting (CNS) in Toronto, Canada
- 2009 Organizer of the workshop *Anesthesia and Sleep: recent theoretical and experimental aspects* at the Computational Neuroscience Meeting (CNS) in Berlin, Germany

Memberships

- 1998- Member of German Physical Society
- 2011- Member of Federation of European Neuroscience Societies (FENS)
- 2010-2014 Elected member of the Board of Directors, Organisation for Computational Neuroscience (CNS)

Chapter 2

Supervision of students

Undergraduates

- 1993-2006: Leader of lecture tutorials accompanying the lecture courses in Experimental Physics, Theoretical Physics and Mathematics at University of Stuttgart, University of Leipzig, Humboldt University Berlin
- 2002-2004: Supervision of student in the software implementation of interface between Matlab, R and C++ at Weierstrass Institute for Applied Analysis and Stochastics Berlin.
- 2004-2006: Supervision of students in the development of software packages for stochastic differential equation solvers (programming language: C/C++) at the Department of Physics at Humboldt University Berlin.
- 2008: Supervision of internship students from Rumania (6 months) at INRIA Nancy.
- 2009: Supervision of student from IUT Nancy to implement a Graphical User Interface in PYTHON at INRIA Nancy.
- 2009: Supervision of internship student from Canada (3 months) at INRIA Nancy.
- 2010: Supervision of internship student from Mexica (6 months) at INRIA Nancy

Diploma students

- 2006: At Department of Physics, Humboldt Universitaet Berlin, Michael RADING has worked on the pattern formation in non-locally interacting neural populations (**Diploma in Physics**, 1 year)

- 2006: At Department of Physics, Humboldt University Berlin, Helmut SCHMIDT has worked on fronts and bumps in heterogeneous neural populations (**Diploma in Physics**, 1 year). Work resulted in publication: H.Schmidt, A.Hutt and L.Schimansky-Geier, Wave fronts in inhomogeneous neural field models, *Physica D* 238 (14), 1101-1112 (2009)

Master students

- 2009: Wahiba TAOUALI has studied at the Ecole Nationale Supérieure des Mines de Nancy and has worked at INRIA Nancy on her **Master 2** with the topic *Modeling of Neurons' populations of the Deep Superior Colliculus : Control of Saccadic Eye Movements*.
- 2009: Maximilien COLANGE has studied at the Ecole Nationale Supérieure (ENS) Cachan and has worked at INRIA Nancy on his **Master 1** with the topic *Dynamical neural model in general anaesthesia*.
- Feb.-June 2011: Remie BOES studies Mathematics at University Henri-Poincaré Nancy and works at INRIA Nancy on his **Master 1** with the topic *Importance of extra-synaptic receptors on anaesthetic action on dendrites*.

PhD-students

- 2008-2011: At INRIA Nancy and University Henri-Poincaré Nancy, Maxime RIO is working on *The detection of multivariate synchronization in experimental brain signals*.
- 2011-2014: At the Humboldt University Berlin, the University Henri-Poincaré Nancy and INRIA Nancy (co-tutelle), Christian WEBER is working on *Stochastic nonlinear dynamics in neural fields with application to general anaesthesia*.

Chapter 3

Summary of PhD-project

Motivation

The PhD-thesis has the title *Analysis and Modelling of Spatio-temporal Signals* and shows results on studies of event-related potentials in experimental encephalographic data (EEG) obtained during cognitive experiments. Such potentials are amplitude modulations in multivariate EEG-signals occurring synchronously in a subset of signals in a certain time window. Moreover, the evoked potentials occur always for identical experimental conditions and hence represent markers in cognitive experiments. They play an important role in experimental neuropsychology applying EEG. To learn more about such multivariate signal features, the task of the PhD work was to extract mathematical models for single evoked potentials. Such models were low-dimensional ordinary differential equations.

Methods

By virtue of the high dimension and the temporally transient nature of experimental EEG-data, the work identified two major problems: to model the evoked potentials, (i) at first it was necessary to detect the time windows of their occurrence and (ii) the multivariate signal had to be projected optimally in these time windows to a low-dimensional multivariate signal. These tasks have been solved as follows:

- (i) A clustering technique was developed to detect the time windows of the evoked potentials. This technique extracted a cluster quality measure based on the standard un-supervised cluster technique K-Means, which reflected the (time-dependent) probability for an evoked potential. This approach considered all time series in the multivariate EEG-signal.

- (ii) Knowing these time windows, an extended Principal Component Analysis has been developed to project the EEG-signal optimally to a low-dimensional space and, synchronously, determine ordinary differential equation systems for the projected signals. Since this projection technique is described in analytical terms, it is fast and more efficient than previously developed tools.

Results

The clustering method has been applied to artificial and few experimental datasets and extracted successfully evoked potentials in time-windows in good accordance to previous results. The detection method has worked very well even for rather noisy signals. Moreover, low-dimensional differential equations have been extracted for some EEG-signals.

Chapter 4

List of publications

Peer-reviewed publications after the PhD

1. C. Uhl, A.Hutt and F.Kruggel, Improvement of Source Localization by Dynamical Systems Based Modeling, *Brain Topography* 13(3), 219-226 (2001)
2. A.Hutt, M.Bestehorn and T.Wennekers, Pattern formation in intracortical neuronal fields, *Network: Computation in Neural Systems* 14, 351-368 (2003)
3. item A.Hutt and H.Riedel, Analysis and Modeling of Non-stationary Multivariate Time Series and Application to Middle Latency Auditory Evoked Potentials, *Physica D* 177 (1-4), 203-232 (2003)
4. A.Hutt, A.Daffertshofer and U.Steinmetz, Detection of phase synchronisation in non-stationary multivariate time series and application to phase ensembles and chaotic data, *Physical Review E* 68, 036219 1-10 (2003)
5. A.Hutt, An Analytical Framework For Modeling Evoked and Event Related Potentials, *International Journal of Bifurcation and Chaos* 14(2), 653-666 (2004)
6. A.Hutt, Effects of nonlocal feedback on traveling fronts in neural fields subject to transmission delay, *Physical Review E* 70, 052902 1-4 (2004)
7. F.Atay and A.Hutt, Stability and Bifurcations in Neural Fields with Finite Propagation Speed and General Connectivity, *SIAM Journal for Applied Mathematics* 65(2), 644-666 (2005)
8. A.Hutt and F.M.Atay, Analysis of nonlocal neural fields for both general and gamma-distributed connectivities, *Physica D* 203(1-2), 30-54 (2005)

9. A.Hutt and T.D.Frank, Critical fluctuations and $1/f^\alpha$ -activity of neural fields involving transmission delays, *Acta Physica Polonica A* 108(6), 1021-1040 (2005)
10. A.Hutt and F. M. Atay, Effects of distributed transmission speeds on propagating activity in neural populations, *Physical Review E* 73, 021906 1-5 (2006)
11. A.Hutt and M.Schrauf, Detection of transient synchronization in multivariate brain signals, application to event-related potentials, *Chaos and Complexity Letters* 3(1), 1-24 (2007)
12. F.M.Atay and A.Hutt, Neural fields with distributed transmission speeds and long-range feedback delays, *SIAM Journal Applied Dynamical Systemes* 5(4), 670-698 (2006)
13. A.Hutt and M.H.J.Munk, Mutual phase synchronization in single trial data, *Chaos and Complexity* (2), 225-246 (2006)
14. A.Hutt and F.M.Atay, Spontaneous and evoked activity in extended neural populations with gamma-distributed spatial interactions and transmission delay, *Chaos, Solitons and Fractals* 32, 547-560 (2007)
15. A.Hutt, Generalization of the reaction-diffusion, the Swift-Hohenberg and the Kuramoto-Sivashinsky equation and effects of finite propagation speeds, *Physical Review E* 75, 026214 (2007)
16. A.Hutt, A.Longtin and L.Schimansky-Geier, Additive global noise delays Turing bifurcations, *Physical Review Letters* 98, 230601 1-4 (2007)
17. A.Hutt, A.Longtin and L.Schimansky-Geier, Additive noise-induced Turing transitions in spatial systems with application to neural fields and the Swift-Hohenberg equation, *Physica D* 237, 755-773 (2008)
18. A.Hutt, Local excitation-lateral inhibition interaction yields oscillatory instabilities in nonlocally interacting systems involving finite propagation delay, *Physics Letters A* 372, 541-546 (2008)
19. A.Hutt, L.Schimansky-Geier, Anesthetic-induced transitions by propofol modeled by nonlocal neural populations involving two neuron types, *Journal Biological Physics* 34(3- 4), 433-440 (2008)
20. A.Hutt, A.Longtin and C.Sutherland, Driving neural oscillations with correlated spatial input and topographic feedback, *Physical Review E* 78, 021911 (2008)
21. H.Schmidt, A.Hutt and L.Schimansky-Geier, Wave fronts in inhomogeneous neural field models, *Physica D* 238 (14), 1101-1112 (2009)

22. A.Hutt, Additive noise may change the stability of nonlinear systems, *Europhysics Letters* 84, 34003 1-4 (2008)
23. N.Rougier and A.Hutt, Synchronous and Asynchronous Integration of Dynamic Neural Fields, *Journal Difference Equations And Applications*, in press (2010)
24. A.Hutt and A.Longtin, Modeling general anesthetic effects in neural populations, *Cognitive Neurodynamics*, 4(1), 37-59 (2009)
25. A.Hutt, Sleep and anesthesia, *Frontiers in Neuroscience*, 3(3), 408-409 (2009)
26. A.Hutt, Oscillatory activity in excitable neural systems, *Contemporary Physics* 51(1), 3-16 (2009)
27. W.Taouali, F.Alexandre, A.Hutt, N.Rougier, Asynchronous evaluation as an efficient and natural way to compute neural networks, In: *Numerical Analysis and Applied Mathematics: International Conference on Numerical Analysis and Applied Mathematics 2009*, AIP Conference Proceedings 1168, 554-558 (2009)
28. A. Hutt and N. Rougier, Activity spread and breathers induced by finite transmission speeds in two-dimensional neural fields, *Phys. Rev. E* 87, R055701 (2010)

Publications in books after the PhD

1. A.Hutt and F.Kruggel, Fixed Point Analysis: Dynamics of Nonstationary spatiotemporal signals, In: S.Boccaletti et al. (Ed.), *Space-time chaos: characterization, control and synchronization* (2002), World Scientific
2. F. M. Atay and A. Hutt, Dynamics of neural fields with distributed transmission speeds, In: A. Deutsch et al. (Eds.), *Mathematical Modeling of Biological Systems, Volume IV* (2005), Birkhaeuser
3. A.Hutt, Finite Propagation Speeds in Spatially Extended Systems, In F. Atay (Ed.), *Complex Time-Delay Systems*, pp. 151-176 (2009), Springer, Berlin
4. A.Hutt, Spatio-temporal instabilities in neural fields and the effects of additive noise, In D.A.Steyn-Ross and M.L.Steyn-Ross (Eds.), *Modelling Phase Transitions in the Brain*, pp. 53-80 (2010), Springer, New York
5. A.Hutt and M.H.J.Munk, Detection of phase synchronization in multivariate single brain signals by a clustering approach, In: R. Wennberg and J.L. Perez Velazquez (Eds.), *Coordinated Activity in the Brain: measurements and relevance to brain function and behaviour*, pp. 149-164 (2009), Springer, New York

Published conference abstracts after the PhD

1. A. Hutt, F. Kruggel, C.S. Herrmann, Fixed Point Analysis: Objective Detection of Components in ERPs and MLAEPs by a Clustering Algorithm, *Journal of Cognitive Neuroscience*, Supplement (2001)
2. A. Hutt, Spatiotemporal modelling of EEG/MEG, 10th German Mapping Meeting, Giessen, September 2001, *Brain Topography* 14(4), 347 (2002)
3. A. Hutt, Segmentation of Multivariate Time Series and Application to ERP-data, 11th German Mapping Meeting, Giessen, September 2002, *Brain Topography* 15(4), 266 (2003)
4. A. Hutt, J. Polzehl, Spatial adaptive signal detection in fMRT, 9th International Conference on Human Brain Mapping, June 2003, New York, USA, *NeuroImage* 19(2) (2003)
5. A.Hutt and M. Schrauff, Detection of Mutual synchronization in single ERPs, *Brain Topography* 17(3), 187 (2005)